SOFT CAPACITIVE SENSORS FOR PROXIMITY, TOUCH, PRESSURE AND SHEAR MEASUREMENTS

by

Mirza Saquib us Sarwar

M.A.Sc. The University of British Columbia, 2014

B.Sc. Bangladesh University of Engineering and Technology, 2011

A THESIS SUBMITTED IN PARTIAL FULFILLMENT OF

THE REQUIREMENTS FOR THE DEGREE OF

DOCTOR OF PHILOSOPHY

in

THE FACULTY OF GRADUATE AND POSTDOCTORAL STUDIES

(Electrical and Computer Engineering)

THE UNIVERSITY OF BRITISH COLUMBIA

(Vancouver)

May 2019

The following individuals certify that they have read, and recommend to the Faculty of Graduate and Postdoctoral Studies for acceptance, the dissertation entitled:

Soft capacitive sensors for proximity, touch, pressure and shear measurements

submitted by Mirza Saquib us Sarwar in partial fulfillment of the requirements for the degree of Doctor of Philosophy in Electrical and Computer Engineering

Examining Committee:

John D. W. Madden
Co-supervisor

Shahriar Mirabbasi
Co-supervisor

Supervisory Committee Member

Hendrik F. M. Van der Loos
University Examiner

A. Srikantha Phani
University Examiner

Additional Supervisory Committee Members:

Supervisory Committee Member

Supervisory Committee Member

Abstract

Sensors are devices that convert a physical stimulus into an electrical signal. Mechanical stimuli such as touch, pressure, strain and shear are very important for a plethora of applications. A lot of these application areas, including consumer electronics, sports, health care and robotics, require the sensor to be soft, stretchable and even transparent. In this thesis we demonstrate three capacitive sensors that are each an evolution of the preceding version. The first sensor is a flexible, transparent, proximity and touch sensor based on mutual capacitance technology - the conventional technology used in most touch-screen devices. The novelty in this research is the sensor's ability to operate while being deformed. This is important for applications where the device is expected to experience a bend or stretch while being interacted with such as in a wearable device and smart clothing. The second sensor in this thesis adds the ability to detect pressure and strain to enable its use in further applications. The sensor uses both mutual capacitance and overlap capacitance to detect the range of stimuli mentioned. The dielectric has cylindrical air gaps that enhance the pressure sensitivity. A 4 X 4 array structure is implemented that demonstrates the detection and differentiation of the different stimuli. However, for artificial skin applications, the ability to sense shear is extremely valuable, for example for helping robots grasp objects. The third sensor developed in this thesis is able to detect proximity and light touch similar to the previous iteration, but with 10X increase in pressure sensitivity (1.3% change in capacitance per kPa applied pressure, compared to 0.13% change for the second sensor) and the ability to detect localized shear (2.2% change in capacitance per kPa of shear stress). The novelty is a patterned dielectric architecture with pillars and sliding supports that enable the top surface of the sensor to slide and buckle like real skin and therefore enable the detection of localized shear. All the sensors use readily available materials (silicone, carbon black and/or polyacrylamide), along with conventional molding and bonding techniques and should be easy to produce in large quantities at low cost.

Lay Summary

This thesis presents three soft and stretchable sensors each an evolution of its ancestor. The first sensor is a transparent, flexible proximity and touch sensor that can operate while being actively bent/stretched. Its applications include wearable devices, smart clothing and flexible hand-held devices that are interacted with while being deformed. The second sensor is highly stretchable and adds the functionality of detecting pressure and strain to the existing ability to detect proximity and light touch, at the cost of transparency. This sensor has applications in human motion mapping for gaming and health care and as artificial skin for robotics and prosthetics. However, for artificial skin applications it is important to be able to detect shear – a sense that enables us to interact with fragile objects. The third sensor is able to buckle like human skin and adds the ability to detect localized shear in addition to proximity, touch and pressure.

Preface

The author is the main researcher in all of the work done in this thesis. It was done under the supervision of Dr. John D. W. Madden and Dr. Shahriar Mirabbasi. They provided guidance, as well as technical and editorial feedback on the work.

Material presented in Chapter 2 has been presented in the Materials Research Society Conference in 2015 titled "Hydrogel Based Flexible and Transparent Capacitive Proximity Sensor" and published in the journal Science Advances in 2017 titled "Bend, stretch, and touch: Locating a finger on an actively deformed transparent sensor". A PCT patent application (WO2016086306A1) has also been filed titled "FLEXIBLE TRANSPARENT SENSOR WITH IONICALLY-CONDUCTIVE MATERIAL". The design, development, fabrication, characterization and analysis has been conducted by the author. Judy Wang, Milind Pandit, Claire Preston and Justin Wyss aided in the fabrication and characterization, under the direction of the author.

Material in Chapter 3 has been presented in the Materials Research Society Conference in 2017 titled "Soft Multi-Modal Sensor—Bend, Stretch, Pressure, Touch and Proximity Using a Gel Electrode Array". The design, development, fabrication, characterization and analysis has been conducted by the author. Claire Preston, Justin Wyss and Tom Searle aided with the fabrication and characterization of the sensors, under the direction of the author.

A provisional patent application has been filed using the materials in Chapter 4 (application No. 62/768840) titled "DEFORMABLE SENSOR FOR SIMULATING SKIN AND OTHER

APPLICATIONS". The design, development, fabrication, characterization and analysis has been conducted by the author. Claire Preston, Alex Abulnaga and Neil Fan aided with the fabrication of the sensors.

Table of Contents

List of Tables

List of Figures

List of Abbreviations

Aam – Acrylamide, to which salt and water were added to create a transparent and stretchable conductors.

CDC – Capacitance to digital converter, used to measure capacitance.

MBAA - N,N′-Methylenebis(acrylamide), a monomer used in synthesizing polyacrylamide gel.

PDMS – Polydimethylsiloxane, used as a stretchable dielectric material in the sensors.

PEDOT:PSS - poly(3,4-ethylenedioxythiophene) polystyrene sulfonate, an electronically conducting polymer.

Acknowledgements

I would like to thank my supervisors Dr. John Madden and Dr. Shahriar Mirabbasi. I would also like to thank my colleagues and my family.

Dedication

Dedicated to my sister, my parents and my grandmother.

Chapter 1: Introduction

1.1 Background

A sensor is a device that translates a physical phenomenon (mechanical, thermal or electrical) into an electrical signal that can be interpreted and used to extract useful information regarding the said phenomenon. Some important mechanical stimuli are – the presence of a light contact, the pressure applied by a press or a weight, the stress and strain due to a stretch and shear forces due to a deformation parallel to the plane of a sensor. Traditionally these sensors have been rigid devices and typically either infrared (IR), piezoelectric, piezoresistive or capacitive in nature. If sensing is required over a large area or an arbitrary surface, a distributed and connected array of individual sensor units is used.

In recent times, with advances in flexible electronics, mechanical sensors have been developed that are soft, stretchable and even transparent. Some of these sensors (implemented in an array) are suitable for large and arbitrary area sensing and even for surfaces that can change dimensions (bent or stretched). Artificial skin or electronic skin refers to sensors that mimic human skin with applications in robotics and prosthetics. Its sensing capabilities include tactile sensing, temperature and other phenomenon [1]. Tactile sensing includes light touch using mutual capacitance [2], pressure [3], [4] and shear [5], [6]. A chronological development of some of these sensors for electronic/artificial skin application is compiled in [7] (Figure 1.1). It shows the progression from early rigid capacitive touch sensor on a computer screen to an array of individual rigid IR touch sensors on a mat placed on an arm, followed by flexible implementations using nanomaterials and stretch-able substrates. Applications for these advanced sensors in addition to electronic/artificial skin [1] include – robotics [8], [9], wearable

devices [10], [11] and smart textile [12]. Certain applications require the sensor to be transparent in addition to being flexible [13]–[17] such as the touch interactive component on top of the display of handheld electronics or wearable electronics. Other applications such as artificial skin, e-textiles and prosthetics require the sensor to be sensitive to multiple modes of stimuli simultaneously such as pressure, strain and shear [8], [9], [18]. The working principles of these sensors are often similar to their traditional counterparts and are typically piezoresistive [19], [20], piezoelectric [21] and, most commonly, capacitive [2], [22]–[24].

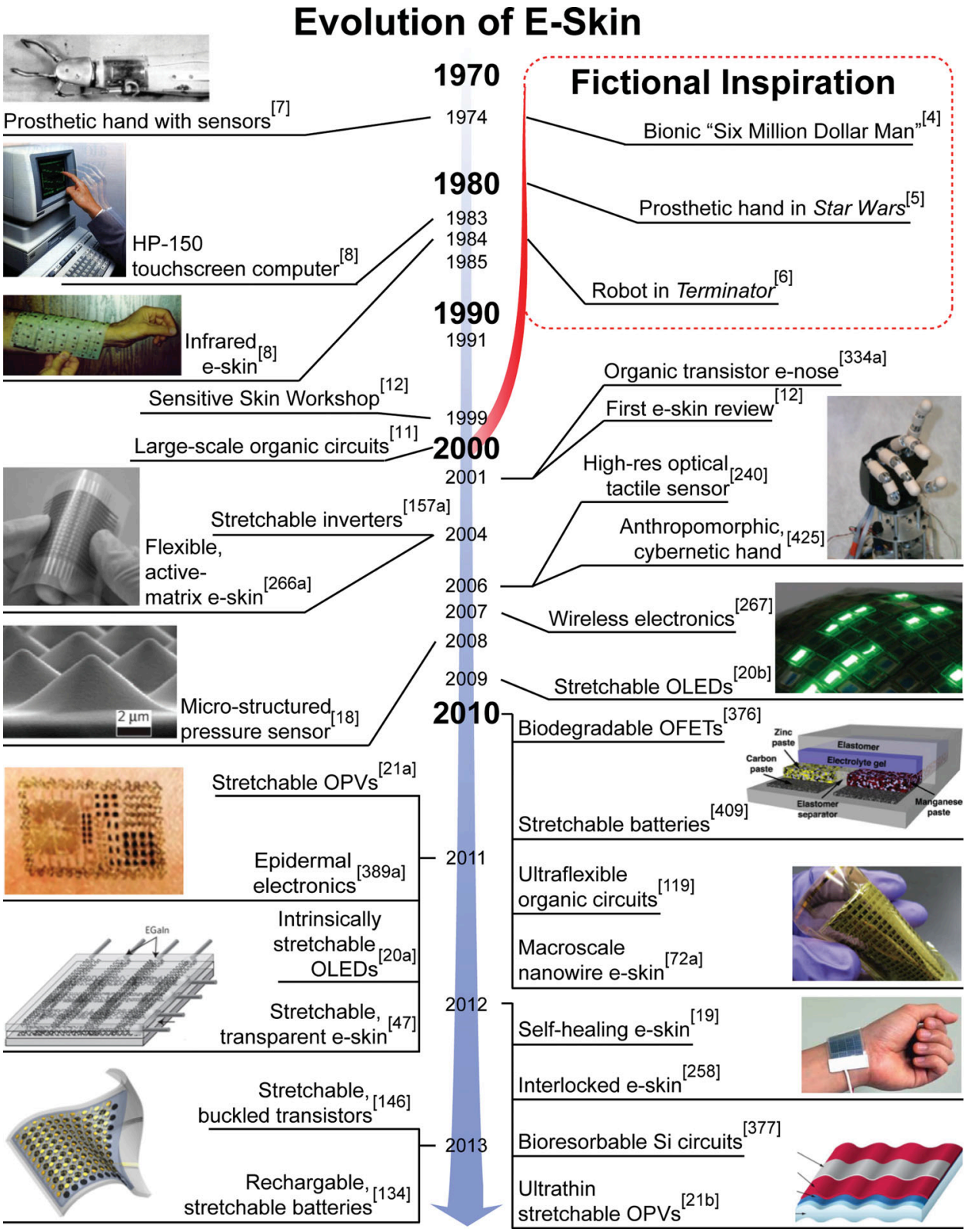

Figure 1.1: Critical milestones in the development of E-Skin technology [7]

The advances in these compliant sensors have been made possible by the development of stretchable conducting materials to be used as electrodes. Examples of such materials include Silver Nanowires (AgNW) [15], [25], CNT [14], conducting polymer [26], hydrogel [17] and liquid metal [27], [28]. These materials offer appealing features to sensors that include high compliance to arbitrary geometries, stretch-ability and even transparency in some cases.

CNTs and AgNW are nanomaterials. They are typically tens to hundreds of nanometers in diameter with large aspect ratios of 1:1000 (diameter : length) and are usually suspended in a liquid and often spray coated or spun on a substrate. Upon transferring to an elastomer, the patterned nanomaterial areas are able to withstand a bend and even a stretch to a limited amount (less than a hundred percent strain maximum) [29]. This is possible due to the entanglement of the nanowire/nanotube structures in the elastomer matrix that can move about to allow such deformations.

In saturated polymers e.g. polyethylene, all valence electrons are used in covalent σ-bonds. Hence the gap between valence band and conduction band is large. In conjugated polymers a π system is formed along the polymer backbone. The Carbon atoms (and sometimes Nitrogen) form three σ-bonds and one π-bond. Pristine conjugated polymers show little conductivity similar to semiconductors. However, like semiconductors, these polymers can be chemically doped, oxidizing the backbone to introduce mobile charge. The charge introduced is neutralized by a counterion from the electrolyte solution. When an electron is added to the conjugated chain, one electronic level is moved from the valence band into the gap region and one level is moved down from the conducting band into the gap region. The new electron sits in the new conduction band. This is called a polaron. Bipolarons are formed by two polarons with the same charge. Polymers such as PEDOT conduct using bipolarons. Compared to metals, their conductivities are orders of magnitude less (~10^5 S/m or less, compared to $6x10^7$ for copper).

Being a polymer, PEDOT is associated with some stretch-ability - however the maximum strain before it cracks is less than 10% [30]. Using additives this can be increased to 176% [30].

Liquid metals can be stretched a significant amount inside a fluidic channel of an elastomer with the maximum strain only limited by the stretch-ability of the encapsulating elastomer [27]. However, the liquid form of this material poses some difficulty in processing and interfacing with the associated electronics such as difficulty in soldering an electronic component on liquid metal.

Apart from liquid metals, hydrogels (strain over 500%) [17], carbon black composites (strain of 500%) [31], are other candidates for a highly stretchable conductor that can be stretched to over a few hundred percent strains with ease, with the added benefit of being in a solid form and therefore comparatively easier to process and interface. Hydrogels are hydrophilic polymers that have recently been shown to be highly stretchable (up to 21 times) [32] and ionically conductive [33]. Keplinger *et al.* [33] and Suo *et al.* [17] are among the pioneers in demonstrating the use of hydrogels as stretchable conductors for actuator and sensor applications respectively. The sensor in [17] can measure large strains of up to 700% and moderate to low pressures of up to 40 kPa.

Inspired by the literature in the field, this thesis explores new sensor architectures and material combinations that can detect proximity, touch, pressure and/or shear while simultaneously being stretchable and with the ability to conform to arbitrary geometries. The research began with the sensing of light contact and deformations (such as a bend and a stretch), followed by sensing pressure and finally - in the last part – shear, in addition to all the stimuli in the preceding segments.

The ability to detect a light touch and proximity during active deformation was pursued since it is an important ability to have for wearable electronics or electronic textile applications.

For example, the sleeve of a wetsuit can be made interactive but the sensor would be strained or twisted or deformed in various other ways with regular movements of the arm. It is therefore important to be able to differentiate the deformations from the desired touch signal. Although there is a myriad of flexible and stretchable touch sensing technologies described in the literature [13], [16], [34], there has been very little work in the detection of proximity and touch during active deformation and differentiating between the different stimuli (this prior work is described in Chapter 2). In the first segment of this thesis a sensor is developed that aims to do just that. Sensing is achieved using a capacitive approach. Mutual capacitance is the conventional technology used in touch screen devices. In this case there are coplanar electrodes that have fringe fields protruding outwards. A finger in proximity or contact acts as a virtual ground and decouples the fields, thereby decreasing the capacitance. This work is presented in Chapter 2.

A logical sequence to the touch sensor was an enhanced version that is able to detect a pressure in addition to a proximity and light touch while being able to differentiate between the different stimuli. To do this we have used a highly stretchable elastomer as the dielectric combined with carbon black composite electrodes, and air bubbles within the dielectric to make it more compliant (and sensitive to pressure). The sensor array is presented in Chapter 3.

Lastly, a further multi-modal sensor that can additionally detect shear was developed, following the earlier work, since shear is a highly sought-after stimulus for numerous applications - especially for artificial skin. Most artificial skin (also known as electronic skin or e-skin) technologies described in the literature are only designed to detect pressure [35], [36], and in fact cannot differentiate between pressure, stretch or bending. Some have the ability to detect shear in addition to pressure [5], [37] but most of these are either composed of individual rigid sensor components, or the flexible sensors contain “bumps” to detect the shear. The bumps do not allow for a smooth skin like experience and no sensor described in the literature has

demonstrated the ability to detect the entire range of stimuli – proximity, touch, pressure and shear. In addition to detecting this entire range of stimuli, the sensor in the third segment of this thesis is a close mechanical analog to human skin. The key to this achievement is a novel dielectric architecture that enables localized buckling similar to human skin. The buckling allows a translational movement of the top surface of the sensor parallel to the base without disrupting the neighboring region. The dielectric architecture also provides a non-linear mechanical characteristic similar to human skin [38]. Electrodes on the top and bottom surface forms a set of capacitors that respond to such a stimulus by changing their capacitance in a signature way that can be used to interpret the direction and magnitude of the horizontal movement or shear. This sensor is the first of its kind to be able to detect a local shear by buckling and stretching at the location of the shear, similar to human skin. The sensor also demonstrates mechanical properties similar to human skin in its non-linearity. This is a critical improvement from the existing shear sensors being applied for artificial skin applications. The shear sensor described in this thesis is soft, smooth and uses readily available materials and fabrication processes, details of which are discussed in Chapter 4. The thesis describes a design and implementation of this and other sensors that can differentiate between multiple modes of interaction. However, further work will be required in software to cleanly distinguish between these signals in a wide variety of interactions (beyond simple finger approach, contact and shear).

1.2 Sensing modes

The most commonly required sensing modes are 1) proximity – approaching close to the sensor but not making any physical contact 2) light touch – the moment of making physical contact with the sensor applying close to zero pressure, 3) pressure, 4) strain – stretching the

sensor along the length or width and 5) shear. Several sensing mechanisms can be used for these stimuli and sometimes the same one can be used for sensing multiple stimuli such as piezoresistive and capacitive. One way to categorize these stimuli and mechanisms is illustrated in Figure 1.2.

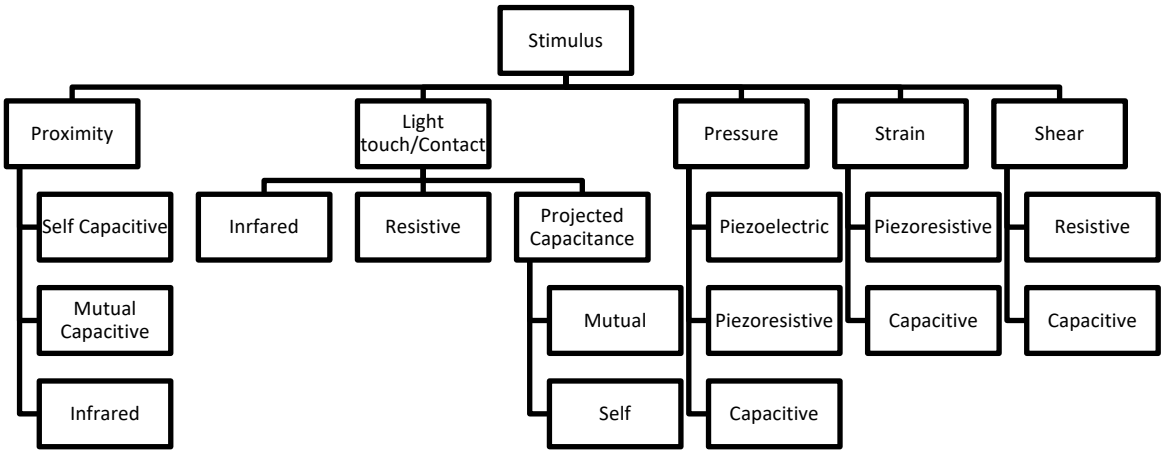

Figure 1.2: Stimuli and corresponding detection mechanisms categorized

1.2.1 Proximity

Proximity of a finger is a stimulus investigated in the last decade or two with the human computer interface industry trying to push the boundaries of the space [39], [40]. In order to add more interactive ability in the limited real estate of a touch screen the solution was to move in the perpendicular axis. The proximity or hover of a finger on a touch screen would enable added interactive features. One commercially available product that incorporated this feature is the Samsung Galaxy S4. The most common method of sensing used is self-capacitance.

1.2.1.1 Self-Capacitance

This is a form of projected capacitance method and it measures the capacitance of a single electrode with respect to ground. The capacitance of the sense electrode, C_s, is with respect to the ground through the air and therefore very small. When a finger is near the sense electrode, it (the finger) acts as a second electrode connected to a virtual ground (human body), increasing the capacitance of the sense electrode [24], [41] as shown in Figure 1.2.

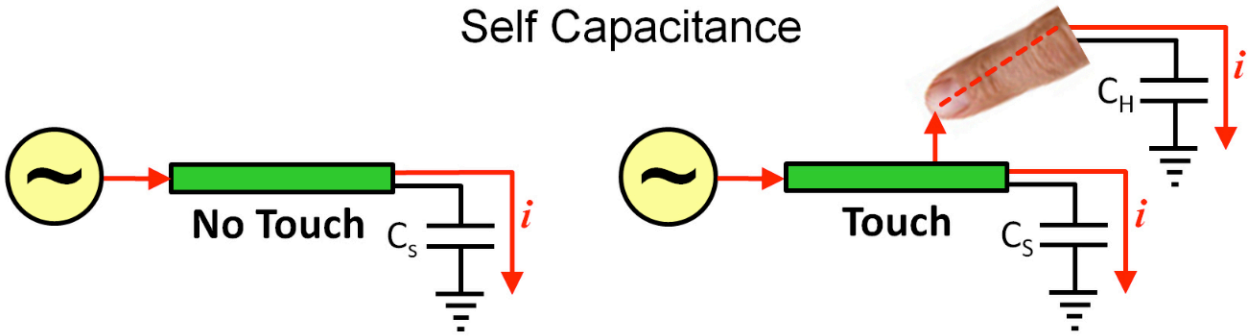

Figure 1.3: Self capacitance working principle [24]

In a self-capacitance touch screen, transparent conductors are patterned into spatially separated electrodes in either a single layer or two layers. Each electrode represents a different proximity coordinate and is connected individually to a controller.

1.2.2 Light touch/Contact

A light touch is often referred to as a touch or a contact. It refers to the act of coming in contact with a surface (or a sensor) without applying any (or minimal) pressure. This stimulus is not detectable with a pressure sensor (unless it is extremely sensitive). The most common use of this is in touch screen sensors used in hand held electronics and other devices. In addition to detecting the presence of a finger (or object such as a stylus), these applications require the

ability to detect a “swipe” which is a rapid movement of the finger on the sensor surface. Among the most common sensing methods used to detect a touch are 1) Infrared, 2) Resistive, 3) Self capacitance and 4) Mutual capacitance.

1.2.2.1 Infrared

This is among the earlier touch sensing methods where there is an array of IR LEDs along the X and Y axis edges of the screen and an array of photoreceptors along the opposing edges of the LEDs as shown in Figure 1.4 (a) [42]. When a finger touches the screen it disrupts the beam and triggers the corresponding photoreceptors in the X and Y edges, which provides information on the location of the finger. Although an elegant approach, this method has a number of shortcomings. Multi-touch is an issue due to the ghosting effect shown in Figure 1.4 (b). If the green spots are the actual position of the fingers the sensor can’t tell if the finger is actually on the green spots or the red spots since it only sees the combination of the co-ordinates where the light beams are broken at X2, X4, Y1 and Y2.

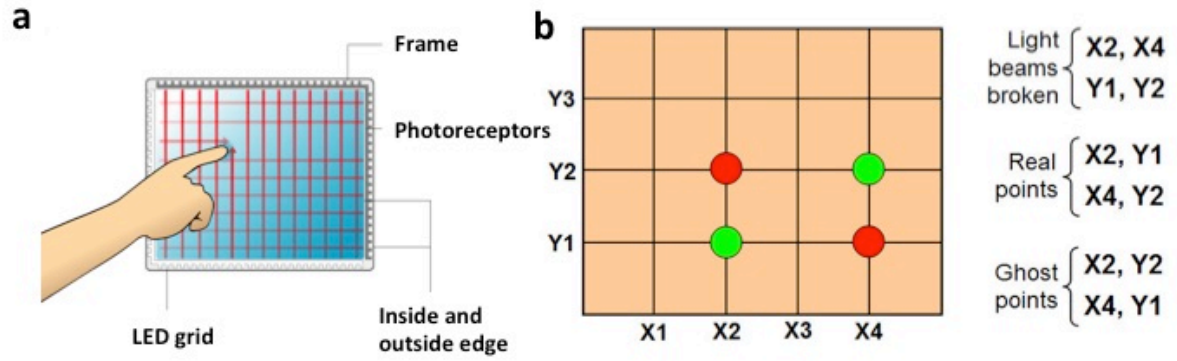

Figure 1.4: a) IR touch sensor b) Ghosting effect in IR touch sensor [42]

In addition to the ghosting effect ambient light can cause interference and a hover or other forms of surface obstruction can cause a false positive.

1.2.2.2 Resistive

Analog resistive is among the first commercially used touch sensing methods on touch screen devices. The operating principle is a simple voltage divider. The sensor consists of two transparent electrode layers as shown in Figure 1.5 (a). The layers are separated by dielectric spacer dots. When a finger is used to touch and press on the top layer, it deforms downwards and makes contact with the bottom layer as shown in Figure 1.5 (b). There are four readout electrodes in total A-B shown in Figure 1.5 (c). When the x-axis location is to be measured a voltage is applied to A, and C is grounded. Upon touching a point on the screen the point comes in contact with the bottom layer and electrode D is used to read the voltage drop at the location of the finger. The finger location is a function of the ratio of the resistances before and after the point of contact along the length of the x-axis. If the finger is at the extreme left of the screen there will be a minimal voltage drop across the length from the edge of the screen to the location of the finger. This corresponds to a small voltage readout. If the finger is in the middle of the x-axis the voltage drop will be half and similarly if it is at the extreme right the voltage drop will be the maximum. When detecting the y-axis location the roles of the electrodes A,C and B,D are reversed.

Although these are simple, low cost and durable, resistive screens have poor optical properties, low sensitivity to a light touch and do not allow multi-touch.

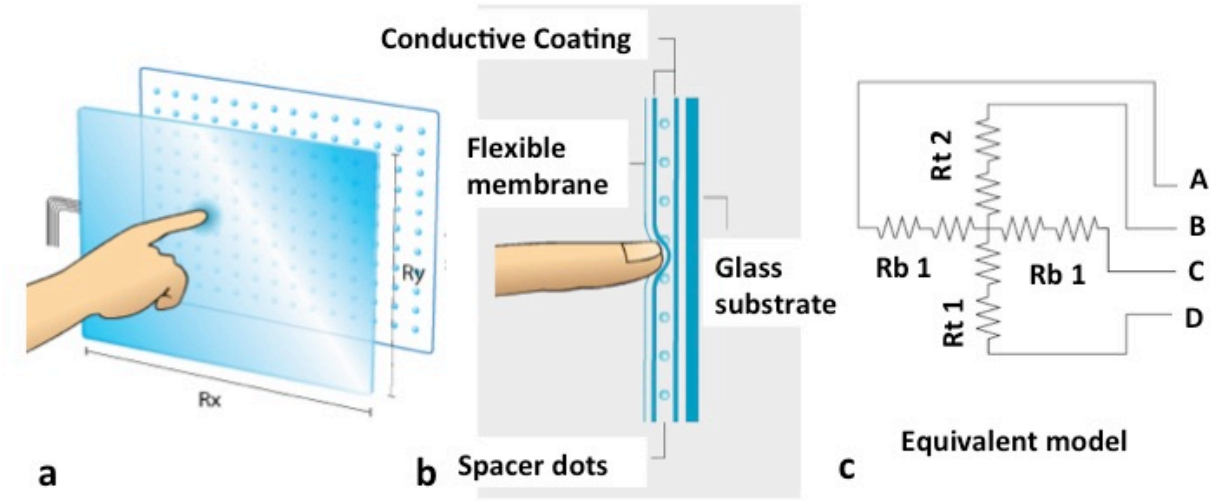

Figure 1.5: Resistive touch sensing a) two electrode layers b) cross-section showing spacers c) equivalent model [42]

1.2.2.3 Self-capacitance

The concept of self-capacitance is introduced earlier in section 1.2.1.1. In addition to detecting a hovering finger, it can also be used to detect the contact or touch of a finger. Two separate electrode designs – 1) single/individual pad and 2) 2D array are illustrated in Figure 1.6 [42]. The single pad design is more often used for a hover or for a combination of hover and touch. The 2D array is predominantly used for touch. In case of the single pad, each pad is individually scanned. This is much slower compared to the 2D array where entire rows and columns are scanned in sequence. The individual pad implementation is also difficult to scale owing to the complexity of routing the interconnects to the readout circuit. The 2D array, although simpler to implement, suffers from the ghost point issue in case of multi-touches, as with the IR touch sensor.

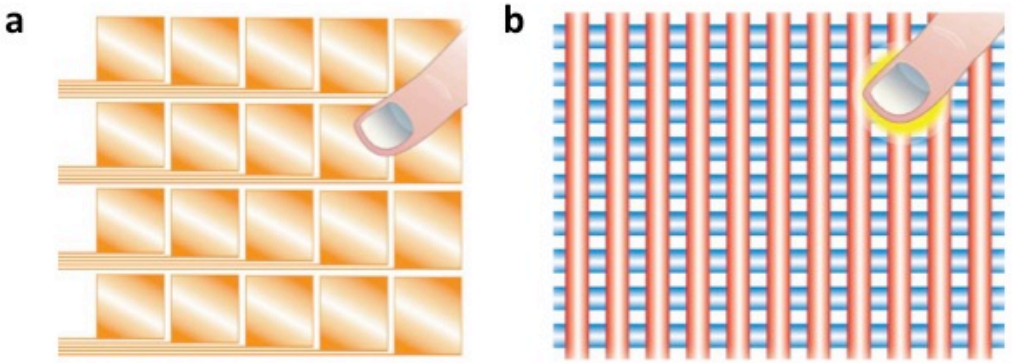

Figure 1.6: Self capacitance electrode designs : a) Individual pad b) 2D array [42]

1.2.2.4 Mutual-capacitance

The gold standard currently in use by the industry is mutual capacitance [43]. The sensor is a capacitor formed by the electric field coupling between two co-planar electrodes (drive electrode and sense electrode) with the electric fields projecting out of the plane as shown in Figure 1.7 (a). When a finger comes in contact with the surface of the dielectric on top of the electrodes (in this case glass) the electric fields couple with the finger (which now acts as a third electrode) and in the process decouples the field with the sense electrode. This decreases the capacitance between the drive electrode and sense electrode and hence provides information regarding the presence of a finger. There are several electrode designs for mutual capacitance that can be two layered and single layered.

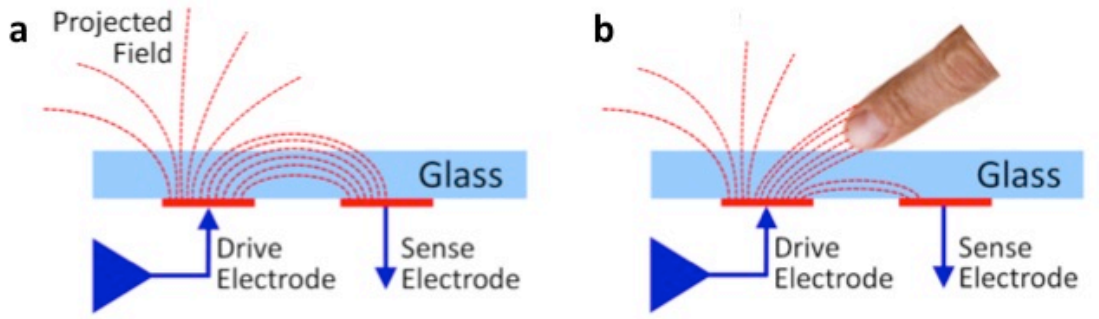

Figure 1.7: Mutual capacitance a) no finger b) with finger [42]

Common two-layered electrode designs for mutual capacitance are bar and stripe (also called Manhattan) and interlocking diamond shown in Figure 1.8. In case of the bar and stripe there are two types of electric field coupling – 1) overlap fields that go through the dielectric between the top and bottom electrodes E_{ov} and 2) fringe fields that project out of the plane and around the edges of the drive electrode into the sense electrode E_f. It is E_f that is responsible for the mutual capacitive sensing. The greater the ratio of $E_f : E_{ov}$ the greater the sensitivity of the sensor. This is enhanced in the interlocking diamond design shown in Figure 1.8 (b). In this case almost the entire mutual coupling is fringe capacitance (denoted by C_M in the figure) with little overlap coupling.

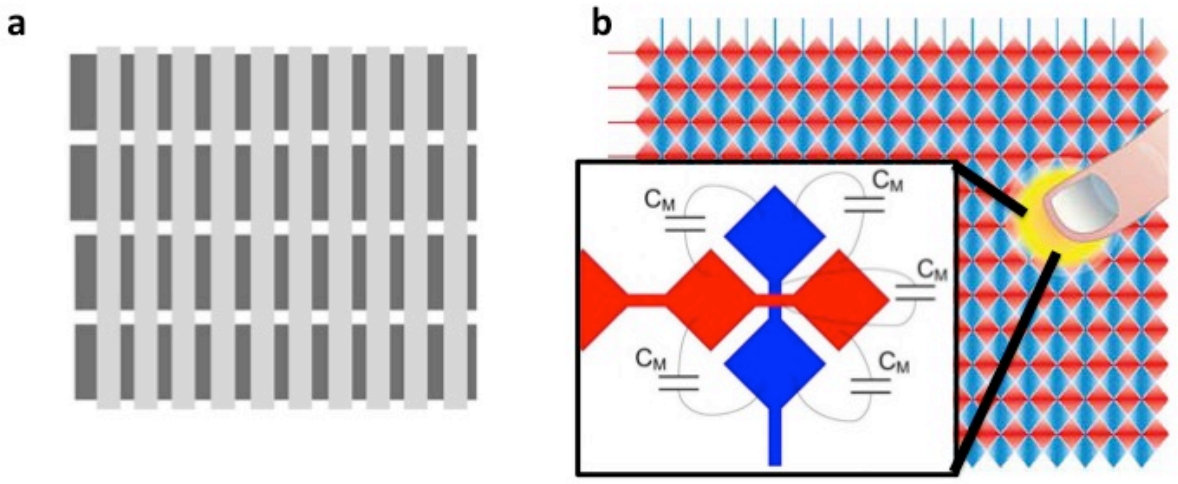

Figure 1.8: a) Bar and stripe design b) Interlocking diamond pattern [42]

Single layered designs are more common in recent times. A few examples are illustrated in Figure 1.9. In the case of single layered architectures, the entire capacitance is due to E_f and there is zero overlap capacitance. This renders it more sensitive at detecting a touch than the two-layered options, at the cost of information regarding deformations (since deformations are better sensed by overlapping electrodes where the deformation of the dielectric between the electrodes bring about changes in the sensor capacitance).

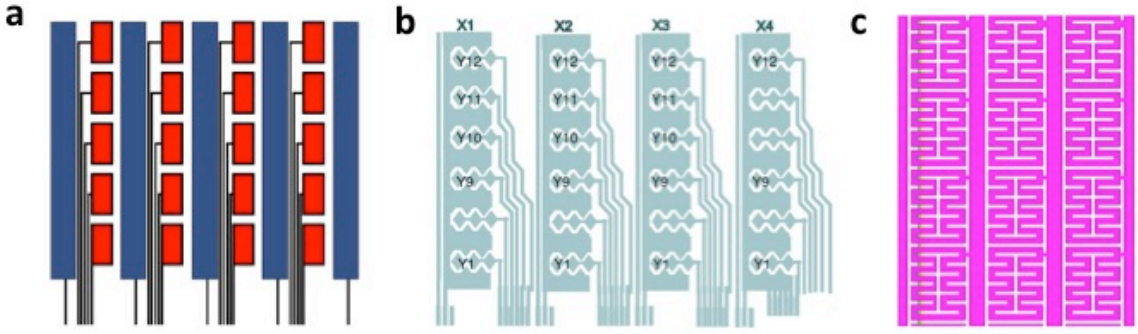

Figure 1.9: Single layer mutual capacitance electrode design a) Synaptic's caterpillar design b) ELAN's caterpillar design c) Alternative design by ELAN

Mutual capacitance offers flexibility in pattern design, high signal to noise ratio, high resolution, enables non-ambiguous multi-touch (no ghosting) and simple interconnects to readout circuit (in comparison to self-capacitance). This is the approach used in the work presented here.

1.2.3 Pressure

Pressure sensors date back to early 20th century with the first patents on a strain gauge based diaphragm pressure sensor being filed around the middle of the century [44]. The main pressure sensing mechanisms include piezoelectric, piezoresistive and capacitive. Although there are a large number of existing applications of pressure sensing, this thesis will be more focused on ones associated with flexible and stretchable platforms.

1.2.3.1 Piezoelectric

The word “piezoelectricity” has its roots in Greek that means electricity by pressure. Certain crystalline materials have molecular structures that at a rest state have the center of gravity of the positive and negative charges coincide but upon application of a stress the charges separate out generating an electric dipole. The concept is illustrated in a simplified diagram in Figure 1.10. When used as a pressure sensor the application of a pressure will lead to the generation of dipoles that in turn generate a potential difference. This potential difference can be read out using appropriate electronics and the voltage or charge can be calibrated to corresponding pressure magnitudes. Although traditionally piezoelectricity has been observed in solid crystals such as quartz, for flexible applications piezoelectricity has been investigated in polyvinylidenefluoride (PVDF) films [45], [46].

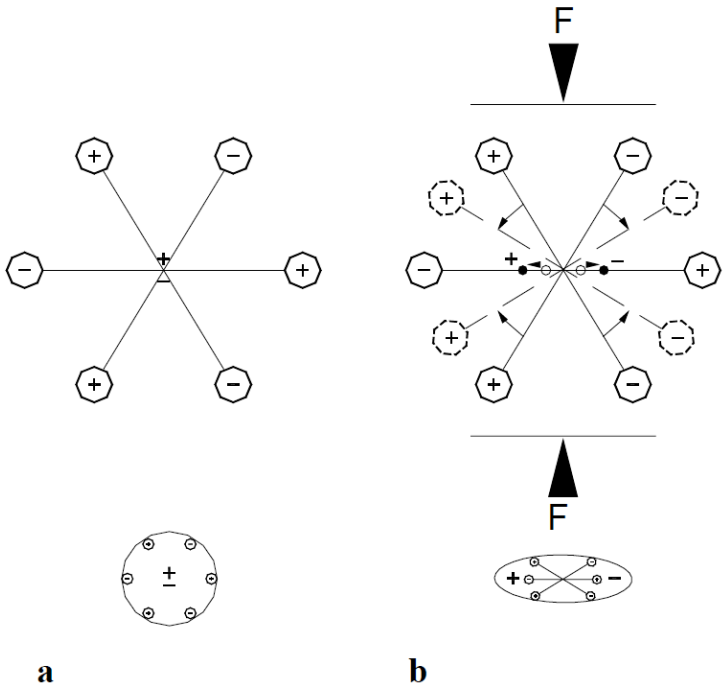

Figure 1.10: Working principle of piezoelectricity

1.2.3.2 Piezoresistive

The piezoresistive effect is the change in electrical resistance of a material due to the application of a stress. In metals it is generally due to geometric changes in dimensions. Resistance is given by the formula $R = \rho \frac{l}{A}$, where R is the resistance, ρ is the resistivity of the material, l is the length and A is the cross-sectional area. A change in l and A will bring about a corresponding change in R. The piezoresistive gauge factor is given by $G = \frac{\frac{\Delta R}{R}}{\frac{\Delta l}{l}}$, where G is the gauge factor. In semiconductors an applied stress impacts the bandgap, which in turn influences

the conductivity. In certain semiconducting materials the effect can be several orders magnitude larger than the geometrical effect in metals.

When implemented as a pressure sensor the basic principle is a piezoresistive strain gauge connected to a diaphragm [47]. When the diaphragm deflects due to the application of a pressure the piezoresistive strain gauges experience a strain and hence a change in resistance, which can later be calibrated to provide the magnitude of the applied pressure.

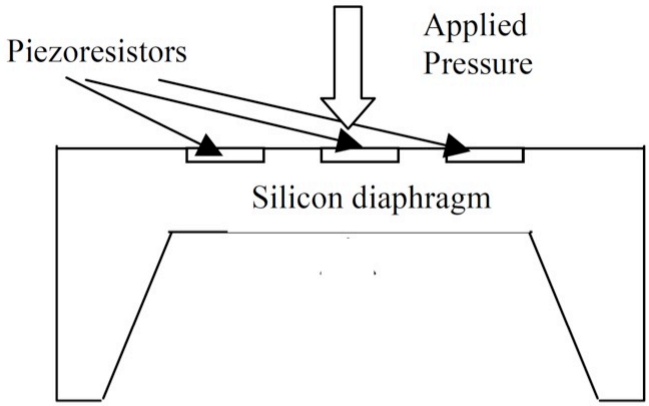

Figure 1.11: Piezoresistive pressure sensor [47]

1.2.3.3 Capacitive

A capacitive pressure sensor operates on the basis of the parallel plate capacitor and increasing area in some cases, equation $C = \varepsilon \frac{A}{d}$. When the two electrodes of a capacitor are pressed and brought closer together reducing the thickness of the dielectric, the capacitance increases in an inverse proportion. This property is used to demonstrate the ability of hydrogels to act as electrodes for use in a pressure sensor in [17] shown in Figure 1.12.

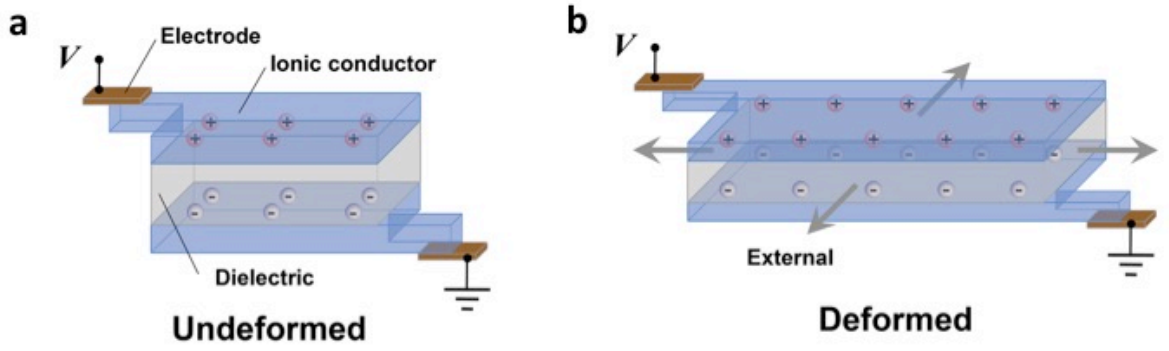

Figure 1.12: Hydrogel electrode based capacitive pressure sensor (a) undeformed (b) deformed [17]

1.2.4 Strain

Strain is the percentage change in length of an object upon application of a stress $\varepsilon = \frac{\Delta L}{L}$, where ε is the strain and L is the length. The Young's Modulus, Y, is a material property that connects stress and strain. $Y = \frac{Stress}{Strain} = \frac{Force/Area}{\Delta L/L}$. Strain can be measured using strain gauges that change an electrical property upon application of a stress. These electrical properties include resistance and capacitance.

1.2.4.1 Piezoresistive

Piezoresistive strain gauges have been introduced in an earlier section. In addition to metal and semiconductor strain gauges, there are soft polymers and nanomaterials-based strain gauges that change their resistance due to a geometrical change in dimensions. Nanomaterials include CNT, AgNW etc. One such CNT based strain gauge is demonstrated in [48] shown in Figure 1.13 where the strain gauge is stretched up to 500%. In addition to direct contact of the CNTs, the authors claim that the conductivity is also due to the tunneling effect of electrons

through the dielectric material. This effect decreases with a strain when the CNT structures are pulled further apart. This contributes to the piezoresistive effect and also the large strains attained.

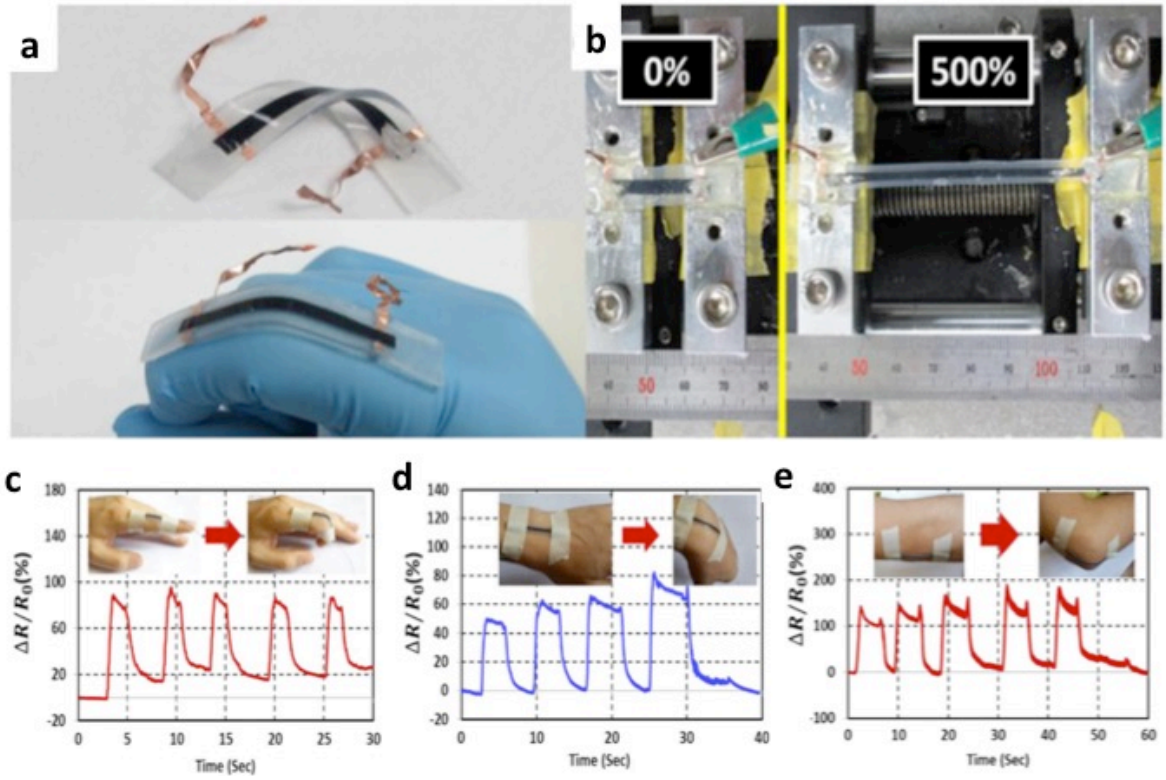

Figure 1.13: CNT based strain sensor a) bent and twisted b) stretched to 500% c) applied on a finger d) on the wrist and e) on the elbow joint [48]

Such highly stretchable strain gauges have important wearable applications in mapping human motions for rehabilitation, gaming etc. [48] where the sensor needs to be soft and demonstrate high stretch-ability with a large dynamic range for strain sensing.

1.2.4.2 Capacitive

A capacitive strain sensor works in the same way as a capacitive pressure sensor being governed by the equation $C = \varepsilon \frac{A}{d}$. A CNT based strain sensor is demonstrated in [49] shown in Figure 1.14 below. Figure 1.14 (a) illustrates the working principle of the sensor. When a strain is applied the length increases by *ΔL*, the width decreases by *ΔW* and the dielectric thickness decreases by *Δg*.

Now, $C = \varepsilon \frac{l \times w}{d}$. When a strain is applied $l' = l(1 + e)$, where *l'* is the new length and *e* is the strain applied. Similarly, $w' = w(1 - \rho e)$, where *w'* is the new width and ρ is the Poisson's ratio, and $d' = d(1 - \rho e)$, where *d'* is the new dielectric thickness. According to this the new capacitance is

$$C' = \varepsilon \frac{l(1+e) \times w(1-\rho e)}{d(1-\rho e)} \quad (1\text{-}1),$$

which reduces to

$$C' = C(1 + e) \quad (1\text{-}2).$$

Thus, application of a strain *e* increases the capacitance proportionately with a capacitive gauge factor $G_c = \frac{\frac{\Delta C}{C}}{\frac{\Delta l}{l}}$ of 1. Figure 1.14 (b) shows a schematic of the sensor. It shows two layers of CNT electrodes with a dielectric in the middle and the whole device encapsulated in an elastomer (using the same material for the dielectric). Figure 1.14 (c) shows an SEM image of the CNT layer.

One important point to note is that the same sensor when used as a pressure sensor can give rise to an increase in capacitance and when used as a strain gauge can also give an increase in capacitance. Therefore, without any knowledge of the type of stimuli, the data is not sufficient

to tell the user what type of stimulus it was. This ambiguity restricts the use of most of such deformation-based sensors for detecting multiple stimuli.

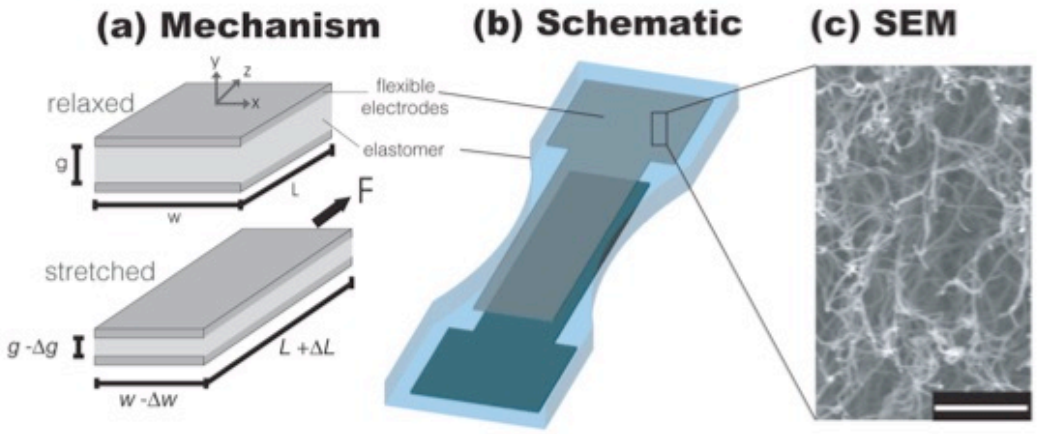

Figure 1.14: a) Working principle of CNT based capacitive strain gauge b) schematic of strain sensor c) SEM image of CNT layer [49]

1.2.5 Shear

The basics of shear stress are illustrated in Figure 1.15. When an object is strained along a plane with surface area A as shown in Figure 1.15 (a) with the bottom of the object anchored, it is strained as shown in Figure 1.15 (b). The shear strain is defined as $\Delta x/l$, where Δx is the displacement along the axis of the shear and l is the height of the object as shown in Figure 1.15. The shear stress is F/A, where F is the shear force applied and A is the surface area of the plane being sheared. The shear modulus is defined as shear strain/shear stress and it is a material property.

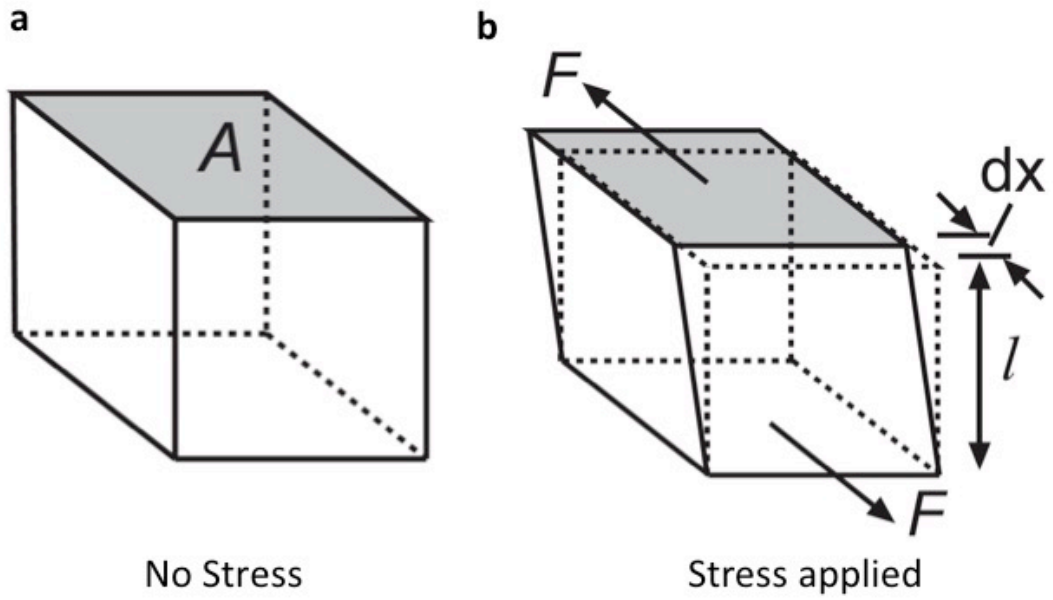

Figure 1.15: a) un-deformed state b) deformed state upon application of a shear force

The main sensing methods to detect a shear are resistive and capacitive. Using these basic methods there are several architectures and implementations in literature. However most of these implementations require a protruding segment on the sensing area that can translate the shear force into a form easily detectable by the sensors. Although there are designs where these protrusions are in the micro scale, for artificial skin type applications it is important for the sensor to be smooth (human skin like) and still be able to detect a local shear.

1.2.5.1 Resistive

There are multiple implementations of a resistive shear sensor but the two most common ones are shown in Figure 1.16 below [50], [51]. Figure 1.16 (a) and (b) [34] shows an implementation where there are four adjacent electrodes with a common electrode in the middle and a micro-structured CNT based conductive composite. Upon application of a directional shear

the resistance between the core electrode and the electrodes along the axis of the shear change. The electrode being pressed on will show a decrease in resistance since the microstructures are now pressing on each other and the magnitude of contact is increased. Conversely the electrode where the shear causes the microstructures to move away will show an increase in resistance.

Figure 1.16 (c) and (d) [35] shows the cantilever implementation of a piezoresistive based shear sensor. In this case the edges of the bends of the cantilever has piezoresistive segments that will change resistance due to the strain applied upon bending the cantilever in the event of a shear as shown in Figure 1.16 (d).

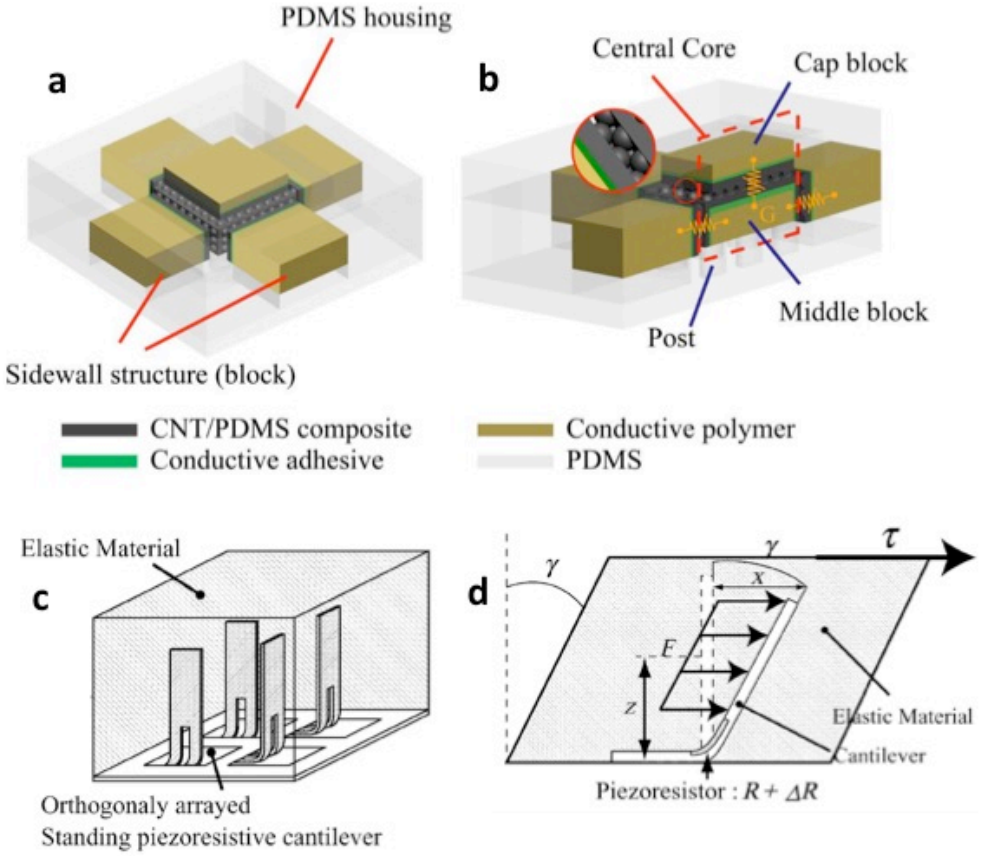

Figure 1.16: shear sensor based on resistive micro-structured conductive composite a) schematic b) cross-section c) cantilever type piezoresistive shear sensor d) cantilever bending upon application of a shear [50], [51].

1.2.5.2 Capacitive

Capacitive sensing is a more common method to detect shear. Once again being governed by the equation $C = \varepsilon \frac{A}{d}$, the shear is sensed when the electrode overlap area of the sense capacitor either increases or decreases. The earliest work on this was done more than two decades back and a notable one among them is by Chase *et al.* [6]. The authors demonstrated the basic sensor architecture shown in Figure 1.17. There is one top electrode E_1 and four bottom electrodes E_{21}, E_{22}, E_{23}, and E_{24}. The top electrode with each bottom electrode forms a capacitor, hence four in total. With the application of a shear the top electrode will move relative to the bottom electrodes and bring about changes in the overlap area with the four capacitances. For example when the shear is in the positive x direction in Figure 1.17, the overlap area with E_{21} and E_{24} will increase and that with E_{22} and E_{23} will decrease. This will give rise to corresponding changes in capacitance formed by the respective bottom electrodes with the top electrode.

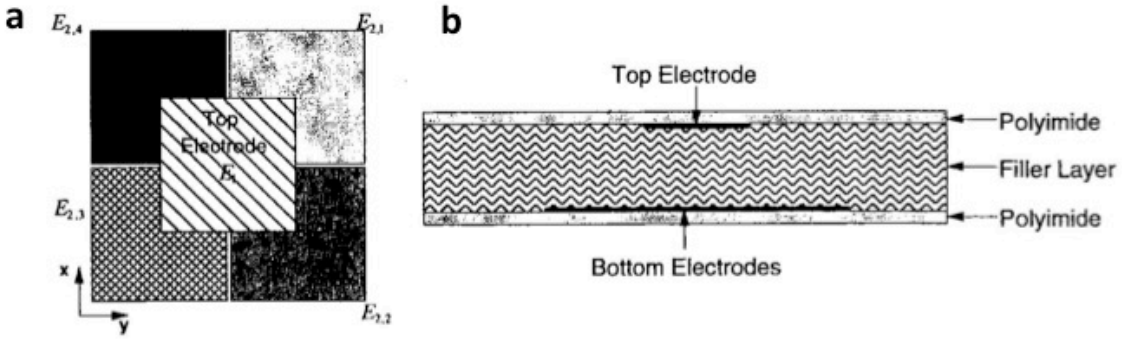

Figure 1.17: Capacitive shear sensor a) top view b) cross-section [6]

In recent times there has been further development of such shear sensors with the basic working principle remaining the same. In [5] Lee *et al.* demonstrate a sensor with four top electrodes and four bottom electrodes connected as shown in Figure 1.18. A cross-section is shown in Figure 1.18. There is a "bump" on top of the sensor, which translates a horizontal force into a perpendicular component as shown in Figure 1.18 (a). When a shear force is applied, one side is pressed down (increasing capacitance) and the other side is pulled up (decreasing capacitance) as shown in Figure 1.18 (d). This sensor is also capable of sensing a normal force as shown in Figure 1.18 (c). In this case all the electrodes are pressed down hence increasing the capacitance.

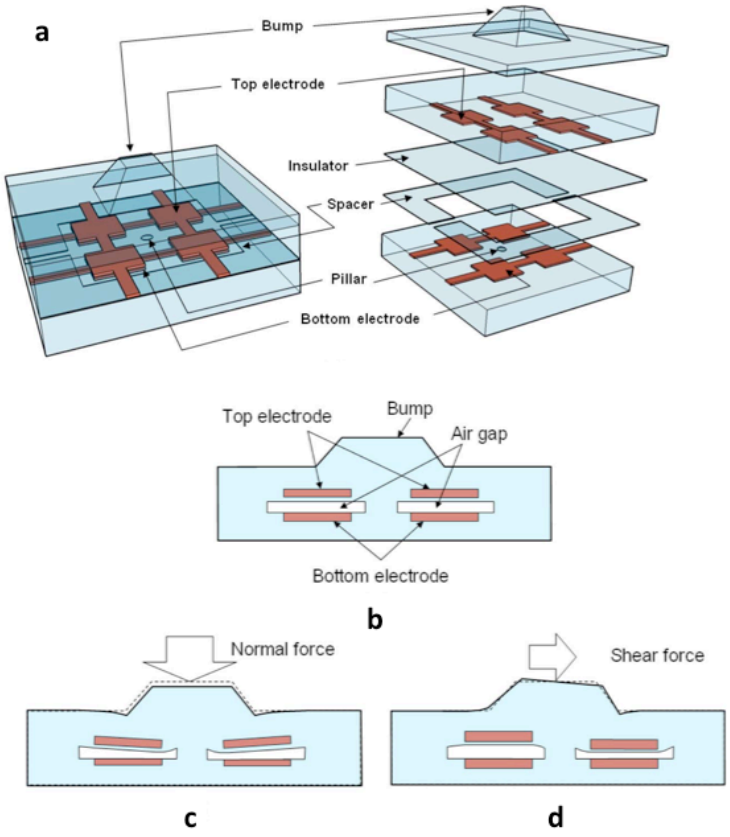

Figure 1.18: a) schematic of shear sensor b) cross-section c) application of a normal force d) application of a shear force [5]

A clever alternative approach to this architecture is proposed by Cheng *et al.* in [37] where the sense electrodes are all on the same layer with floating electrodes on top shown in Figure 1.19. The combination of the bottom electrodes (connected to the readout circuit) and the floating electrode forms one complete capacitive sensing cell. The floating electrode does not have a physical connection to the readout circuit and is only coupled by the electrical fields emerging from the sense electrodes below them. This is demonstrated in Figure 1.19. When a normal force is applied all the top floating electrodes come closer to the bottom sense electrodes and the total capacitance of all the capacitance cells are increased. As in [5] there is a "bump" here that translates the horizontal shear force into a perpendicular component that presses on one side and lifts up the other side as shown in Figure 1.19. This causes the capacitance of the cell on the side being pressed to increase and the other side to decrease.

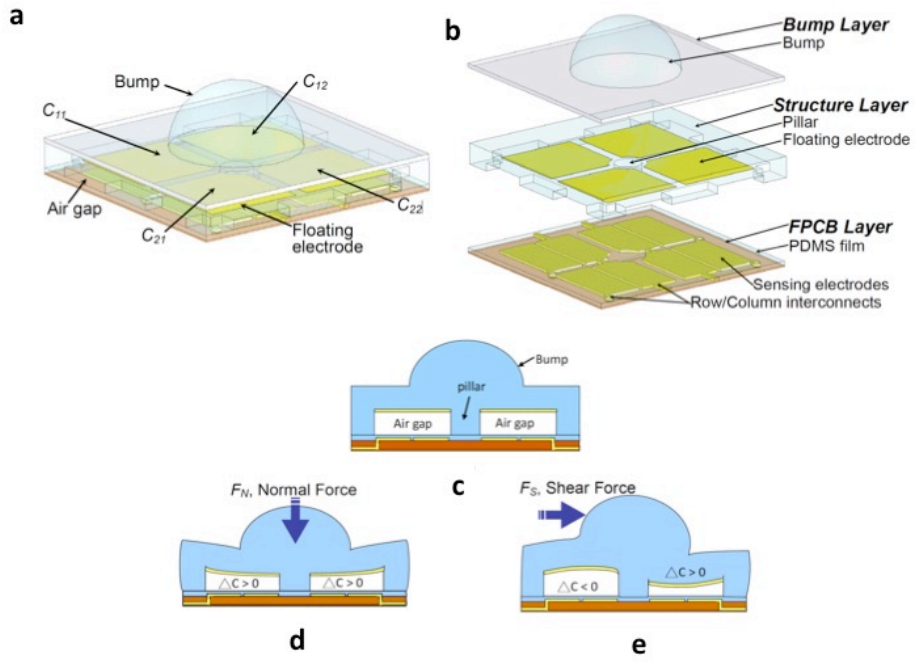

Figure 1.19: a) Capacitive shear sensor 3D model b) blown up diagram c) un-deformed state d) normal force e) shear force

An interdigitated finger approach is demonstrated by Surapaneni et al. in [52] that works using the same principle as the others before. As shown in Figure 1.20 (a) when the top set of electrodes are sheared downwards the top capacitor CAB decreases while the bottom capacitor CAC increases. The interdigitated design allows for a large change in capacitance. A 2D implementation is shown in Figure 1.20 (b).

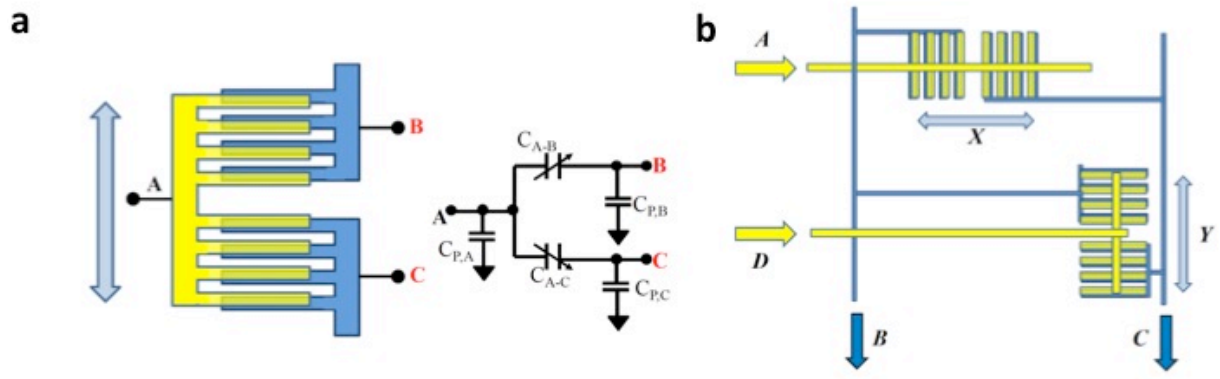

Figure 1.20: a) Interdigitated capacitive sensor and equivalent circuit b) 2D sensor implementation [52]

These are a few commonly used approaches for measuring shear and some of them can be implemented in a flexible platform that could potentially be used for artificial skin applications. However most of these sensors require a "bump" to detect local shear and this is not a desired surface morphology when mimicking human skin.

1.3 Stretchable conductors

The sensors described in section 1.2 can be implemented in flexible and even stretchable forms. This is made possible with the use of stretchable conductors used as the electrodes or as the active materials in the sensors. Among the major ones are Carbon nanotubes (CNT), Silver

nanowires (AgNW), Carbon black composites, conducting polymers (e.g. PEDOT), liquid metal, hydrogel etc.

1.3.1 Carbon Nanotubes

Carbon Nanotubes (CNTs) are structurally similar to a single graphite sheet wrapped in a cylindrical tube [53]. There are single-walled CNTs (SWNT) and multi-walled CNTs (MWNT), which comprises of a concentric array of SWNTs [54].

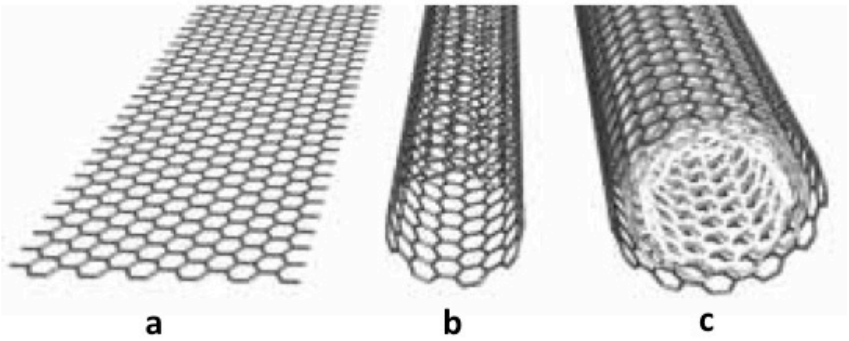

Figure 1.21 a) Graphene sheet b) single walled carbon nanotube c) multi-walled carbon nanotube. [53]

Lipomi *et al.* has demonstrated a stretchable and transparent pressure sensor using CNT based electrodes [14] shown in Figure 1.22. The sensor is an array of CNT strips perpendicular to each other separated by a PDMS dielectric. It is stretchable up to 150% and has a transmittance of 79% and can detect pressures as low as 50~100 kPa. The working principle is shown in Figure 1.22 (c). When pressed the dielectric thickness decreases increasing the capacitance. Similarly, when stretched, the strain causes an increase in area and a decrease in dielectric thickness which also increases the capacitance.

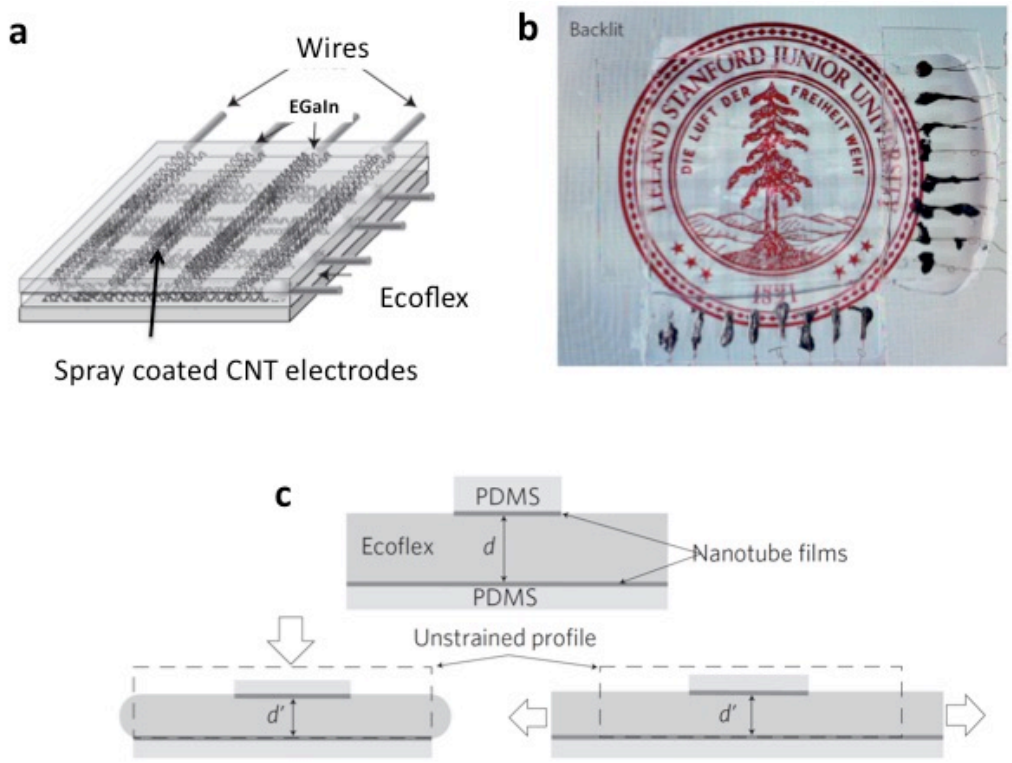

Figure 1.22: a) 3D model of CNT based capacitive pressure sensor b) Image of sensor c) Working principle of sensor [14]

1.3.2 Silver Nanowires

Silver nanowires are cylindrical structures that are tens of nm in diameter and a few microns in length shown in Figure 1.23. They have high conductivity (as low as 8 Ω/□) and transmittance of over 80%.

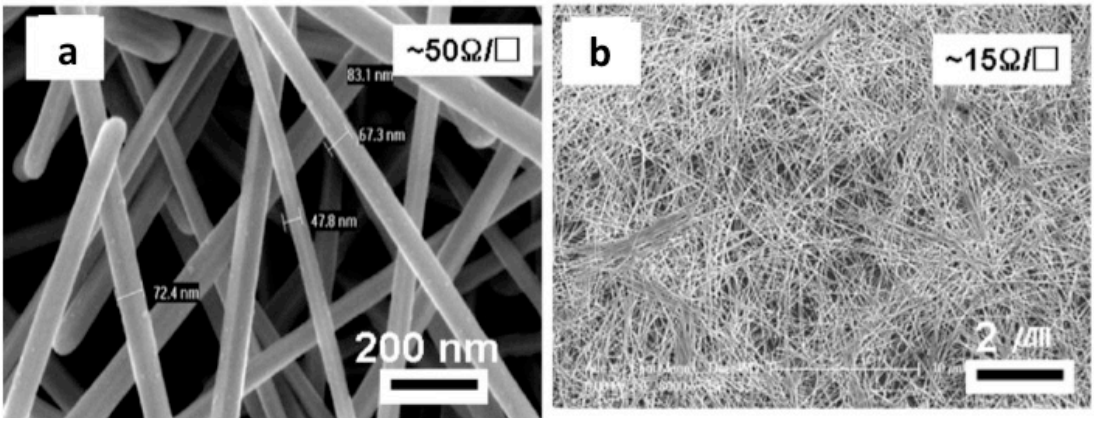

Figure 1.23: Silver nanowires a) scale 200 nm b) scale 2 μm

There are numerous implementations of sensors using AgNW. Among the pioneering attempts is the work by Hu *et al.* [13] shown in Figure 1.24. The implementation of the pressure sensor is similar to the CNT based sensor in [14] with perpendicularly running strips of electrodes separated by a dielectric as shown in Figure 1.24. The sensor is highly transparent and flexible (Figure 1.24). The smallest pressure detectable is around 20 kPa and the highest strain demonstrated is 60%. However similar to [14] both pressure and strain lead to an increase in capacitance and therefore render it difficult to identify the type of stimulus without prior knowledge.

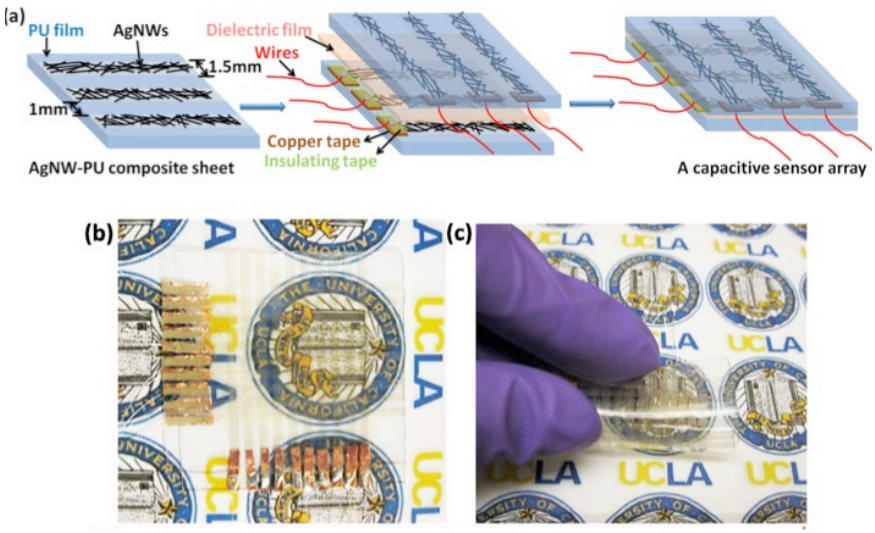

Figure 1.24: a) fabrication steps of pressure sensor b) image of pressure sensor c) bending the sensor

1.3.3 Conducting polymers

These are a unique class of polymers that intrinsically conducting without any conducting fillers (e.g. CNT or carbon black composites) [55]. The conductivity arises from a π conjugation and is achieved through simple chemical or electrochemical oxidation/reduction by a number of anionic or cationic species called "dopants", i.e. the polymeric backbone of these materials need to be oxidized/reduced to introduce charge centers before conductivity is observed. Analogous to solid state semiconductors, in case of "doped" conducting polymers (CP) the π bands become the valence band and the π* bands become the conduction bands. The band gap is generally greater than 1eV in most CPs. These are different from "ion-conducting" polymers, which will be discussed in a later section. Examples of conducing polymers are poly-pyrrole, poly-aniline, poly-3,4-ethylenedioxythiophene (PEDOT) with PEDOT being most popular in recent times due to its high transmittance. PEDOT is positively doped and typically with poly-styrenesulfonic acid (PSS) whose sulfonate anionic groups act as the counterions to balance the doping charges.

Typically their stretch-ability is less than 10%, however the state of the art in this field is almost 200% with the addition of ionic liquid additives as shown in [56] where the authors demonstrate its application in stretchable interconnects. Figure 1.25 (a) and (b) shows patterns of PEDOT:PSS with additional conductivity enhancers being stretched and Figure 1.25 (c) and (d) shows PEDOT based interconnects being twisted while lighting up an LED.

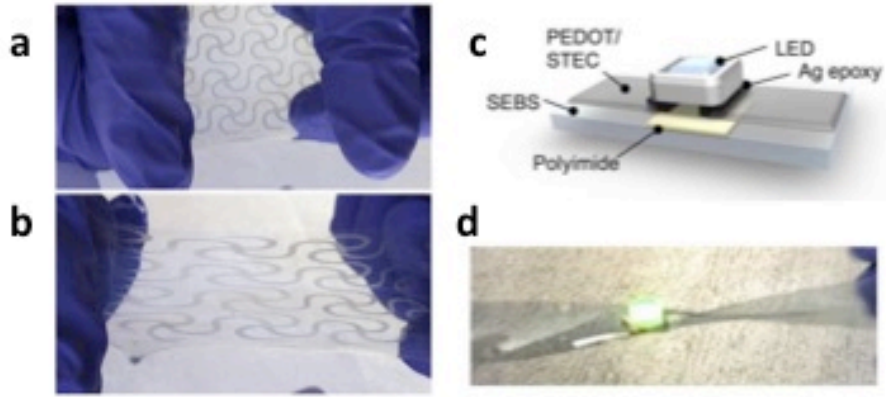

Figure 1.25: PEDOT:PSS with STEC enhancers a) patterned b) stretched c) schematic of LED with PEDOT based interconnect d) PEDOT based interconnect being twisted

Various types of flexible and stretchable sensors have been demonstrated with PEDOT:PSS as the conductive material for the electrode.. One such flexible, transparent touch sensor is shown in Figure 1.26 [57]. The sensor is fabricated on a PET substrate by ink-jet printing PEDOT:PSS suspension in interlocking diamond pattern (discussed earlier in Figure 1.8 (b)). Upon contact the mutual capacitance between the sense electrodes decrease shown in the heat map in Figure 1.26. Transmittances as high as over 80% are reported in this research.

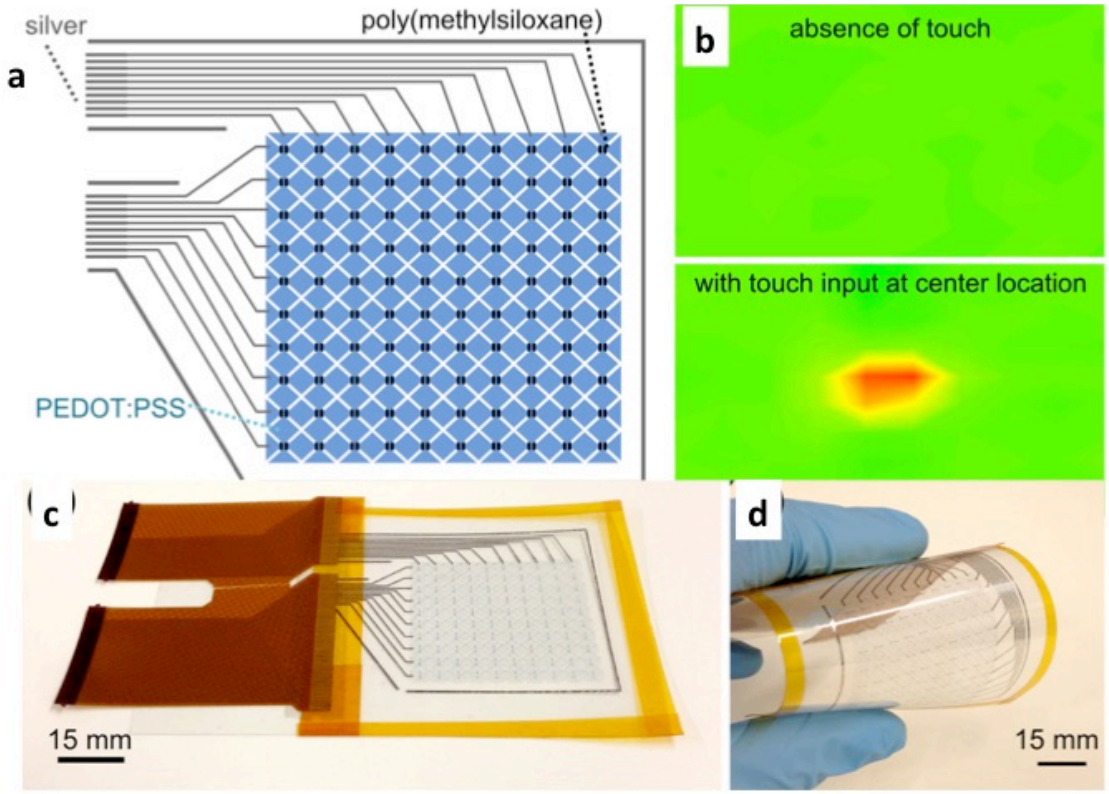

Figure 1.26: a) PEDOT electrode based touch sensor b) heat map showing the absence and then the presence of a touch c) image of touch sensor d) bending the touch sensor

A piezoresistive approach towards pressure sensing using PEDOT:PSS is demonstrated by Choong *et al.* in [58]. A pyramid microstructure based sensor is shown with a composite of PEDOT:PSS and a polyurethane dispersion as the piezoresistive layer grafted on the microstructures shown in Figure 1.27. Upon application of a pressure the piezoresistive layer of PEDOT:PSS gets deformed and leads to a change in resistance proportional to the pressure. It can also be used to measure strain. Although the PEDOT:PSS and PU composite can be stretched to up to 100% the piezoresistivity is linearly demonstrated up to a strain of 50%.

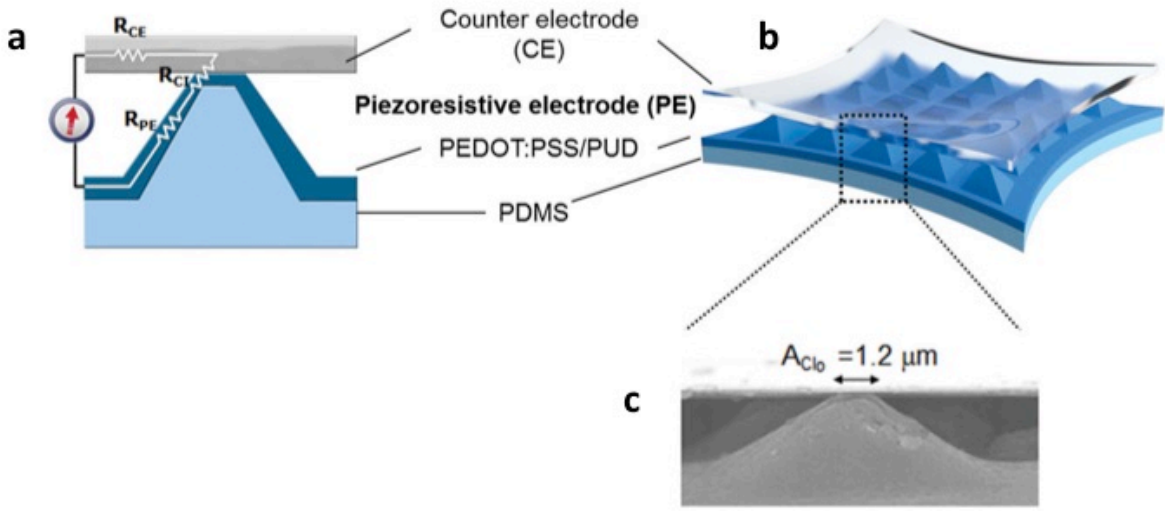

Figure 1.27: a) single pyramid microstructure with piezoresistive coating b) microstructured pyramid array c) SEM image of pyramid [58]**.**

1.3.4 Liquid metal

Liquid metal mercury has been around for over a century, however due to its toxicity it is not useable for most applications. Eutectic GaIn (E-GaIn) liquid metal, which is much less toxic, has been used to devise various sensors. Being a metal, it offers high conductivity in comparison to all its competitor materials or composites available for flexible and stretchable applications. Being a liquid, it can be deformed to the limit only set by the encapsulating elastomer. A number of implementations of liquid metal as a stretchable conductor are shown in Figure 1.28 [27].

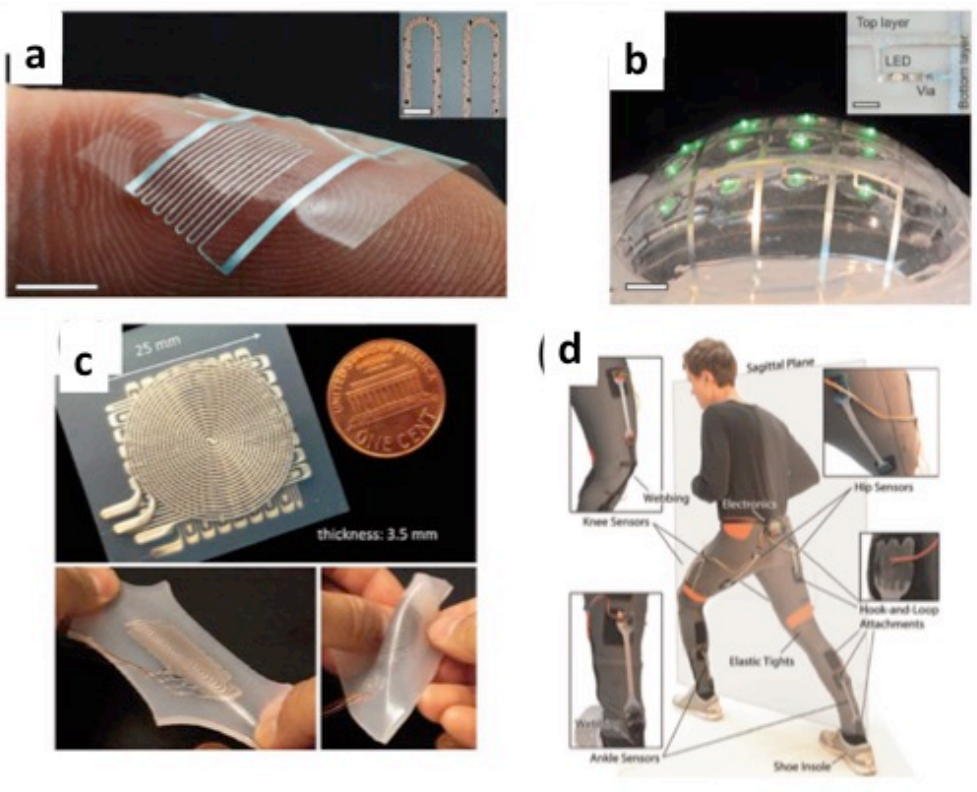

Figure 1.28: a) biphasic lines of liquid metal as interconnect b) liquid metal interconnect lighting an array of LEDs c) Liquid metal in elastomeric microchannels changes resistance when deformed due to changes in geometry of the metal. d) Detecting gait in soft wearable sensors [27]

A pressure sensor that works similar to ones in section 1.3.1 and 1.3.2 is proposed by Li *et al.* in [28] and shown in Figure 1.29. The sensor consists of an array of microfluidic channels inside an elastomer (Ecoflex) filled with liquid metal. Upon application of a pressure the liquid metal channels get closer to each other thereby increasing the capacitance in proportion to the pressure being applied.

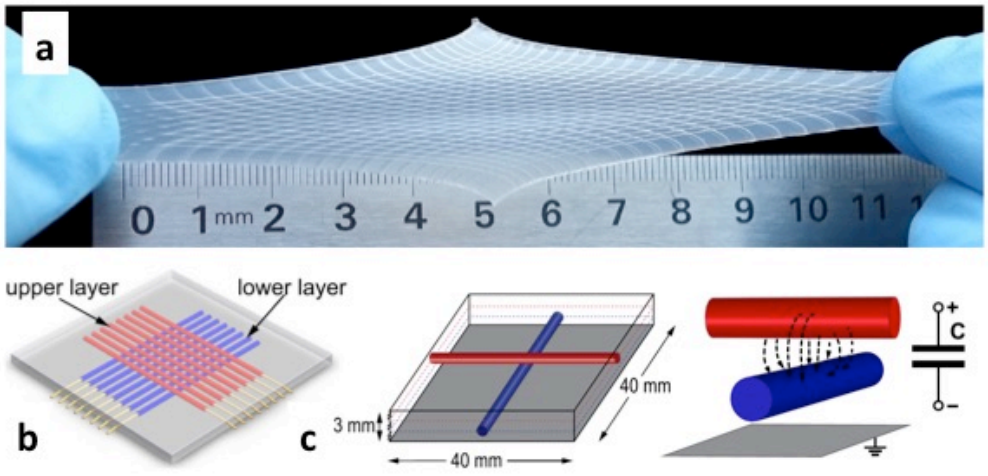

Figure 1.29: a) array of liquid metal electrodes in an elastomer being stretched b) schematic of an array of liquid metal electrodes for capacitive pressure sensing c) single pressure sensing element

1.3.5 Hydrogels

Hydrogels are highly hydrophilic polymers that can be composed of water up to 90% of their total volume. These polymers have been used in numerous applications such as polyacrylamide used in cosmetics, diapers, DNA gel electrophoresis etc. Polyacrylamide is highly transparent and stretchable (certain formations can stretched be up to 21 times the unstretched state [32]). In recent times hydrogels have been investigated as stretchable conductors. Although hydrogels do not form delocalized charges like conducting polymers discussed in section 1.3.3, they are able to conduct ionically in the presence of a salt. The conductivity however is very low (0.06 Ω-m) but for numerous applications this is ample.

Among the pioneering attempts at using hydrogel as electrodes is the dielectric elastomer actuator using hydrogel shown in [33]. In this case a VHB tape dielectric is sandwiched between two layers of polyacrylamide gels as electrodes. A high voltage is applied to the gels which causes the elastomer actuator to contract. Following this application the same research group

demonstrated the use of hydrogels as electrodes for a capacitive pressure sensor [17] with a working principle similar to Figure 1.22 and Figure 1.24, as shown in Figure 1.30 (a). In this case a similar structure to the actuator with VHB tape as the dielectric is implemented (Figure 1.30 (a)). Upon application of a pressure the dielectric thickness decreases which leads to an increase in capacitance. This sensor can also be used as a strain gauge as shown in Figure 1.30 (b) and (c). A pressure sensor array is implemented as shown in Figure 1.30 (d)-(f).

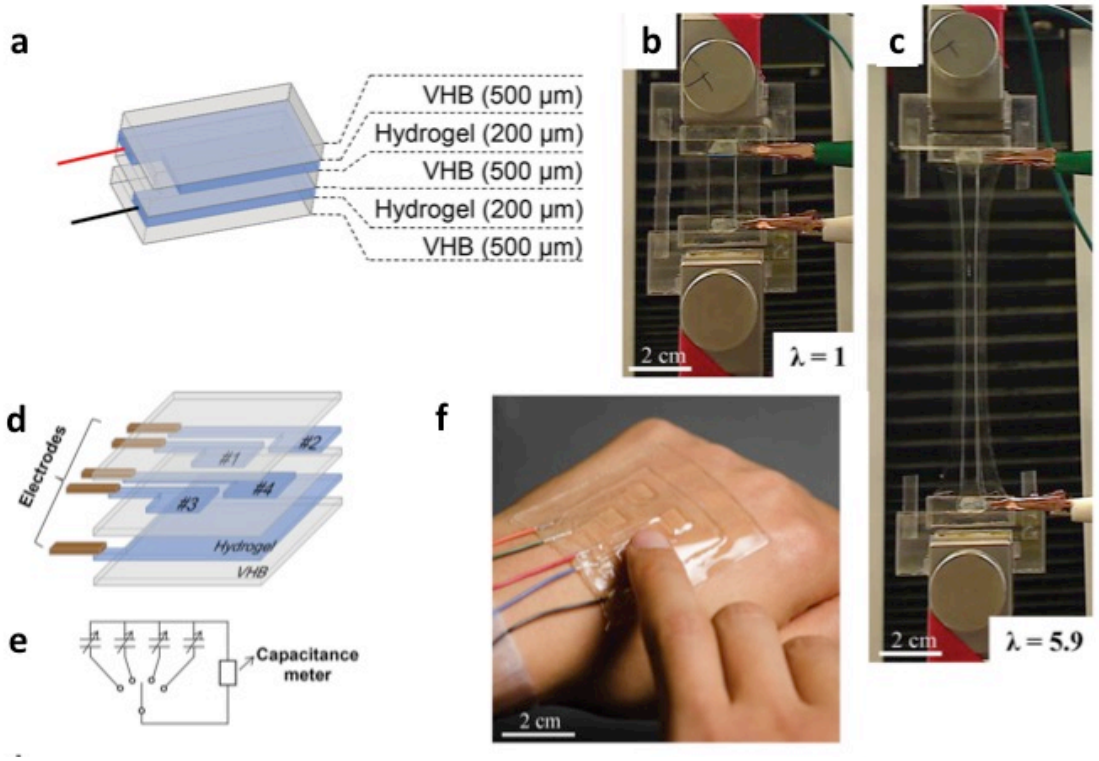

Figure 1.30: a) schematic of capacitive sensor b) upstretched c) stretched sensor d) schematic of array of capacitive pressure sensor e) circuit diagram of sensor f) image of pressure sensor

The sensor can detect pressures as low as 10 kPa and has a transmittance of 98% (gel only) [33]. The material is readily available and low cost ($1 per kg in bulk) and is a feasible candidate for commercial scaling in comparison to competing exotic and more expensive

materials such as CNT or AgNW. Challenges include water retention and inability to conduct direct current. Unless encapsulated properly, the water in the hydrogel will evaporate rendering the sensor incapable of functioning. Additionally, the application of a direct current or voltage will lead to an undesirable electro-chemical reaction. Therefore, this technology is suited only for applications that require alternating current/voltage signals.

1.4 Motivation

Although there is a significant amount of work in this field, there is room for improvement. In case of soft and flexible sensors, work needs to be done to detect and differentiate between multiple stimuli and also detect the desired stimulus while the sensor is being deformed (for applications in wearable devices, smart clothing flexible handheld devices etc.). This thesis aims to investigate these arenas.

The first sensor (Sensor I) in this thesis is a touch and proximity sensor that is stretchable and is able to detect a touch/hover while being bent/stretched. Most soft sensors in literature that are pressure sensors cannot detect a very light touch/contact. This ability is necessary for gestures such as a swipe – commonly used in handheld devices. Highly sensitive pressure sensors [59] in literature can be used to solve this issue but they are deformation based (i.e. in case of a capacitive sensor it works based on the change in the distance between electrodes of the sense capacitor or in case of a resistive sensor, it works based on the deformation of the piezoresistive electrodes). This means that it is difficult for these sensors to differentiate between a touch and a deformation such as a bend/stretch. There are flexible (but not stretchable) touch and proximity sensors [57] that operates using mutual capacitive technology - the same technology used in touch screen devices such as phones, tablets, laptops etc. and therefore are

not deformation based. Since they are not stretchable they are not ideal for applications for on-skin wearable devices or smart clothing. Additionally, they are not able to detect the presence of a deformation being solely mutual capacitance based. Sensor I in this thesis operates using the same mutual capacitive sensing however the architecture of the electrodes combined with the materials used renders the sensor highly sensitive to a hovering finger or a light touch and while it suppresses the effects of deformation on the sensor capacitor it is still able to detect and easily differentiate deformations such as a bend/stretch. A light touch brings about a large **decrease** in capacitance (approximately 20%) while a bend/stretch will bring about a small **increase** (approximately 2-3%) in capacitance. Being small in magnitude and in the opposite direction as a light touch, it is possible to detect the presence of a deformation while easily differentiating it from the desired stimulus – a light touch.

Following sensor I, a second sensor – sensor II is developed that adds pressure and strain sensitivity to existing proximity and light contact sensing. In this segment, instead of only detecting the presence of a deformation, the aim was to be able to quantify the magnitude of common deformations such as a pressure/strain while at the same time have the ability to detect a light touch/proximity and differentiate between the different stimuli. This is achieved by combining mutual capacitive sensing and overlap capacitive sensing. A light-touch/proximity by a human brings about a decrease in capacitance while a deformation such as a pressure or strain leads to an increase in capacitance. This difference in the direction in sensor response to the different stimuli enables easy differentiation between them. Although there are numerous highly sensitive pressure sensors in literature that can also detect strain, none have demonstrated the ability to detect the proximity/light-contact of a human finger. This ability is important in artificial skin applications in robotics where the robot is expected to physically interact with humans. Additionally, for artificial skin applications, shear sensitivity is very important. It is our

ability to sense shear that enables us to interact with fragile objects (e.g. an egg) and also conduct dexterous manipulation of objects. This is the objective of the third segment of this thesis.

The third sensor – sensor III, is a novel artificial skin technology with the ability to detect localized shear in addition to pressure, light touch and proximity. The features of the state of the art in artificial skin sensor technology in comparison to this sensor is depicted in Figure 1.31 below. This figure illustrates a few notable technologies that are able to detect multiple stimuli. However only the sensor in Chapter 4 is able to detect the entire range: touch/proximity, pressure and shear. It is also the only sensor that additionally provides a close mechanical analog to human skin by providing a similar smooth surface and a non-linear elastic modulus.

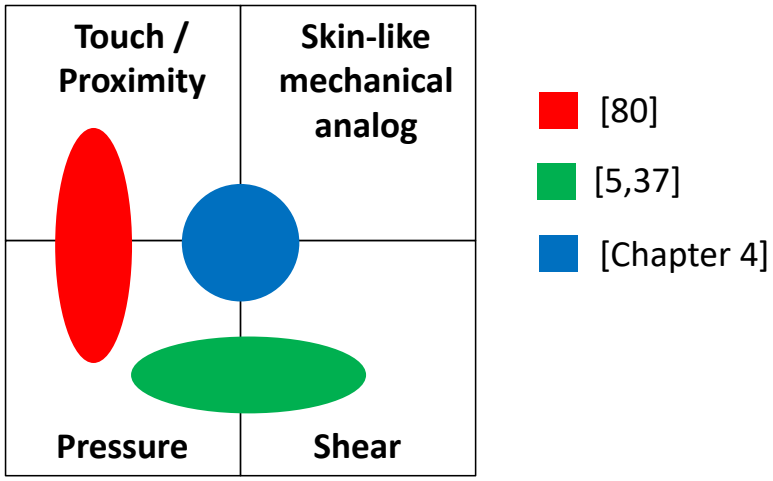

Figure 1.31: State of the art of artificial skin technology compared to this thesis. Each quadrant represents a mode of sensing, with overlap into the quadrant indicating that this type of sensing is possible.

The sensor is capacitive with a novel dielectric architecture, which enables the surface of the sensor to buckle and stretch locally upon application of a shear in a manner similar to human skin. Similar to Sensor II, this sensor incorporates a combination of mutual capacitance and overlap capacitance to give the sensor the ability to detect a light human touch and differentiate

between a human touch and contact with most inanimate objects such as wood, plastic etc. In addition to functional aspects, the sensor also resembles human skin in mechanical properties. Human skin demonstrates a non-linear elastic modulus with a low modulus *E1* for small strains and a higher modulus *E2* for larger strains. Sensor III demonstrates a similar non-linearity. This is the first attempt at creating an artificial skin technology that has similar mechanical characteristics of skin in addition to its functional characteristics. The ability of this pressure/shear sensor to differentiate between the contact of a human versus most inanimate objects (such as wood, plastic, paper etc.) is important for artificial skin applications in robots that are required to physically interact with humans and coexist in our society.

Chapter 2: Transparent Proximity and Touch Sensor

2.1 Summary

The development of bendable, stretchable, and transparent touch sensors is an emerging technological goal in a variety of fields, including electronic skin, wearables, and flexible handheld devices. Although transparent tactile sensors based on metal mesh, carbon nanotubes, and silver nanowires demonstrate operation in bent configurations, we present a technology that extends the operation modes to the sensing of finger proximity including light touch during active bending and even stretching. This is accomplished using stretchable and ionically conductive hydrogel electrodes, which project electric field above the sensor to couple with and sense a finger. The polyacrylamide electrodes are embedded in silicone. These two widely available, low-cost, transparent materials are combined in a three-step manufacturing technique that is amenable to large-area fabrication. The approach is demonstrated using a proof-of-concept 4 × 4 cross-grid sensor array with a 5-mm pitch. The approach of a finger hovering a few centimeters above the array is readily detectable. Light touch produces a localized decrease in capacitance of 15%. The movement of a finger can be followed across the array, and the location of multiple fingers can be detected. Touch is detectable during bending and stretch, an important feature of any wearable device. The capacitive sensor design can be made more or less sensitive to bending by shifting it relative to the neutral axis. Ultimately, the approach is adaptable to the detection of proximity, touch, pressure, and even the conformation of the sensor surface.

2.2 Introduction

With advances in micro-fabrication technology electronic devices are getting smaller, lighter and multifunctional. Human computer interface is no longer just limited to a keyboard but is becoming more organic with touch screens and voice control. There are over 200 million smartphones in the US alone that use a touch screen for input. A lot of electronic devices are evolving from being a brick form factor that can be hand held, towards a wearable form such as on the wrist or integrated in clothing. Wearable devices demand high conformability, motivating interest in so-called Electronic Skin [60] and, more recently, Ionic Skin [17]. Previous devices have shown the ability to detect touch [13], [59], [61], [62], stretch [14], [49], [63], [64], bending [65], or touch and stretch without the ability to distinguish between the two [17], [65]. Some of these can be made transparent [13], [15], [59], [62], [66].

Current touch screens are mutual capacitive touch sensors with Indium Tin Oxide (ITO) as the transparent electrode material. Some ITO-alternative materials provide the added benefit of being flexible and even stretchable. One such implementation of a conducting polymer based solution is demonstrated by Ma *et al.* in [57] where the ITO is replaced by PEDOT in a diamond interlocked architecture shown in Figure 1.26. The sensor is able to detect a light touch and is transparent up to 80%, however it is not stretchable being fabricated on a PET substrate. A truly wearable device would require the material to have the ability to be strained to sustain unobstructed movements of the part of the body where the device resides.

For HCI applications the ability to detect a very light touch, fluid movements or a “swipe” and detecting a touch at multiple locations or “multi-touch” are crucial. Although very sensitive pressure sensors can be used to detect a light touch, only projected capacitive sensors can be used to detect a light touch and the fluid gestures in consideration. Even the resistive touch screen

sensors aren't adept at detecting fluid motions. Additionally, for applications in a wearable device, the sensor is more effective if it can operate while being simultaneously deformed.

There have been several reports of stretchable touch sensors and some even transparent, using materials such as CNT, AgNW and hydrogel. Lipomi *et al.* shows in [14] a capacitive pressure sensor based on CNT electrode arrays shown in Figure 1.22. A similar work by Hu et al. in [13] using AgNW is shown in Figure 1.24 and finally Sun *et al.* demonstrated a sensor using the same principle but using hydrogel in [17]. Although all of these offer commendable specifications in terms of transmittance and stretch-ability, since all these sensors depend on the deformation of a dielectric, a "swipe" is not a feature they can offer.

Kim *et al.* demonstrated in [16] for the first time, a stretchable transparent touch panel that detects a light touch and fluid motions of a finger satisfying all the requirements for a wearable HCI device. It is based on a sheet of hydrogel as the sensor with four electrodes at the edges. Upon contact with the hydrogel surface, the impedance is measured from all the electrodes to the point of contact. The impedance is dependent on the distance from the location of contact to the electrodes. This information can then be used to detect the location of the finger. However, this technique has significant non-linearity and also does not enable the detection of multiple locations or a feature commonly known as "multi-touch". The sensor can be used to detect a stretch but both a stretch and a touch results in a similar response and therefore it is difficult to distinguish between them if they are happening simultaneously. Thus, there still remains room for improvement.

We observe that literature shows individual sensors with the desired features exist but none demonstrate all the functionalities in one single sensor. In this thesis we have attempted to develop a solution where all of these features are offered in one single sensor. Our stretchable proximity and touch sensor is able to operate while being actively deformed (i.e. bent or stretched) and is transparent to enable integration on a flexible display. It operates using mutual capacitive sensing.

The electrode material used is hydrogel (polyacrylamide) in a PDMS substrate. The capacitance changes by 20% with a light touch and about 10% with the proximity of a finger. A 4 X 4 array of 16 taxels is implemented with a readout circuit with multiplexers cycling between the taxels to provide information on the entire interactive surface.

2.3 Working principle

In this thesis we have developed a stretchable and transparent touch sensor that satisfies the major requirements for a wearable HCI device. It is 1) transparent, 2) stretchable, detects a 3) light touch, 4) swipe, 5) multi-touch and 6) is able to operate while being actively deformed. We achieve the required immunity to mechanical deformation in a touch sensor by making use of projected electric fields that extend beyond the device to couple with and enable detection of a nearby finger (Figure 2.1 (a)). The approach of the finger leads to a drop in capacitance between the electrodes. The drop occurs because the electric field, whose strength is indicated by color, is increasingly directed toward the finger, reducing the charge shared between the two electrodes. A cross-grid array of ionically conductive hydrogel electrodes is created with the electrodes capacitively coupled through a silicone elastomer matrix, producing a field that extends beyond the surface of the device. The materials and methods are deliberately chosen to be low cost and appropriate for large format mass production.

In this implementation, each array element is composed of a disc-shaped electrode and its interconnections (Figure 2.1 (b), red) separated from a loop electrode (Figure 2.1 (b), blue) by a dielectric layer. The loop and disc coupling allows for better vertical projection of the field than a simple crossing of lines. The finger acts as a third electrode, which capacitively couples to the sensor element, as represented by the variable capacitor C_F in Figure 2.1 (b), reducing the coupling

between electrodes, C_M. These loop and disk elements are placed in a sensor array depicted in Figure 2.1 (c).

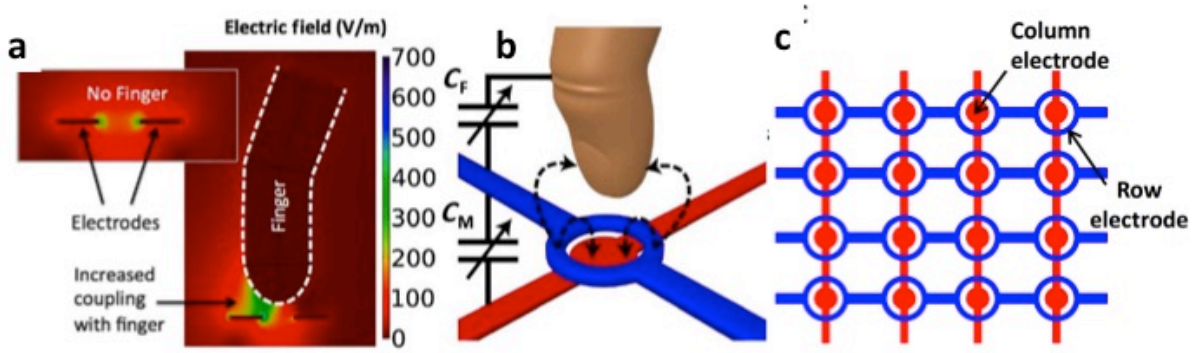

Figure 2.1: (a) Mutual capacitive coupling is simulated between two planar electrodes (shown in the inset without a finger). The coupling between electrodes is reduced by the presence of a finger, which acts as an electrode itself. (b) Finger approaching a pair of electrodes that are in the form of a loop and disc. The finger reduces the coupling between the electrodes (CM) by coupling itself with the projected field (CF is increased). (c) Two-dimensional array of loop-disc electrode pattern, with the loops on top.

2.4 Fabrication

A simple three-step fabrication process, mold-bond-polymerize (MBP; Figure 2.2 (a)-(c)), produces a unibody sensor. The fabrication process is similar to that used in microfluidics device fabrication [67]–[69] to mass produce products such as lab-on-chip devices [70]. Polyacrylamide, the hydrogel used to form the electrodes, is widely used in cosmetics and DNA gel electrophoresis. An ionic resistivity of 0.06 Ω·m (measured for a 2.74 M concentration of NaCl) is established by the presence of the salt in the hydrophilic polymer that contains 90% water. The dielectric that surrounds the electrodes is the widely available silicone elastomer polydimethylsiloxane (PDMS).

In the MBP process flow developed to fabricate the sensor, PDMS (Sylgard 184 silicone elastomer) was mixed in a 10 (base):1 (cross-linker) ratio and then degassed to get rid of the air bubbles. The uncured mix was then poured into molds (Figure 2.2 (a)), and the molds were then placed into an oven at 80°C for an hour. The molds were made of aluminum and formed films that were 55 mm × 55 mm across and 700 μm in thickness. The cured PDMS films with patterned grooves were then peeled off. The molds contained 1-mm-wide and 400-μm deep channels that formed the gel interconnects between the loops (top electrodes) or discs (bottom electrodes). The discs were 1.2 mm in diameter, whereas the loops had an outer diameter of 5 mm and an inner diameter of 3 mm. The loops and discs were 400 μm deep. A uniform-thickness middle dielectric layer was obtained by spin coating a 400-μm-thick uncured PDMS layer on a silicon wafer at 300 rpm for 20 s. The dielectric was then similarly cured at 80°C for an hour.

The three cured layers were then plasma-bonded (Figure 2.2 (b)) using a Harrick Plasma Cleaner (PDC-001) by exposing the surfaces to be bonded to oxygen plasma at a pressure of 600 mtorr for 110 s. The final PDMS shell with perpendicularly running channels has crossover points (referred to as tactile pixels or taxels) 5 mm apart from each other. The number of contacts in the cross-wire array approach is 2n for the case of an array of n × n = n2 taxels. In the proposed architecture, the space consumed by the interconnects is minimal when the array size is scaled up, especially compared to structures that have two distinct electrodes for each sensor element. In the case demonstrated here, the number of taxels is 16, the number of lines is 8, with 4 on each axis and each taxel element has a diameter of 5 mm.

The fabrication of the electrodes begins with the pre-gel solution. It is prepared starting with a mixture containing 2.2 M acrylamide (AAm) (A8887, Sigma-Aldrich) and 2.74 M NaCl. The concentrations of AAm and NaCl were similar to those used by Sun *et al.* [17]. Ammonium

persulfate [AP; 1.5 weight% (wt%)] (A9164, Sigma-Aldrich) was added as an initiator, and 0.06 wt% of the cross-linker N,N-methylenebisacrylamide (M7279, Sigma-Aldrich) was dissolved, with respect to the weight of the AAm monomer. The mixture was then degassed. N,N,N′,N′-tetramethylethylenediamine (TEMED; 1.0 wt%) (T7024, Sigma-Aldrich) was added as the accelerator, causing rapid polymerization. The stoichiometry of AP and TEMED was developed for specifically timed polymerization. Upon the addition of the accelerator, the mixture was injected into the channels within 1 min Figure 2.2 (c), and the mixture polymerized as it flowed through the channels. The process was timed such that the polymerization was completed as the channel was filled. An alternative to this is to use Irgacure 2959 (from Sigma Aldrich) as a UV photoinitiator. Instead of AP and TEMED, Irgacure is added in the ratio 0.1 wt% with respect to the weight of Aam. The sensor is then exposed to UV for 5 mins.

Finally, silver-plated copper wires with a diameter of 250 μm were inserted into the openings of the channels, and the channels were then sealed using silicone epoxy (Sil-Poxy from Smooth-On).

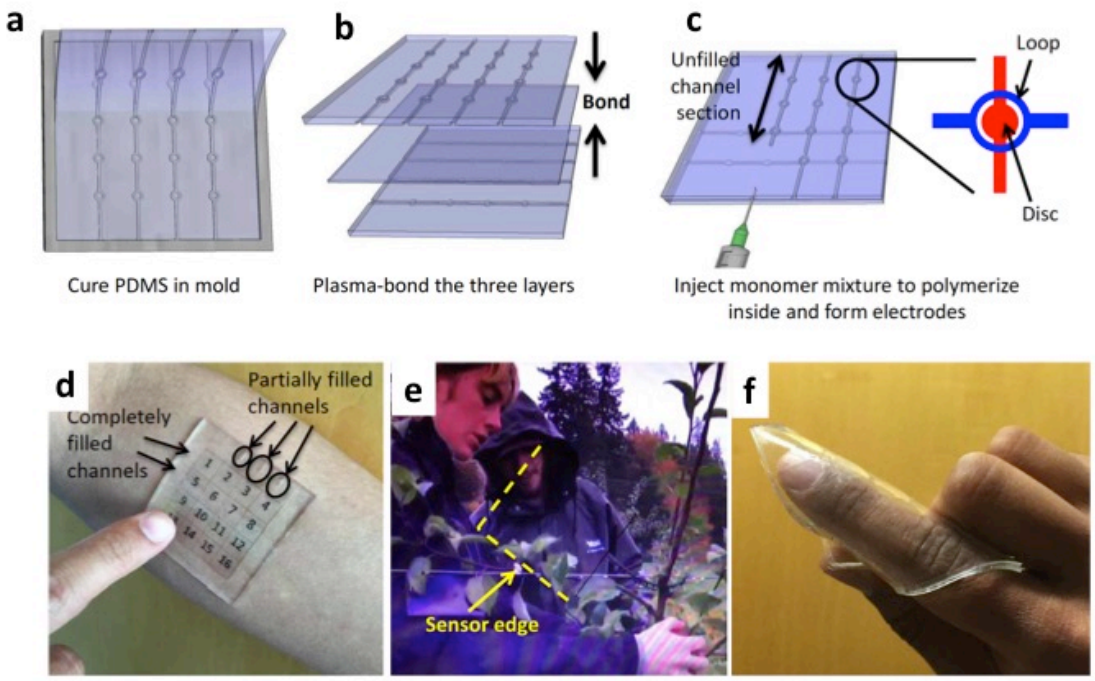

Figure 2.2: (a) Curing PDMS in a mold. (b) Plasma-bonding three layers forming perpendicular channels on top and bottom of the dielectric. (c) Injecting the monomer mixture inside the channels and polymerizing them to form the ionically conducting electrodes (d) Sensor array sitting above a forearm and a printed number pad. (e) Sensor array on an LCD with a video playing demonstrating transparency. Two edges of the sensor are indicated by the dashed lines. A third edge is just visible, extending perpendicular to the lower line. (f) Sensor array wrapped around a finger demonstrating conformity.

An array is shown in Figure 2.2 (d) on a forearm with a printed number pad under it to illustrate the transparency. Three channels are left with unfilled regions to demonstrate how filling makes these channels nearly invisible. The sensor is placed on a liquid crystal display (LCD) playing a video in Figure 2.2 (e) to demonstrate that the sensor is barely detectable. The edges are highlighted by dashed lines and labeled as “sensor edges.” Figure 2.2 (f) shows the sensor wrapped around a finger, an indication of its conformability.

The transmittance of the freestanding sensor in air is measured to be 90%. The light attenuation includes reflective losses at the air-sensor interfaces due to refractive index mismatch (estimated to account for 6% of the 10% loss) and at the hydrogel-PDMS interfaces (less than 1% loss). The remaining 4% loss is primarily the result of surface imperfections. Both, surface scattering and reflections could readily be reduced by adding antireflection coatings [71] and using molds with an optical finish. When the sensor is placed on a surface of relatively high index, such as on an LCD, as shown in Figure 2.2 (e), the reflection losses and surface scattering effects are essentially halved, which helps explain why it is difficult to see the sensor (that is, the sensor is transparent).

2.5 Results and Discussions

2.5.1 Light touch and proximity:

To detect single or multi-touch with a small number of electrical connections, the mutual capacitance concept is implemented (Figure 2.1). The lateral position of a finger can be detected on the basis of the capacitance changes observed. Each combination of row and column electrodes is scanned sequentially, and the capacitances of all taxels are determined to create a map (Figure 2.3 (a)), in this case indicating the presence of the finger at the intersection of row 1 and column 3, that is, element (1,3). The loop and disk design of the electrodes depicted in Figure 2.1 (b) is such that the fringe field exposed to an approaching finger is large, thereby bringing about a significant change in capacitance due to the presence of the finger. When the finger reaches the interface, it yields a 13% decrease in capacitance at the taxel being activated (Figure 2.3 (a), white shaded bar). Unlike other conformable capacitive sensor implementations, in this approach, no

force is required to obtain the change in signal. The proximity approach allows for noncontact gestures to be detected, as in Samsung's "Air View." Contact gestures such as the translational motion of a finger on the sensor surface, commonly referred to as a "swipe," can also be sensed without the need to press firmly, minimizing stiction on the soft surface. In the previous designs, including the recent use of gel electrodes [17], touch sensitivity is achieved by physical deformation, which also leads to sensitivity to stretch, and may explain why these works have not presented the ability to detect touch during stretch. The fringing fields result in some sensitivity also in the neighboring taxels (as seen from the map in Figure 2.3 (a)). Each bar in the map corresponds to a loop-disc taxel arranged as in Figure 2.1 (c). To investigate the proximity detection capabilities of the sensor, we clamped a finger in a fixed position, and the sensor array, placed on an elevator stage, was vertically moved closer to the finger. The clamping not only determines relative sensor-finger vertical position but also holds the lateral position fixed. The corresponding capacitances were recorded. Figure 2.3 (b) shows the relative magnitude of the change in capacitance as a function of distance from the surface. The sensor is demonstrated to be highly sensitive to a finger in very close proximity (lightly touching the surface). The change in capacitance falls off when the finger is further from the surface but is still significant even at 2 cm.

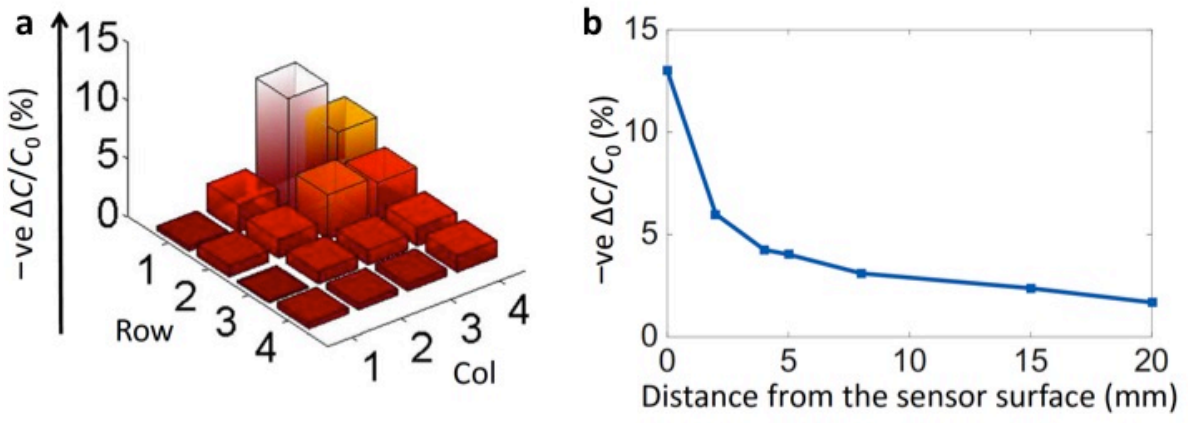

Figure 2.3: a) Map showing the localized change in capacitance due to a touch by a finger (b) Change in capacitance due to a hovering finger at various distances from the top of the sensor. The change in capacitance upon approach of the finger is negative, as indicated

2.5.2 "Swipe" and "multi-touch" detection:

The sensor is able to detect gestures such as a swipe, where a finger in light contact with the sensor is moved across the array (as shown in Figure 2.4 (a)). The use of projected fields makes the approach very sensitive to such gestures, where there is only very light contact. The $\Delta C/Co$ maps in Figure 2.4 (a) show that the finger partially activates neighboring taxels, which can be used to find the center of mass of the activation using further signal processing to enhance the spatial resolution, if needed. Another common gesture used in commercial touch screen devices is the multi-touch capability (shown in Figure 2.4 (b)), in which the presence of one, two, and then three fingers is detectable.

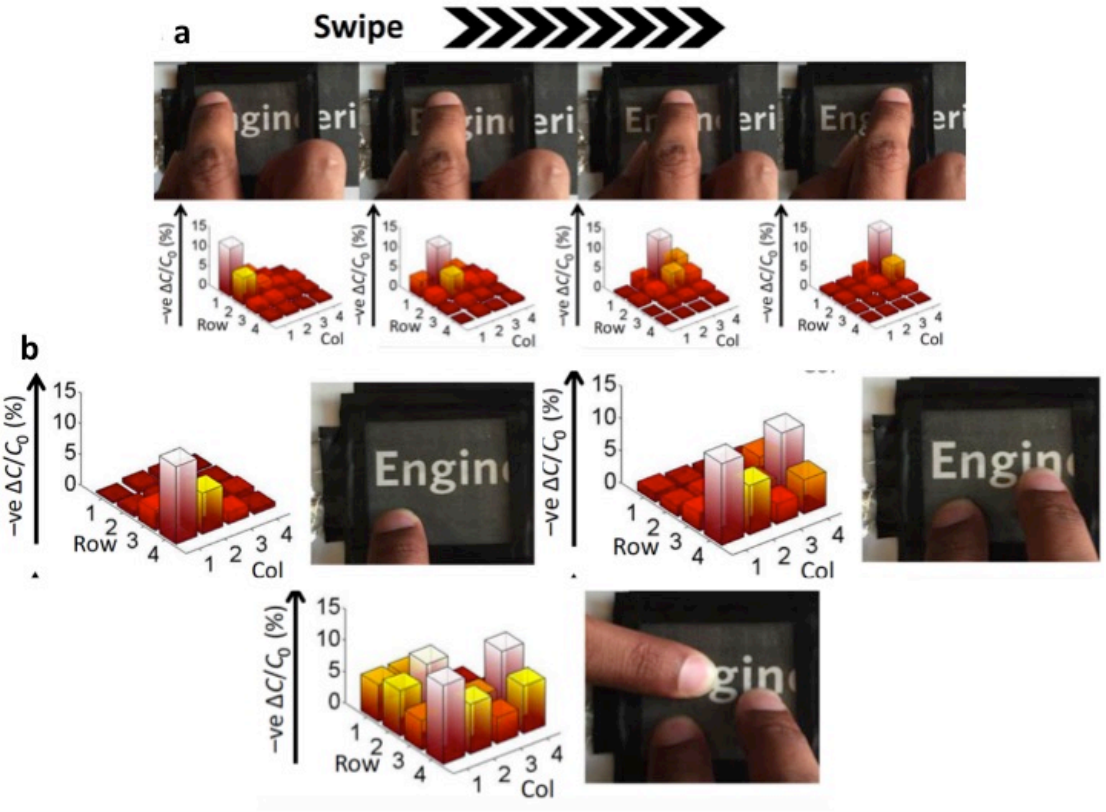

Figure 2.4: Sensor response to a) a "swipe" b) “multi-touch”

2.5.3 Touch while stretching:

To determine the sensitivity of touch sensing to stretching, we clamped the sensor in a dynamic mechanical analyzer. A controlled sinusoidal stretch of 5-mm amplitude (corresponding to a strain of 7%) at 0.11 Hz was applied, and the corresponding capacitance was recorded.

The stretch and the result of touch during stretch are shown in Figure 2.5, with the sinusoidal stretch onset after 40 s. It is observed that the capacitance increases with a stretch and follows the magnitude of the strain. Some change in capacitance is expected from the increase in overlapping electrode area and the reduction in dielectric thickness brought about by the stretch. While being stretched, the sensor was lightly touched three times between 65 and 110 s after the start of

measurement (as shown in Figure 2.5). This brought about a significant decrease in capacitance. The finger contact signal is much larger than the change due to stretching. There is some jitter in the touch response because the finger itself bounces upon contact.

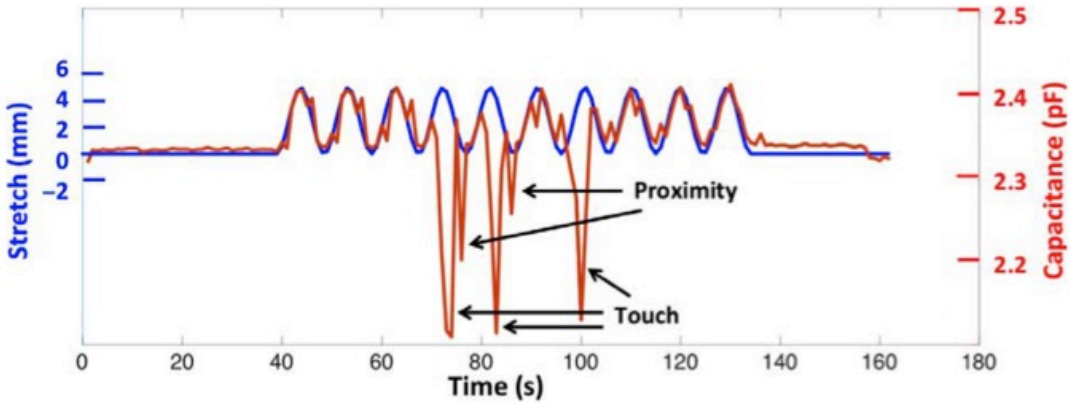

Figure 2.5: Touch while stretching

2.5.4 Touch while bending:

To investigate the effects of bending, we folded the sensor array from the planar state shown in Figure 2.6 (a), in which capacitance is uniform, to a state in which the right hand corner is brought up toward the camera viewpoint, leading to a small radius of curvature (~10 mm) along the bend line (seen in Figure 2.6 (c)). Figure 2.6 (d) shows a small increase (~2%) in capacitance along the fold line. The relative immunity to bending is not surprising because the thickness of the dielectric (400 μm) is much smaller than the bending radius of curvature (10 mm), leading to approximately ±2% strain in the top and bottom electrodes. The sensor is touched while being bent, as shown in Figure 2.6 (e), and the resulting change in capacitance is plotted in Figure 2.6 (f), which shows a large decrease in capacitance at the location of the touch, indicating easy detection of the touch during bending. In the figure, the vertical axis shows a negative change in capacitance, whereas in the neighboring plots, the change in capacitance is positive, with the

vertical axis being positive change and this change is represented by dark blue instead of red and yellow. Finally, folding of the sensor array in the opposite direction (Figure 2.6 (g)) yields a similarly small increase in capacitance along the axis of bend (Figure 2.6 (h)) as that seen with the opposing fold. These demonstrations of detection of a finger while being actively stretched and/or bent are important in applications where the device may be folded as part of its normal use, such as application to the surface of a flexible display to create a touch screen.

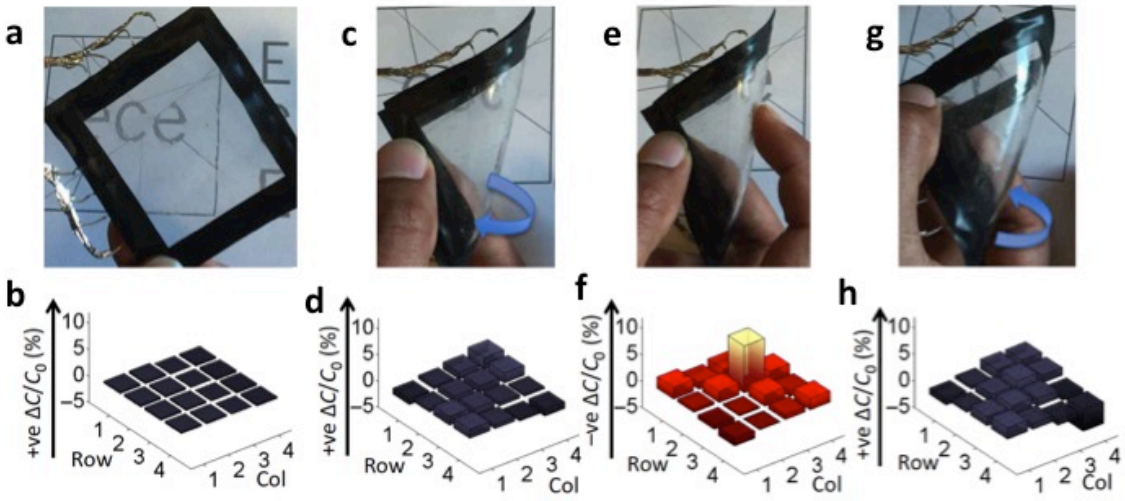

Figure 2.6: (a) Sensor in steady state. (b) Stable capacitance map for steady state. (c) Sensor folded in an anticlockwise direction. (d) Resulting small positive change in capacitance of the taxels along the axis of bend where capacitance increases with positive y-axis. (e) Sensor being touched while being bent. (f) Negative change in capacitance map showing the taxel touched having a change in capacitance of 10%, reduced slightly by the change due to the bend where the capacitance decreases with positive y-axis. (g) Sensor being bent in the clockwise direction. (h) Positive change in capacitance map showing the axis of bend and a similar response that in (d).

2.5.5 Enhance sensitivity to bending:

The design of the electrodes makes the sensor relatively immune to bending and stretch, whereas the presence of a finger is strongly captured. This is made possible by the electrode pattern (loop and disc in this case, which projects field) and the use of a relatively thin sheet with the positive and negative electrodes equally spaced on either side of the neutral axis (which reduces sensitivity to bending). In some cases, it is desirable to determine the overall shape of the surface. The sensitivity to bending can be increased if desired by modifying the geometry.

Figure 2.7 shows the increased response to bending achieved when the electrodes are offset relative to the neutral axis, so their strains are no longer equal and opposite during bending. In this case, the top layer is made thicker such that the neutral axis is aligned with the top electrode layer instead of the dielectric, so the bottom electrode layer would experience a large strain and thereby detect a bend more readily. The radius of the curvature in Figure 2.7 is ~10 mm. As seen from the cross-sectional diagram in Figure 2.7, the bottom electrode layer is 640 μm away from the neutral axis and therefore experiences a strain of ~6.4% (whereas the top electrode remains unstrained being on the neutral axis). This results in a larger change in capacitance (~5%) compared to the previous iteration (~2%) with the dielectric along the neutral axis (Figure 2.6 (c) – (h)). The grayscale plot in Figure 2.7 shows the axis of bend corresponding to the bending action in the image above it. Under bent conditions, the sensor is still able to detect a touch, as seen from Figure 2.7 (c). This opens the possibility of designing the sense electrodes to be more or less sensitive to particular modes of deformation or touch. There is the possibility of making certain elements more sensitive to bending or stretching while making other elements less sensitive by modifying, for example, their geometry and neutral axis offset, which would enable complete reconstruction of the surface conformation.

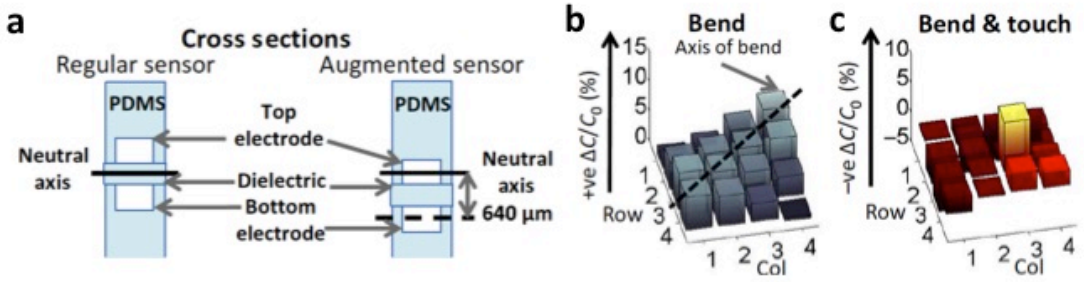

Figure 2.7: (a) Diagram of the design and results from an augmented bend sensor (compared with the regular sensor with the neutral axis aligned with the dielectric), with the neutral axis aligned with the top electrode layer, which (b) enhances the detection of bend but still enables (c) the simultaneous detection of touch

2.5.6 Mechanical characterization:

2.5.6.1 Strain cycling:

A potential challenge with any multilayer composite structure such as the sensor arrays is failure by delamination. An initial study of the general robustness of the sensor array was performed, in which the sensor was clamped and stretched by 10%, followed by a buckle with a radius of curvature of 16 mm (corresponding to a surface strain of 6%) as shown in Figure 2.8 (a) – (c). This cycle is repeated 500,000 times at a frequency of 1 Hz in a water bath. The bath ensures that any changes seen are not due to evaporation of water from the gel. The sensor is unclamped and tested for finger touch sensitivity during the cycling at the point of maximum bending. No significant drop in performance is observed over the test, and there is no visible damage to the sensor array, as evident from the plot in Figure 2.8.

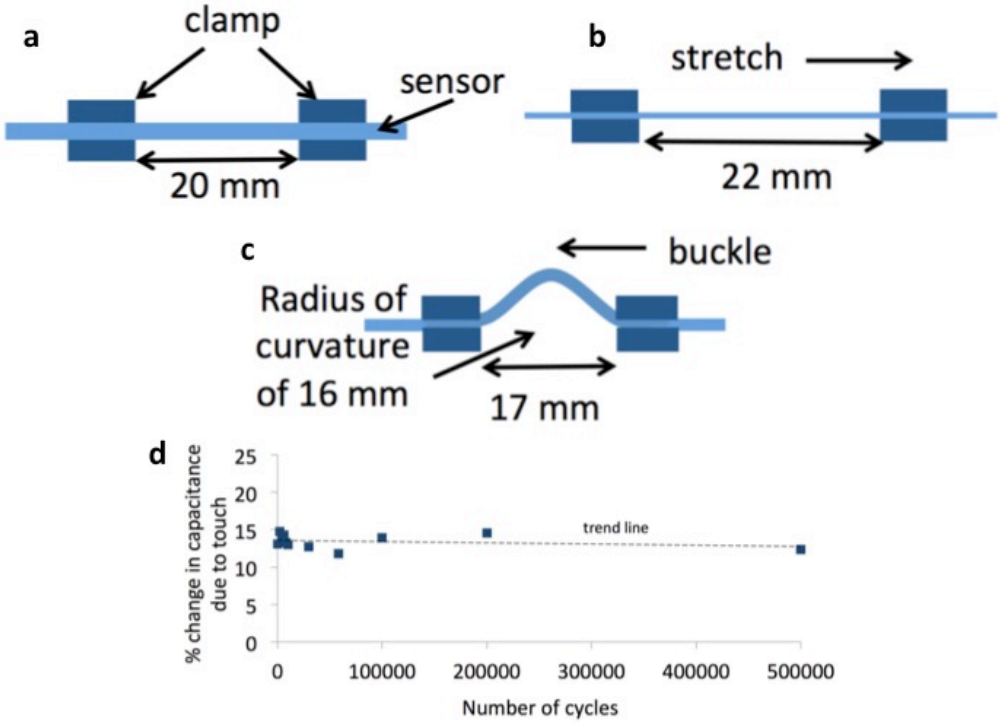

Figure 2.8: (a) sensor un-stretched (b) stretched (c) buckled (d) change in capacitance due to a touch over half a million cycles

2.5.6.2 Temperature cycling:

The sensor array was also heated to 80°C for 15 min and cooled to −10°C for 15 min. Following these temperature exposures, the sensor responded to a touch as before (the taxel sensitivity was initially 14%, and afterward was 13%, within the typical variation range resulting from slight changes in finger position and orientation).

2.5.7 Readout electronics:

The readout circuit uses an off-the-shelf capacitance to digital converter (CDC). Two multiplexers are used to cycle through the array of taxels. One multiplexer is connected to the rows of electrodes and the other to the columns. An ATMega 2560 micro-controller is used to control the cycling of the multiplexers, readout the capacitance from the CDC and finally feed the data through a serial port to a computer. The block diagram of the system is shown in Figure 2.9 and the readout circuit is shown in Figure 2.10. The entire 4 × 4 array of 16 taxels was sampled three times per second.

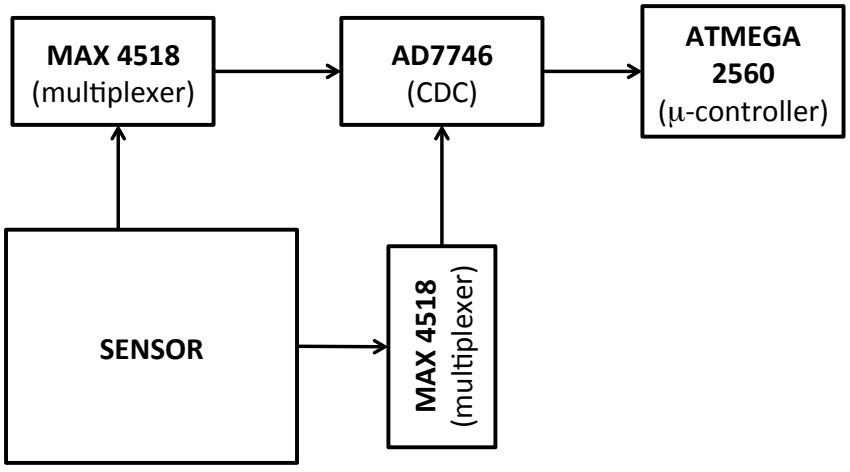

Figure 2.9: Block diagram of readout circuit

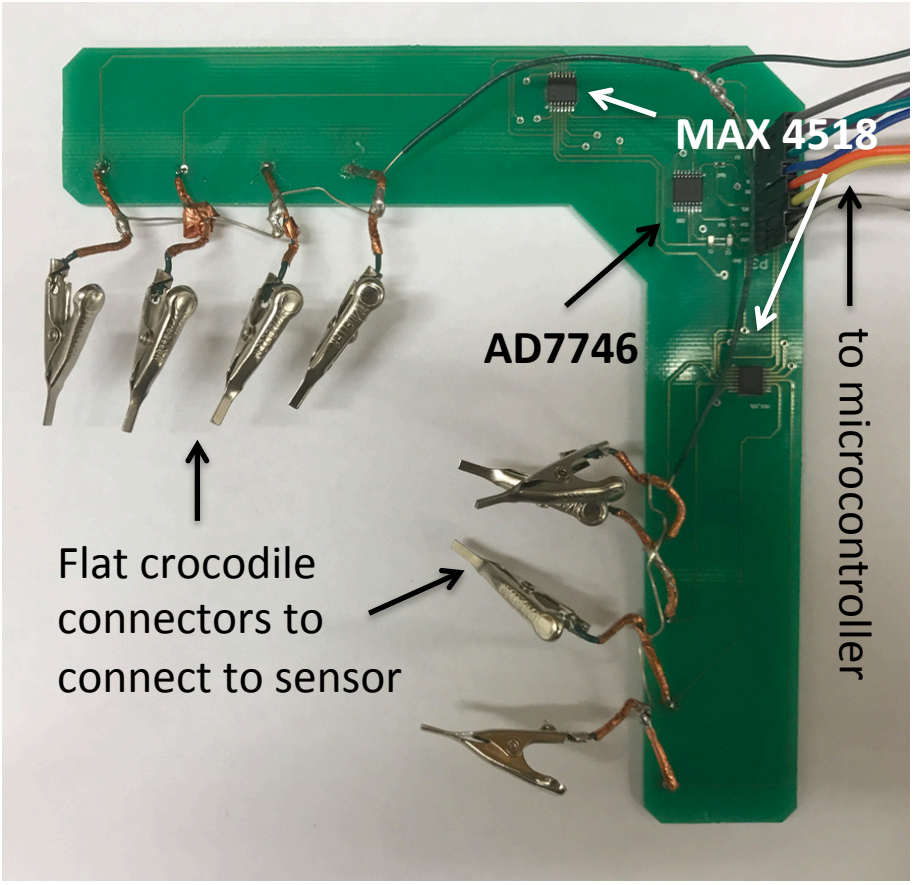

Figure 2.10: Readout circuit showing the clips used to connect to the sensor (4x4), the multiplexers (MAX 4518, and the CDC for capacitive measurement (AD7746).

To be effective for portable and mobile applications, sensing devices should be of low power, and the footprint of the interface electronics should be small to facilitate compact-form factors. Here, the readout electronics is based on well-established capacitive sensor readout circuits that are widely used in mobile devices. Although we used an Arduino platform together with a capacitance-to-digital converter (CDC) chip, a custom single-chip solution can be envisioned that has approximately double the 5-mm X 6-mm footprint of the CDC and has an average power consumption of less than 1 mW. At this power level and with 8 hours of continuous operation per

day, the proposed system can be expected to last 3 months without recharging using a typical smart-watch battery.

2.5.8 Dimensional scaling:

Keplinger et al. [33] have shown that gel-based ionic conductor pairs can propagate signals with a highly effective diffusion rate. For the sensor array case, a limit on the maximum dimensions of the sensor is set by the RC time constant of the most distant taxel, the refresh time, τ, and the number of taxels, n. The RC time constant is important because if a taxel is probed on too short a time scale or at too high a frequency, the resistance of the interconnects will dominate and the capacitive signal will be small. Assuming the taxels are individually addressed sequentially, the RC time constant should be less than or approximately equal to the measurement time for each taxel, given by τ/n. The maximum sensor array dimension, Lmax, is then approximately

$$Lmax \leq \sqrt[3]{\frac{\sigma \alpha l t_i t_d \tau}{2\beta \varepsilon_r \varepsilon_o}} \quad (2\text{-}1)$$

In this equation, a square array is assumed with the dimension of each taxel being l × l, the conductivity of the interconnects is represented by σ, the thickness of the interconnect is t_i and that of the dielectric is t_d, and the permittivity of the dielectric is $\varepsilon_r\varepsilon_o$. Here, αl is the average width of each interconnect (with α being the fraction of the width consumed by the interconnect), whereas β represents the ratio of the taxel and parasitic capacitance to that of an l X l parallel plate capacitor. As expected, increasing the width of the conductor, αl, and the thickness, t_i, will allow the size to be increased by reducing resistance of the conductor. Increasing the capacitance by reducing the dielectric thickness or increasing the permittivity will reduce the dimensions. The estimate in Eq. 2-1 suggests that the sensor array area can be very large, approximately 50 m X 50 m in a 20-cm

grid refreshed every half a second. Such a format might be used to detect the presence of feet (instead of fingers).

An attractive feature of any capacitive technology is that its resolution scales in proportion to the dimension of the electrodes. Like a parallel plate capacitor whose dimensions are uniformly scaled up or down, the magnitude of the projected capacitance also scales linearly, as do the vertical and lateral resolution. To demonstrate this a COMSOL multiphysics simulation is used. In the model shown in Figure 2.11 (a) a finger touches the taxel (2,2). The simulation is initiated with the width of the electrodes as 2 mm and spacing between them as 5 mm (edge to edge) and thickness as 0.4 mm (set 1). This gives rise to a change in capacitance of 18% at the taxel being touched while the adjacent taxels experience a change in capacitance of 8% providing sharp localization of the finger. The system is then scaled down by 10 times (set 3), which effectively made the electrodes thinner and brought the taxels closer together. The changes in capacitance for the taxels along the 2nd row are plotted in Figure 2.11 (b). It is observed that the relative change in capacitance $\Delta C/Co$ for a 0.4 mm thick electrode with a finger diameter of 10 mm is exactly the same for the 0.04 mm thick electrode case with a finger diameter 1 mm (can be the tip of a stylus).

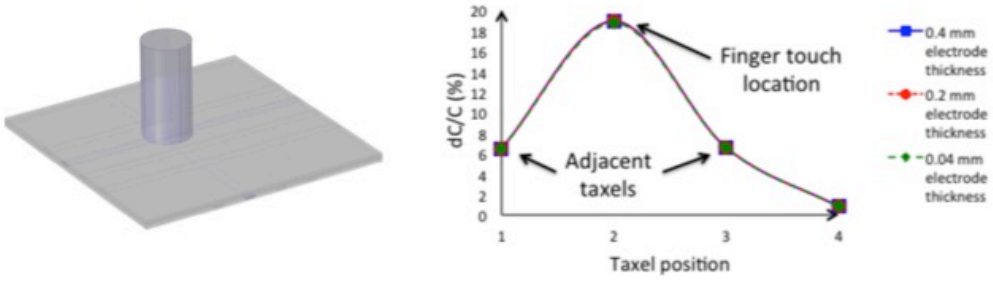

Figure 2.11: (a) COMSOL model for a finger on an array of electrodes (b) plot showing change in capacitance with the location of a taxel with the finger being on top of the 2nd taxel

The scaling of the sensor array therefore has no effect on the functionality of the sensor. The smaller the electrodes, the finer the lateral resolution. However, it does cause the lateral and vertical resolution to change with the scaling factor. The scaling of resolution is the same in the vertical direction. This implies that devices can be constructed to sense at much larger or smaller scales than the millimeter levels shown here, subject of course to limitations of fabrication methods and instrumentation considerations. Microelectromechanical system (MEMS) devices sense capacitances that are 1000 times smaller [72] than those of our devices, suggesting that operation with micrometer resolution is possible if desired.

2.6 Conclusions

With flexible displays having been implemented by Sony, Samsung, Plastic Logic, and others, and with stretchable electroluminescent materials and displays emerging [73], [74], it is interesting to consider how these interfaces can be made interactive. The transparent sensor array, when laminated onto the surface of a deformable display, promises to enable touch screen selection and gesture-based interactions even during bending and stretching. If the device is also made sensitive to stretch (independently), image distortion could be corrected. In general, the compliance and transparency offer the promise of applying the sensor arrays to virtually any surface.

Implementing a unique electrode architecture, the sensor presented here was made preferentially sensitive to proximity of a finger and light touches but relatively insensitive to deformations such as a stretch or bend. The sensor response to a deformation is a small increase in the sense capacitance (approximately 2-3%) which is much smaller and in the opposite direction

than a decrease in capacitance due to a proximity/touch (approximately 15%). This enables easy detection of a proximity/touch even while the sensor is deformed.

Intuitively, the next stage in evolution for this sensor is to be able to detect and quantify applied deformations (such as a pressure) in addition to its existing ability to detect proximity and light touch while being able to differentiate between the different stimuli. The sensor would provide combined information enabling finger location and applied pressure detection, including the discrimination of stretch, bend, and touch-related deformations.

Chapter 3: Stretchable proximity, touch, pressure and strain sensor

3.1 Summary

Advances in highly deformable sensors are needed in order to enable emerging devices for wearable electronics, medical devices and soft robotics. Stretch-ability is necessary to enable the sensor to conform to arbitrary geometries such as the contours of a part of a human body (e.g. the wrist), for wearable applications and/or smart clothing. For artificial skin applications in robotics and prosthetics, multiple modes of sensing are desired that include light contact, pressure and even proximity. This chapter demonstrates a single stretchable sensor that is able to detect proximity, light touch, normal pressure and stretch and is able to distinguish between the different stimuli. The working principle is a combination of well-established mutual capacitive and overlap capacitive methods. The proximity of a finger brings about a decrease in capacitance of ~5% while a light contact decreases the sensor capacitance by 10%, both using mutual capacitive effects. Application of a normal pressure brings about a 0.13% increase in capacitance per unit kPa pressure applied and offers a capacitive gauge factor of 0.35 for a stretch, both using overlap capacitive effects. Deformations bring about an increase in capacitance, a change in the opposite direction of the response due to the proximity or light contact of a human finger. This combined with cumulative information from an array of sensor units provides paths towards differentiating between the different stimuli.

3.2 Introduction

In recent times there has been a significant interest in skin like, stretchable pressure sensors for numerous applications ranging from artificial skin [4], [75], robotics [8], smart clothing [12], [76], wearable devices [77], [78], health monitoring [79] etc. Typically the sensors are either capacitive or resistive in nature with stretchable sense electrodes. The electrode materials described in the literature include silver nanowires (AgNW) [15], [25], CNT [14], conducting polymers [26], hydrogels [17], liquid metals [27], [28] and carbon black filled composites [31]. Liquid metal, hydrogels and carbon black filled composites [31] have demonstrated the ability to be stretched significantly, but each also has disadvantages. Liquid metal is difficult to process and pattern since it flows, with most of its applications being in a micro-fluidic channel form. Carbon black is a suitable candidate as a stretchable conductor, as are hydrogels, even though they are much higher in resistance compared to the competing stretchable conductors. Sintake *et al.* [31] demonstrate a carbon black based strain sensor that can be strained as high as 500%, and Sun *et al.* [17], demonstrate a highly stretchable pressure sensor that detects strains up to 500%, as well and very low pressures (as low as 1 kPa). The sensors are capacitive in nature and detect pressures and strains based on the deformation of the electrodes that lead to an increase in capacitance. Being deformation based sensors these cannot detect the proximity or the presence of a finger lightly touching the surface. Rocha *et al.* [80] have demonstrated a sensor that is able to differentiate between the proximity of a finger and applied pressure using two separate sensors integrated in the same substrate (mutual capacitive for proximity and piezoresistive for pressure), which increases complexity of fabrication and readout and is not able to detect strain.

In this research we introduce a single sensor (shown in Figure 3.1 (a)) that combines the ability to detect and differentiate between the proximity of a finger or light touch (applying close

to zero pressure) and deformations such as a press (or pressure), strain (over 300%). The sensor geometry and fabrication are simple and it uses readily available materials. The working principle is a combination of projected capacitance technology (used in touch screen devices) for the proximity and light touch sensing (similar to [2]) and overlap capacitance for sensing the deformations such as pressure and strain. The combination of this working principle, the patterned dielectric architecture and collective information from an array of sensor elements enable the detection and differentiation of the different mentioned stimuli. The dielectric architecture is composed of cylindrical air gaps of diameter 2 mm spaced 3 mm apart (center to center) with a height of 1 mm shown in Figure 3.1 (b) and (c). This architecture reduces the elastic modulus of the sensor and hence enhances pressure sensitivity (compared to one without the patterned dielectric). Several soft pressure sensors in literature have demonstrated introducing air gap structures to enhance pressure sensitivity. Choong *et al.* uses pyramid structures in [58], Zhuo *et al.* in [81] uses rectangular channels and Mannsfeld uses pyramids in [3]. However, none of these sensors demonstrate the ability to detect the proximity/light contact of a human finger.

The implementation of the projected capacitance technology gives the sensor the ability to differentiate between the contact of a human (a material with high dielectric constant and acts as a virtual ground) and inanimate objects like plastic or wood (that has small dielectric constants). This ability is of great importance for robotic skin applications for robots that interact with humans. One example of its importance is a safety locking mechanism of a robot hand using this sensor when working with humans in the same work space to avoid accidents. If the robot hand is completing a programmed task but a human gets in the way, the sensor detecting the presence of a human will prevent the robot hand from proceeding with the task and come to a complete halt until the human is at a safe distance.

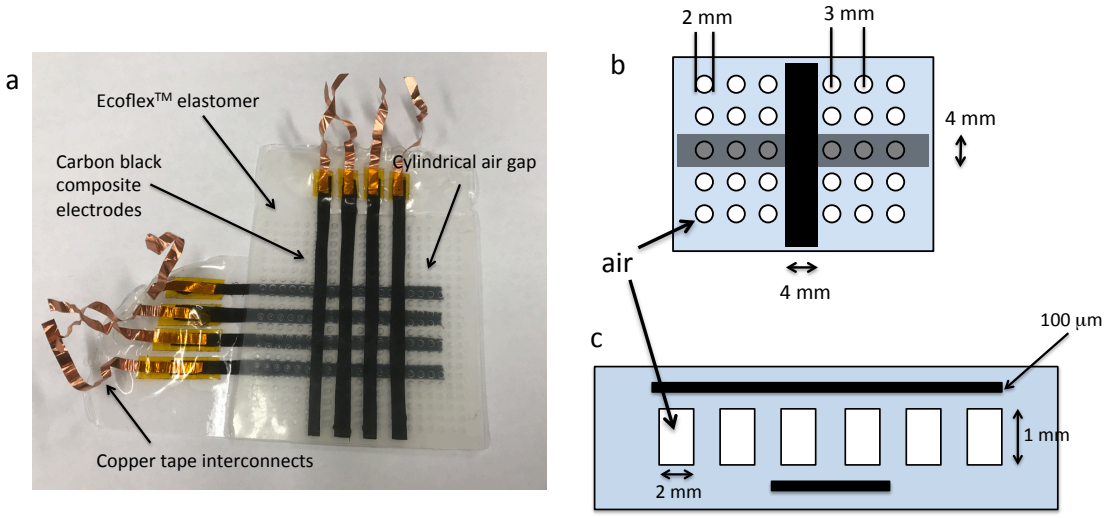

Figure 3.1: (a) Image of a 4 X 4 implementation of the sensor (b) top view (c) cross-section

The elastomer used is Ecoflex™ and the stretchable electrode is a carbon black filled composite. Ecoflex™ is a safe elastomer which is commonly used to make toy face masks. It has a skin-like feel and is safe to touch which is why it is used to make face masks. Carbon black fillers are widely used in tires and other rubber objects. It is readily available in bulk and easy to use. The sensor implementation discussed in this research is a 4 X 4 array of sensing cross-points or "taxels". As will be shown, light touch by a finger leads to a ~10% decrease in capacitance while a pressure leads to an increase in capacitance of 0.13%/kPa. In case of strain the capacitive gauge factor is ~0.35. Light contact of a cardboard or plastic has little change in capacitance (2-3% increase).

3.3 Working Principle

Projected capacitance is the component of the capacitive coupling between two electrodes due to the fringe fields (Figure 2.1). Human beings can act as a virtual ground. When a finger (or

a grounded metal) approaches the electrodes (or lightly touches the surface), the finger acts as a third electrode, decouples the electric field between the sensor electrodes, and thereby reduces the capacitance (Figure 3.2 (a)). This response is different from that caused by deformation-based stimuli such as a pressure, which leads to a change in capacitance in the opposite direction (i.e. an increase).

Upon application of a pressure the sensor is deformed such that the electrodes are closer together (Figure 3.2 (b)) thereby increasing the capacitance (according to $C=\varepsilon A/d$). A lateral strain increases the area of the electrode (shown in Figure 3.2 (c)) and reduces the dielectric thickness. This results in an increase in capacitance. The device is thus sensitive to proximity, pressure and in plane strain.

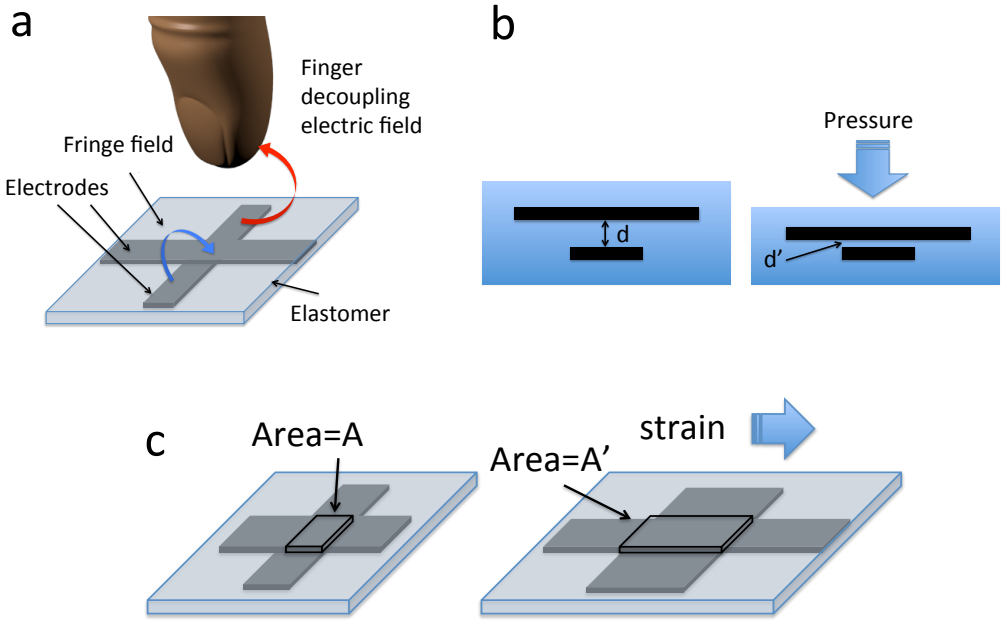

Figure 3.2: (a) Finger reducing coupling of sensor electrodes (b) application of a pressure resuling in a reduced dielectric thickness (c) application of a strain increasing the area of overlap of sensor

A simple flowchart describing these basic stimuli is shown in Figure 3.3 below. This considers the case of a finger interacting with a single taxel and stretching the sensor along its plane. For more complicated stimuli sophisticated machine learning techniques may be implemented. One such complicated scenario is described in the results section regarding the distinction between the retraction of a finger after a touch and application of a pressure.

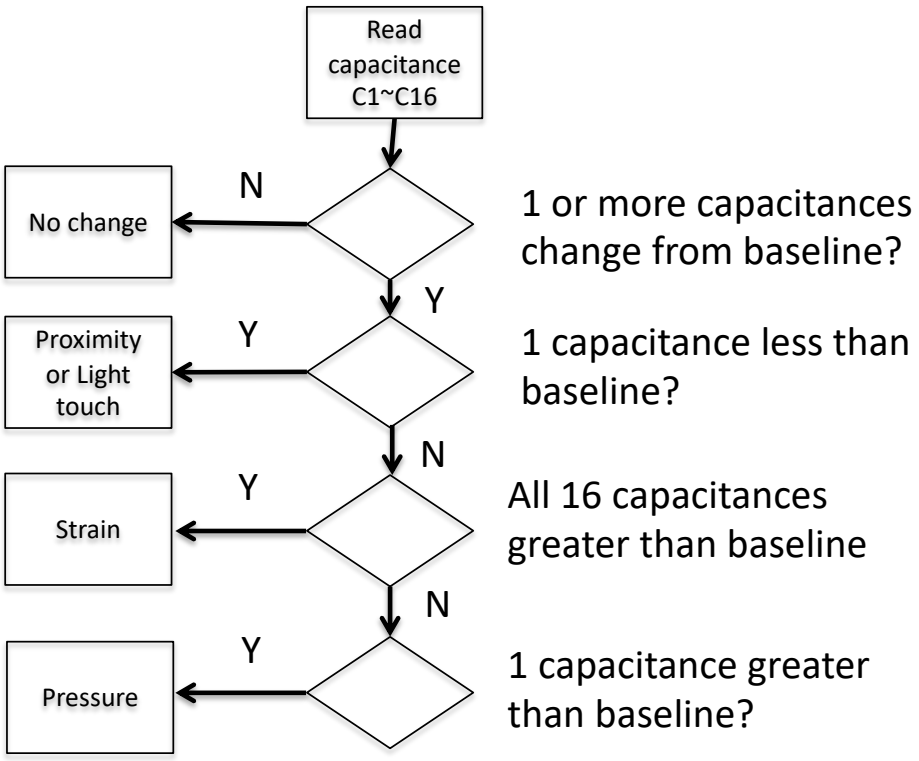

Figure 3.3: Flowchart describing simple interactions with the sensor

The dielectric architecture is illustrated in Figure 3.1 (b) and (c). The air gaps render the sensor easily deformable and bring about a large increase in capacitance when compressed due to the decrease in volume of air. This makes the sensor more sensitive to pressures compared to using

a solid dielectric and also aids in differentiating between the different stimuli as discussed in a later section.

The sensor has a similar 4 X 4 electrode array layout as the sensor in Chapter 2, hence, the same readout electronics are used for this sensor as those presented in Chapter 2, shown in Figure 2.10.

3.4 Fabrication

The fabrication of the sensor is a simple three-step process as illustrated in Figure 3.4. The first step involves casting the patterned dielectric in a 3D printed mold and spinning a base layer (Figure 3.4 (a)). The elastomer used is Ecoflex^{TM} 00-30, which is degassed prior to molding to get rid of any air bubbles. The dielectric is 1.5 mm thick with air gaps in the form of cylinders of height 1 mm and radius 1 mm at a pitch of 2 mm center to center. The base layer is spun at 300 rpm and cured at 60^{o}C for 10 mins. The second step is to pattern the sensor electrodes (Figure 3.4 (b)). The electrode material is a carbon black composite made by mixing carbon black particles (H30253 Carbon Black Super P® Conductive) with Ecoflex^{TM} 00-30 in the ratio 1:10 by weight. The electrodes are rectangular strips (resistivity $\rho = 0.1$ Ω-m) of 4 mm width (4mm edge to edge distance), 5 cm length and 100 μm thick. A second set of electrodes is patterned on the base layer. At the edge of the electrodes, copper tapes are added, buttressed by Kapton tape to be connected to the readout circuit. An encapsulating layer of Ecoflex is spun at 300 rpm on top of the electrodes on the dielectric layer (Figure 3.4 (c) left). The dielectric layer now encapsulated, is peeled off from the mold. An adhesive layer of Ecoflex is spun on the electrodes of the base layer (Figure 3.4 (c) right). The dielectric layer is immediately but carefully laid down on the uncured Ecoflex adhesive layer to bond the dielectric layer with the base layer (Figure 3.4 (d)). The whole sensor

is then cured in the oven at 60ºC for 20 mins. The electrodes are aligned such that they are perpendicular to each other, forming row and column electrodes. The intersections of the row and column electrodes are called taxels. Each of these is a location where the sensor can detect the mentioned stimuli.

In order to scale up the fabrication process a combination of existing manufacturing processes may be implemented. The molding step can be done in a larger mold. Alternative to the carbon black composite, CNTs, may be spray coated through a shadow mask to pattern the electrodes. The adhesive layer of uncured elastomer may be applied using automatic film applicators such as Elcometer 4340. The different layers can be aligned and bonded together using a roll-to-roll process.

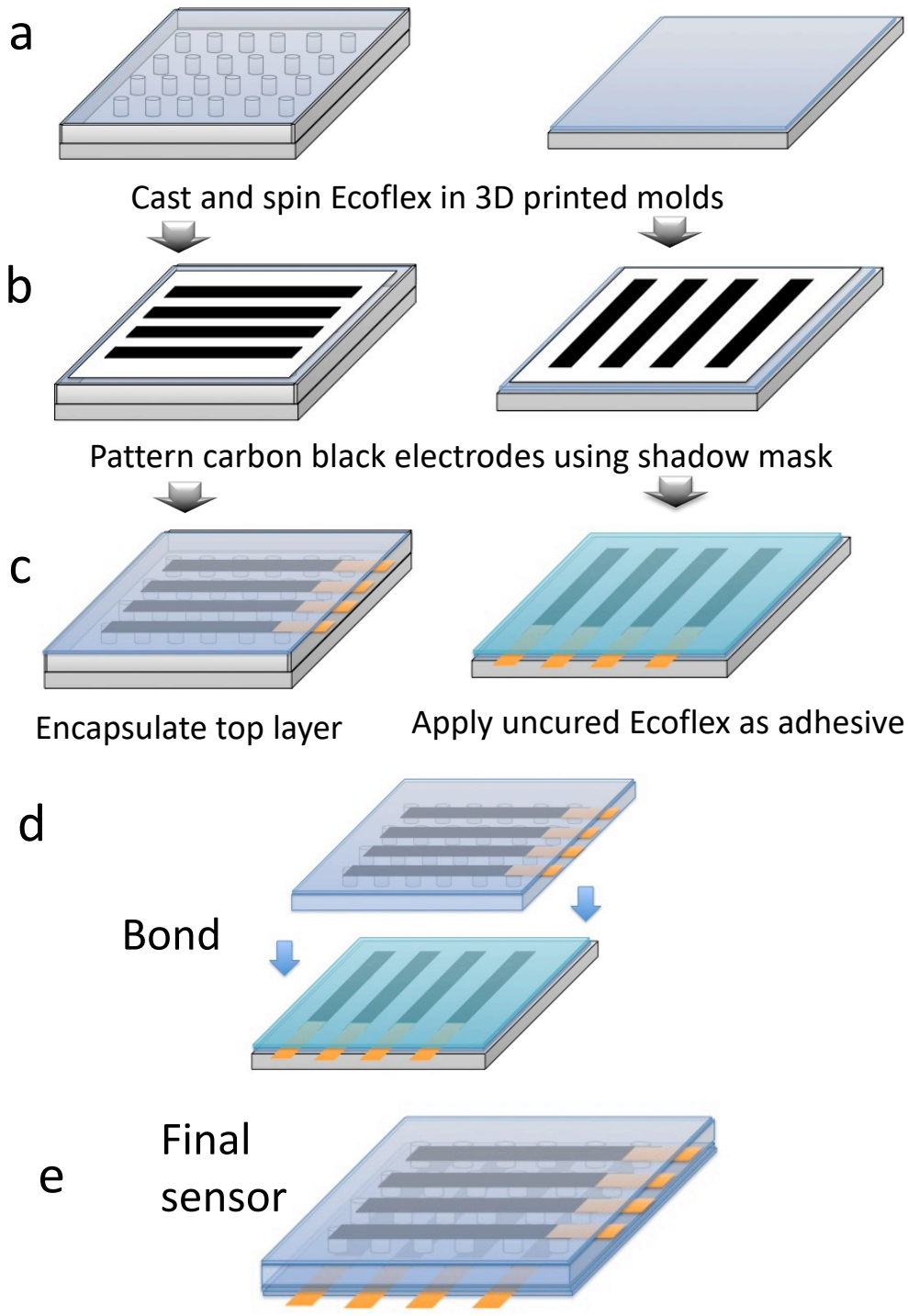

Figure 3.4: Fabrication of sensor (a) casting and spinning Ecoflex in mold and on petri dish respectively (b) patterning carbon black electrodes using a shadow mask (c) (left) apply Ecoflex to encapsulate top layer (right) apply uncured layer of Ecoflex as an adhesive (d) bond the two layers (e) final sensor

3.5 Results and discussion

3.5.1 Proximity and light touch

Similar to the sensor in Chapter 2, proximity and light touch detection is implemented using mutual capacitance. The lateral position of a finger can be detected on the basis of the capacitance changes observed. Each combination of row and column electrodes is scanned sequentially. A sample case using the taxel R2C2 on the second row and second column is used for demonstration purposes as shown in Figure 3.5. The four signals of each plot in Figure 3.5 correspond to the signals coming from the four column electrodes and the four plots correspond to the signals coming from the four rows. Therefore, the signal coming from the taxel R2C2 is the green signal in the second plot from the top. The first interaction with the sensor is a hovering finger. It is observed in the case of proximity at time t=10 s, the activated taxel decreases in capacitance by approximately 5%. However, the neighboring taxels also experience a decrease in capacitance of a very close magnitude to the activated taxel. This is because the fringe fields of the neighboring taxels (which are 4 mm apart) span a region that is close enough to couple to the finger (width of approximately 15 mm).

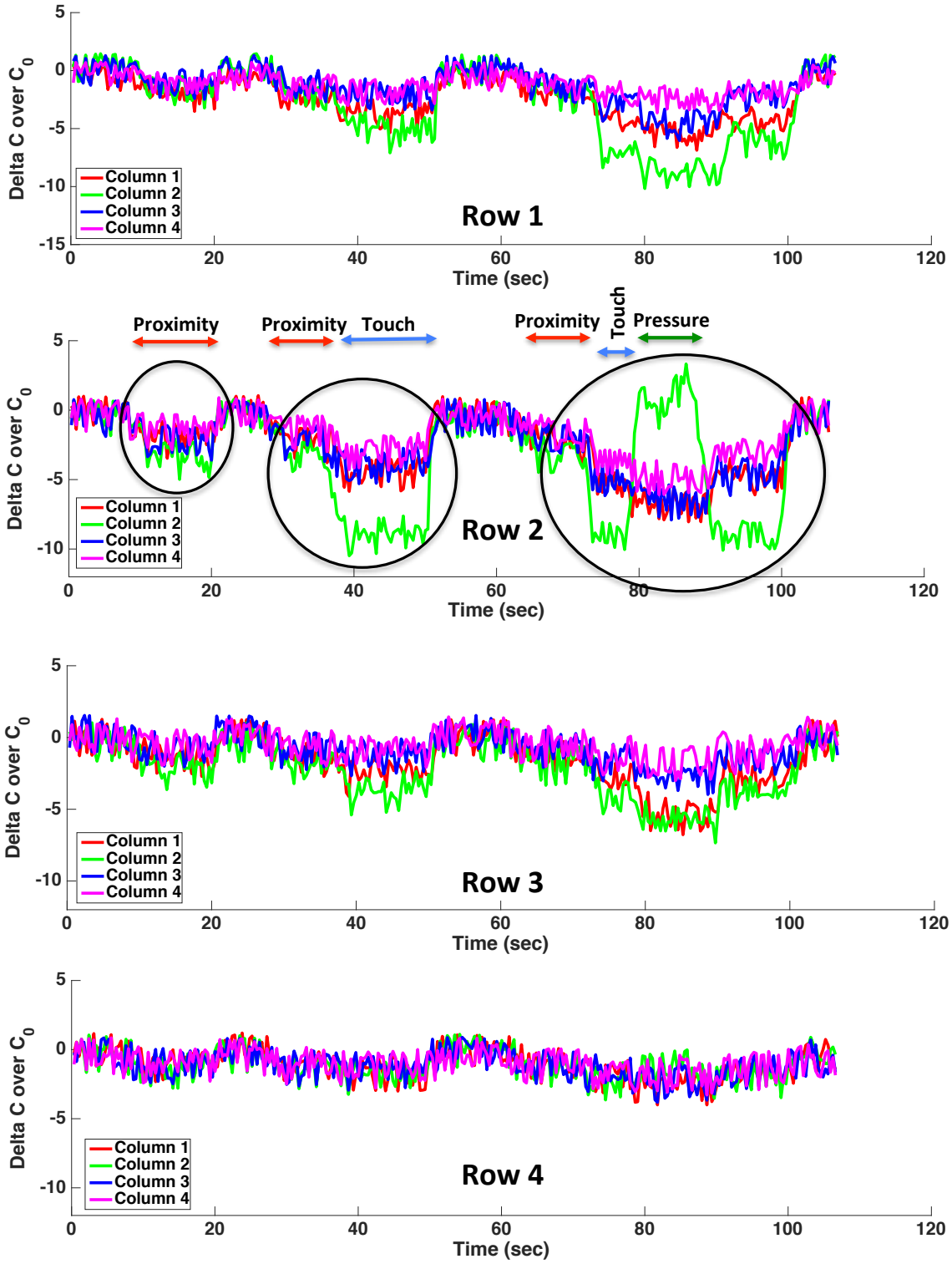

Figure 3.5: Response of sensor to a proximity, light touch and press of a finger on taxel (row 2, column 2), demonstrating the use of neighboring taxel response to differentiate between the different stimuli

Again in Figure 3.5, the second interaction with the sensor is a touch - following a hover. Upon touching the taxel R2C2 (applying close to zero pressure) at time t=40 s (as seen in Figure 3.5), its capacitance decreases by approximately 10% while the maximum decrease observed by the neighboring taxels is 5%. This is because upon contact, the coupling with the finger is much larger than through air (when it is hovering). Upon retracting the finger, the capacitance returns to the baseline value along with the neighboring taxel capacitances.

The third interaction is a hover followed by a touch and then a pressure at taxel R2C2. The proximity and touch interactions are similar to before. A small pressure is applied at t=80s such that the capacitance of taxel R2C2 returns close to its baseline value. Now, without any information from the neighboring taxels it is difficult to assess this stimulus because this return to steady state is similar to the act of retracting a finger after a touch at time t=50 s. However, upon application of the pressure it is observed that the neighboring taxels still demonstrate a decreased capacitance throughout the entire time the pressure is applied, and even when the pressure is released- until the finger is retracted. This is because even though the physical deformation is only experienced by taxel R2C2, the fringe field coupling still exists between the finger and the neighboring taxels. When retracting finger at time t = 50s where the neighboring taxels also return to their baseline value at the same time.

This ambiguity in detecting a pressure only arises when the pressure is applied by a human finger. In case of pressures applied by an inanimate object such as wood or plastic there are very small changes in sensor capacitance due to mutual capacitive effects and any change in sensor capacitance is caused predominantly by changes in overlap capacitance. Therefore, the pressure applied by a plastic finger would not be preceded by a decrease in capacitance as in the case of a human finger. The application of a pressure by the plastic finger will only be registered as an

increase in capacitance due to the decrease in dielectric thickness between the capacitor electrodes, in which case interpreting the results can be done using the simple flow chart in Figure 3.3. However, in order to incorporate interactions with a human finger a more detailed flowchart is necessary as the one shown in Figure 3.6.

Here, assuming the interacting object is comparable to the size of a single taxel, the algorithm begins by sorting the changes in capacitance from the baseline values ΔC_{ij} according to their magnitudes with the maximum negative value being the first element in the array and the maximum positive being the last element in the array. Once sorted it searches for any changes that are above the noise threshold. Any changes large enough to be considered a stimulus is then investigated based on their direction of change. All positive changes are brought about by non-human objects such as wood or plastic that does not have mutual capacitive effects. If a single taxel experiences an increase in capacitance it is a pressure applied, however if the entire array experiences an increase (above a certain threshold) it is a stretch. If there are negative changes in capacitance it is likely that a human finger (or a grounded metal) is interacting with the sensor. If the decrease in capacitance is beyond the touch threshold then it is considered to be a touch, otherwise it is a hovering finger. Once a touch is detected, a flag is enabled which is checked every cycle. If the touch flag is found to be enabled in the previous cycle, then the taxel that was assigned a touch is checked to see if it is still activated as a touch or if the capacitance change is reduced. If reduced, the neighboring taxels are checked to see if they experience reduced capacitance due to the proximity of the finger. In that case this will be a pressure applied similar to the situation at t=80s in Figure 3.5. Otherwise it is the retraction of the finger from a previous touch position similar to the situation at t=50s in Figure 3.5.

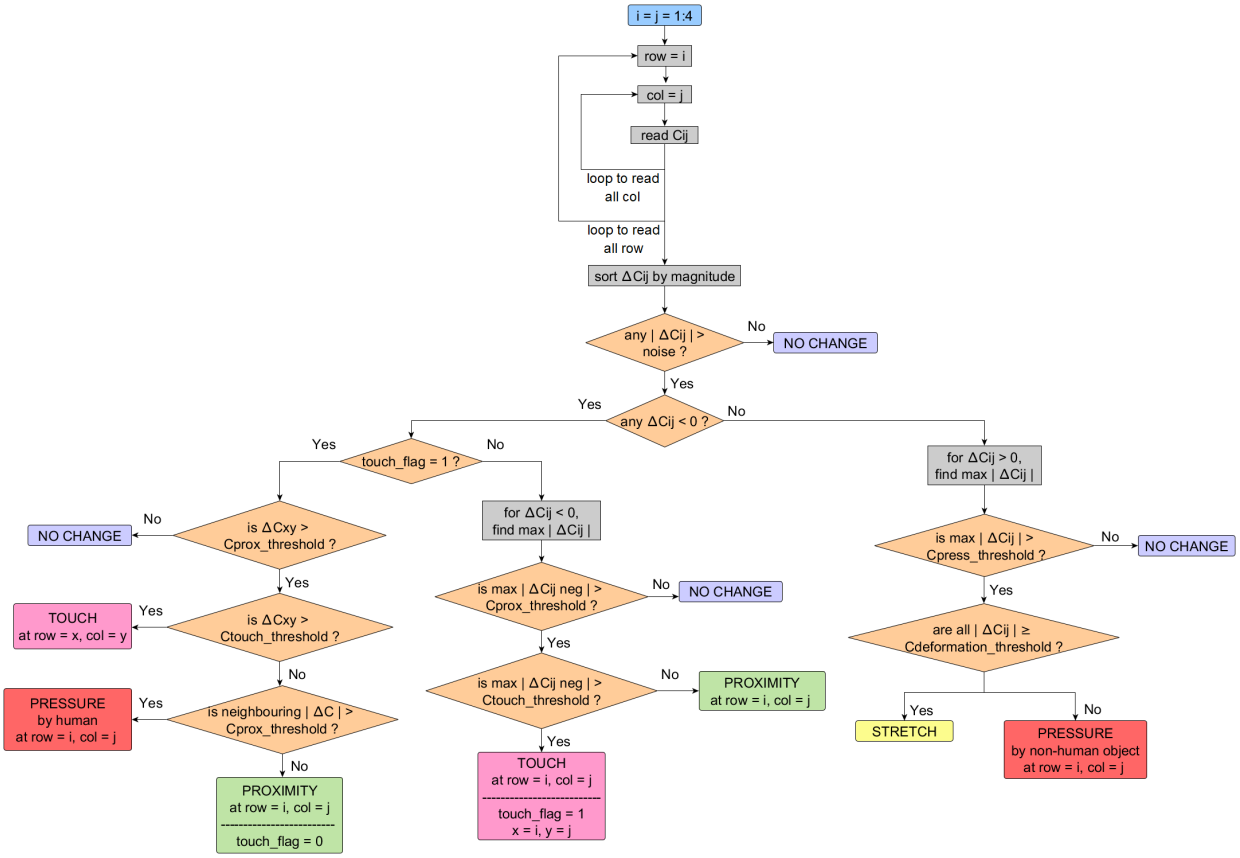

Figure 3.6: Detailed flowchart incorporating complex interactions in order to detect proximity, shear and stretch produced by an object comparable in size to the taxel spacing.

This investigation demonstrates that with data from an array of sensors that has a resolution that is around the magnitude of the interacting finger it is easy to differentiate between hover, touch and press. This differentiating capability can be further enhanced by increasing the pressure sensitivity of the sensor such that upon applications of a very small pressure the increase in capacitance will be very high such that it crosses the steady state value and therefore removing the ambiguity between a retracting finger and a press.

3.5.2 Pressure and displacement

To investigate the pressure sensitivity different loads are applied using a dynamic mechanical analyzer and a load cell. In order to maintain constant area a small indenter of 14 mm X 14 mm cross-sectional area and height 50 mm was used. The experimental setup is shown in Figure 3.7 below.

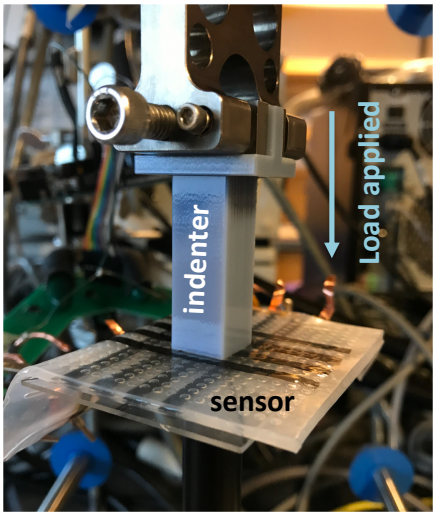

Figure 3.7: Experimental setup to apply normal pressure

Experimental data of applying 5 cycles of sinusoidal load stimulus of 0.1 Hz frequency and 4 N load amplitude (peak to peak) are plotted in Figure 3.8 below. A small force of approximately 0.2 N is applied before the experiment is commenced to ensure proper contact of the indenter with the surface of the sensor. It is observed that the capacitance follows the load in a similar sinusoidal manner as shown in Figure 3.8 (a). The displacement of the surface of the sensor due to the

application of the force is plotted versus ΔC/C, and again follows the applied load, with some creep.

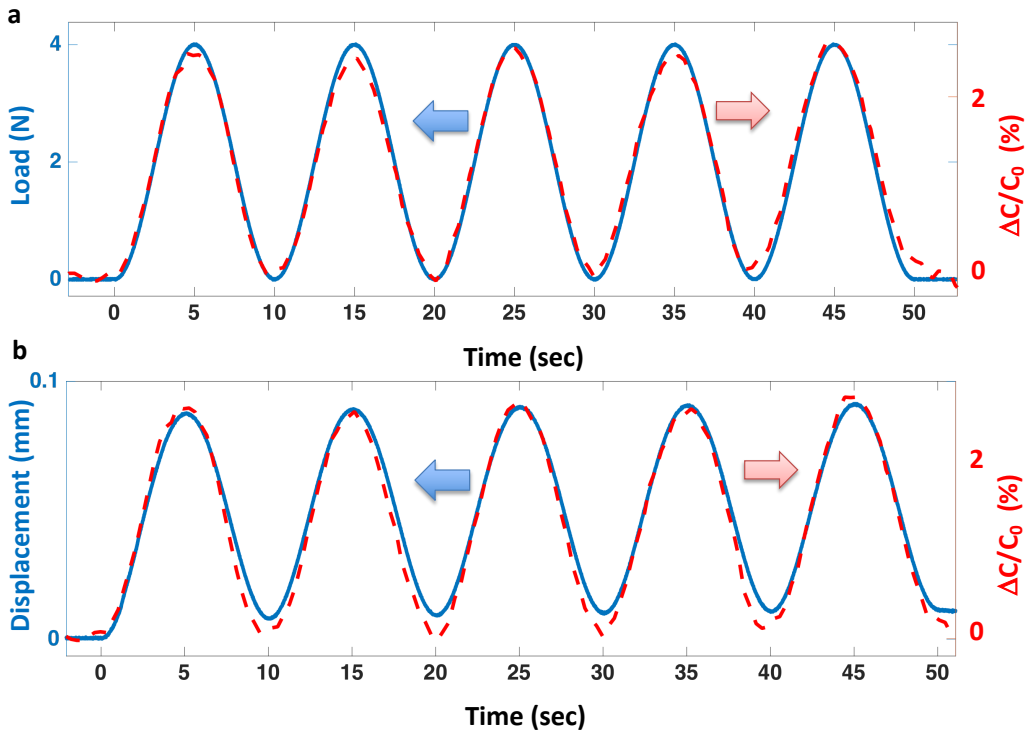

Figure 3.8: (a) load applied with % change in capacitance (b) displacement of the sensor surface and % change in capacitance

A range of normal loads are applied, corresponding to strains of up to 20%. The $\Delta C/C_0$ is plotted against the applied pressure in Figure 3.9. The change in capacitance is fairly linear with the applied pressure (observed from the linear fitted line in blue in Figure 3.9). A sensitivity of 0.13% per kPa pressure is obtained from the linear fit in the range 20-80 kPa. The smallest pressure detected is 20 kPa. To put this in perspective a cube of sugar applies a pressure of 0.3 kPa so there is still work to be done to increase the pressure sensitivity of this sensor.

Theoretically, the sensor baseline capacitance for a single taxel 4 mm X 4 mm, incorporating overlap and fringe fields should be ~0.6 pF according to the Equation (3-1) [82].

$$C = \frac{\varepsilon WL}{d}\left(1 + \frac{d}{\pi W} + \frac{d}{\pi W}\ln\frac{2\pi W}{d}\right) \times \left(1 + \frac{d}{\pi L} + \frac{d}{\pi L}\ln\frac{2\pi L}{d}\right) \quad (3\text{-}1)$$

However, the readout circuit reads 1.5 pF. The readout circuit introduces significant parasitic capacitance, $C_{parasitic}$, in turn causing the readout value of $C_{readout} = C_{0real} + C_{parasitic}$ to be greater than the real baseline value of the sensor capacitance C_{0real}. This results in the apparent sensitivity to be lower than the actual sensitivity since the ΔC value is divided by a larger $C_{0apparent}$ value to get $\Delta C/C_0 = \Delta C/C_{0apparent}$, but in reality, the actual sensor C_{0real} value is much smaller. If the real and smaller magnitude of C_{0real} is obtained from the sensor, then ΔC will be divided by a smaller value of C_{0real} which will increase the magnitude of $\Delta C/C_0 = \Delta C/C_{0real}$ for any given stimulus. This is proved in Chapter 4 where a custom readout circuit V2 is designed for sensor III with much lower parasitic capacitance which leads to a smaller baseline C_0 and therefore the apparent sensitivity is greater and much closer to the real sensitivity than when measured using this readout circuit V1.

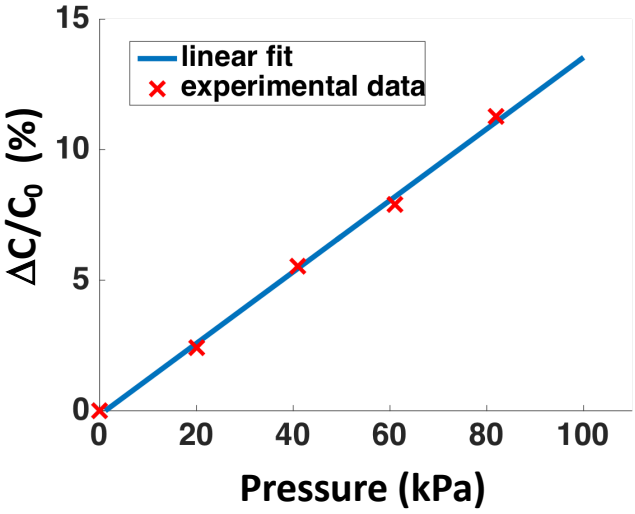

Figure 3.9: ΔC/C₀ VS Pressure

For larger loads (over 4 N) a creep effect is observed as shown in Figure 3.10 (a) where it is seen that upon releasing the load (to 0 N) at time t = 18 s, the surface displacement remains at 60 μm instead of returning to 0 mm. This is characteristic of a viscoelastic material. Plotting load with $\Delta C/C_0$ for the same five cycles in Figure 3.10 (b) and displacement with $\Delta C/C_0$ in Figure 3.10 (c) shows that the capacitance follows a similar trend as displacement rather than load. This is intuitive from the definition of a parallel plate capacitance $C = \varepsilon \frac{A}{d}$. This sensor is therefore a better displacement sensor, and in order to attain proper force values for a time varying signal, load history needs to be taken into consideration and modelled.

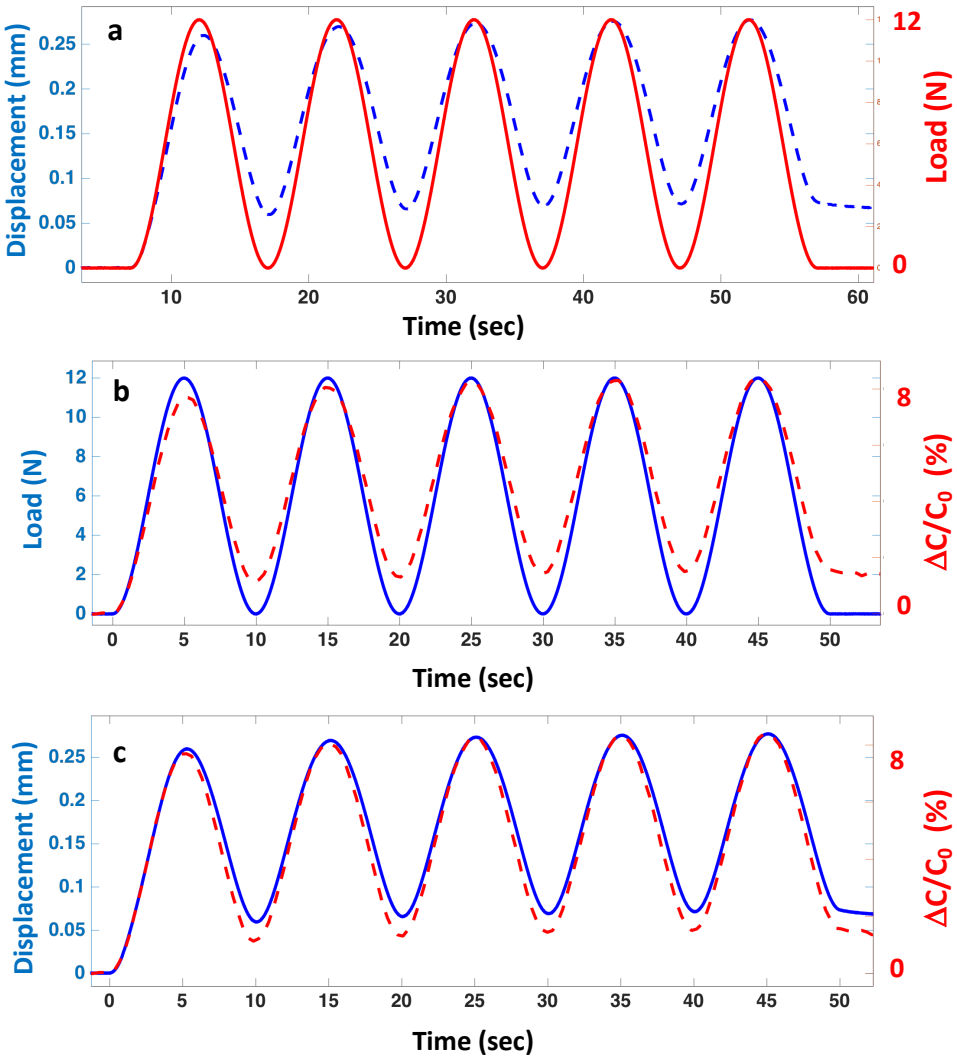

Figure 3.10: (a) Applied sinusoidal load and displacement for 5 cycles (b) Applied load and $\Delta C/C_0$ with time (c) Displacement of sensor surface with $\Delta C/C_0$

3.5.2.1 Mechanical characterization

The loading and unloading cycles for a range of applied compressive loads are shown in Figure 3.11 below where the applied pressure is plotted against the normal strain. It is observed that the initial ramp responses to loading for all four applied loads coincide and appear

approximately linear in the range shown. An elastic modulus of approximately 500 kPa is calculated from the gradient of the linear part of the loading segment. This results in the linear $\Delta C/C_0$ relation with increasing pressure shown in Figure 3.9. Upon unloading there is a gap or apparent hysteresis between the loading and unloading half cycles, which is characteristic of creep. We infer from this that the sensor material is viscoelastic in nature. Additionally, the cycles following the first cycle also indicate that creep is occurring.

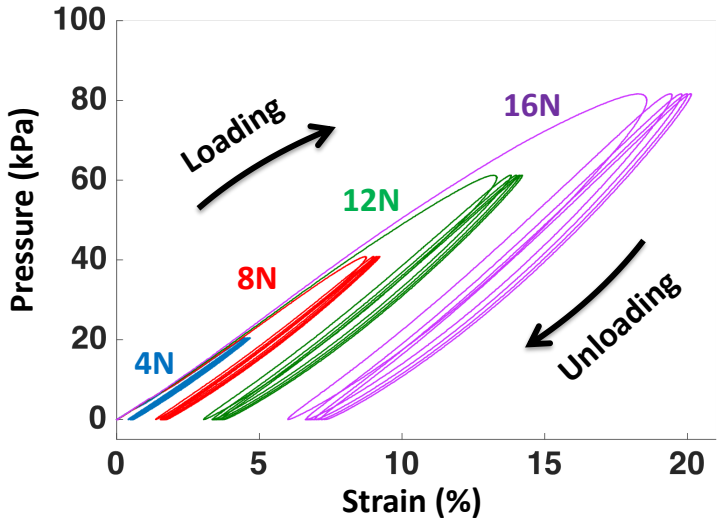

Figure 3.11: Pressure VS strain - loading and unloading

In comparison to a sensor with solid dielectric the patterned dielectric with air gaps (bubble dielectric) has an elastic modulus of half as large, due to the presence of the air gaps. This is shown in Figure 3.12. A more compliant dielectric means greater deformation of the dielectric for a given pressure, and in turn a greater change in capacitance, thereby increasing the sensitivity to pressures applied. It is observed that applying a 61 kPa pressure on the sensor with patterned dielectric, a 7.7% change in capacitance is attained, which is 2.8 times the 2.7% change using the sensor with a solid dielectric. The change (hence sensitivity) is greater than the

expected value of 2 times (the elastic modulus is 2 times greater for the solid dielectric case). This additional increase in $\Delta C/C_0$ is due to the fact that the baseline capacitance C_0 in case of the sensor with a solid dielectric (C_0=2.8 pF) is greater than the baseline capacitance of the sensor with the patterned dielectric (C_0=2.4 pF). This is because the effective dielectric constant of the patterned dielectric is a combination of air and Ecoflex™ which is less than solid Ecoflex™.

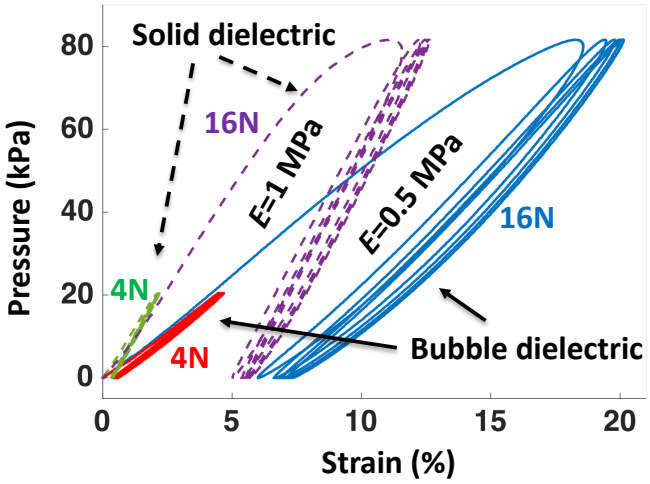

Figure 3.12: Comparing loading and unloading of bubble dielectric with solid dielectric

In order to investigate the viscoelastic nature of the sensor a step load of 10 N (51 kPa) is applied as shown in Figure 3.13. The strain increases rapidly with the applied step in force and then continues to increase with a pattern similar to an exponential decay. Upon releasing the load, the strain once again decreases abruptly and then gradually decreases with an exponential decay.

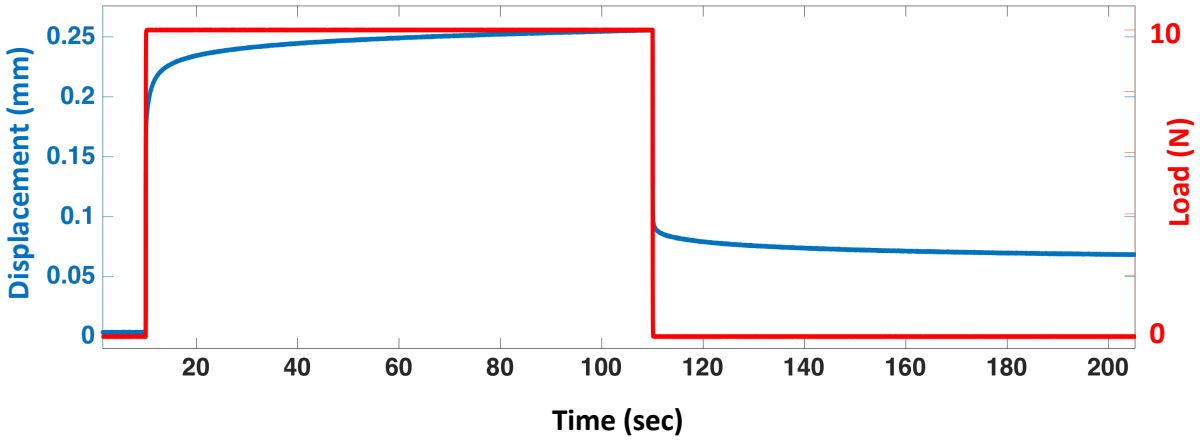

Figure 3.13: Response of sensor to a step load

We can see from the step response that the initial response is like that of a spring (represented by a material modulus *E1*), which is responsible for the initial rise in strain. The exponential decay can be modeled using a Voigt model, i.e. a spring (*E2*) and dashpot ($\eta 2$) in parallel to each other and in series with the first spring (*E1*). Finally, strain continues to decrease with time. This can be attributed to a second dashpot ($\eta 1$) in series with the first spring (*E1*) forming a Maxwell model. The complete model, also known as the Burgers model, is shown in **Figure 3.14** below.

We investigate the load step response in further detail. In the model shown in **Figure 3.14**, the strain across the elements of the Voigt model is the same and the stress across the elements of the Maxwell model is the same. Using these conditions and Laplace transforms, it can be shown that for a step in stress, σ_o, the strain is given by:

$$\varepsilon(t) = \sigma_0[\frac{1}{\eta_1}t + \frac{1}{E_1} + \frac{1}{E_2} - \frac{1}{E_2}e^{-\frac{E_2}{\eta_2}t}]. \quad (3\text{-}1)$$

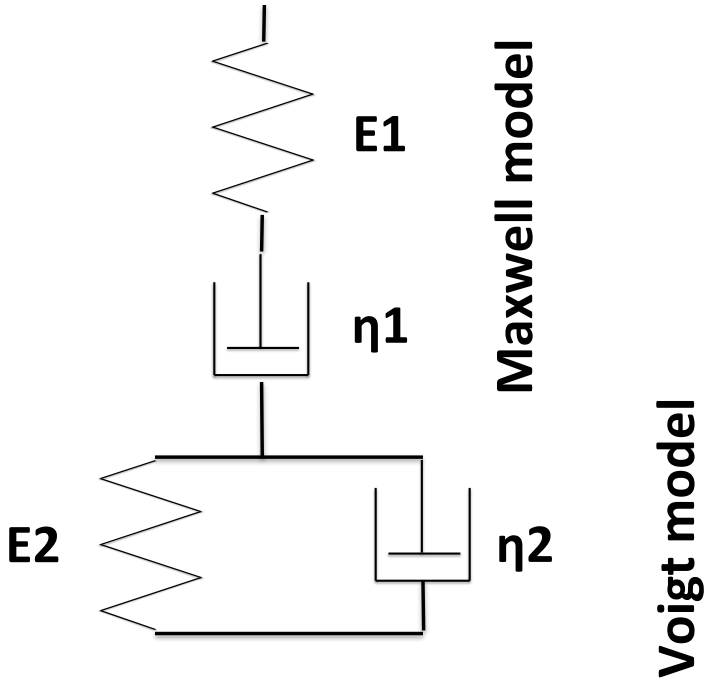

Figure 3.14: Burgers model, used to describe the viscoelastic response of the sensor.

Using least square fitting in Matlab, for the parameters $\eta 1$ = 5.08 GPa·s, $E1$ = 500 kPa, $\eta 2$ = 360 MPa·s and $E2$ = 2.4 MPa the model described shows a close fit to the experimental data, as shown in Figure 3.15. The value of $E1$= 500 kPa from the Matlab simulation is similar to the magnitude of elastic modulus of the sensor determined experimentally in the earlier part of this section. The strain rate at long times – which corresponds to the creep rate – is estimated to be 6.9 X 10^{-6} /s from the slope, as shown in Figure 3.16. From Equation 3-1 this corresponds to a value of $\eta 1$= 7.3 GPa.s, which is close to the simulation parameter of 5.08 GPa.s. (An overestimate is expected, since the Voigt element is still responding as well.)

At short times, displacement and force are directly proportional to each other, as only the spring $E1$ is activated. The high frequency/short time response is derived from the step load

applied. According to the model, the response should be instantaneous, but in fact $\Delta t=0.03$ s is the time required for the displacement to reach the elastic spring limit, as shown in Figure 3.17. However, this limit is determined by the speed at which the dynamic mechanical analyzer can apply a fast step load, as seen in the inset of Figure 3.17. The mechanical model is valid at least up to the time constant of the mechanical characterization system, which is ~ 0.03 s, or 33 Hz. At shorter times, the stress and strain are still proportional, suggesting the model is valid up to at least the sampling rate of the instrument – which is 100 Hz (0.01 s). As long as changes in capacitance are measurable at such rates, the sensor response to force and displacement should be effective to at least 100 Hz which is similar to the refresh rate of touch screen sensors in hand-held devices.

Due to the viscoelastic nature of the sensor, for constant forces or slow moving stimuli the sensor needs to be investigated further to be able to predict the load applied accurately from the change in capacitance with the time varying stimulus. In other words, the sensor is good for measuring displacement of the surface, but shows a time dependent and history dependent response when used as a pressure sensor. This time and history dependence is expected to be evident at times longer than about 1 s, as seen from Figure 3.12.

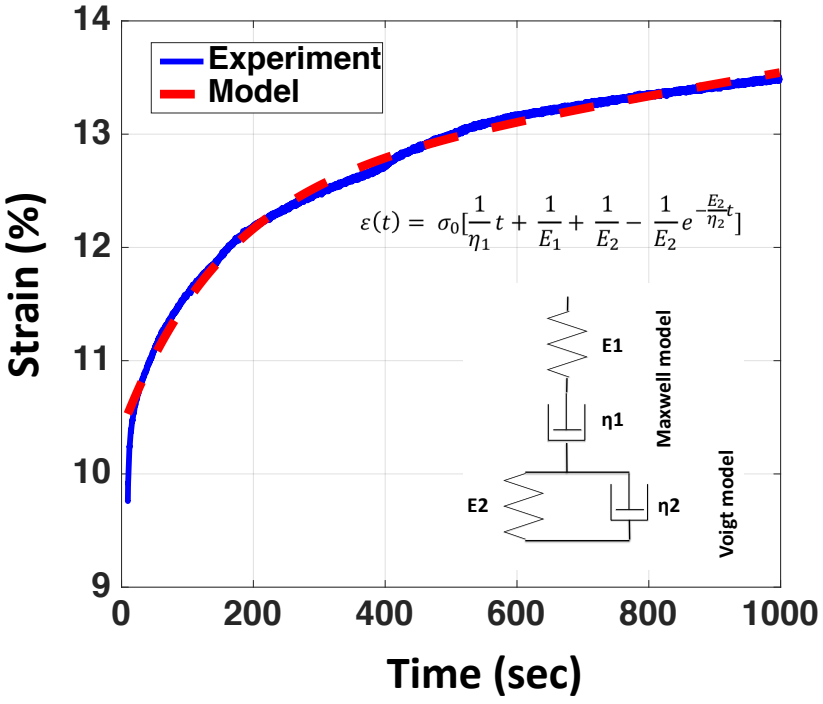

Figure 3.15: Model and experimental data for sensor response for a load step stimulus

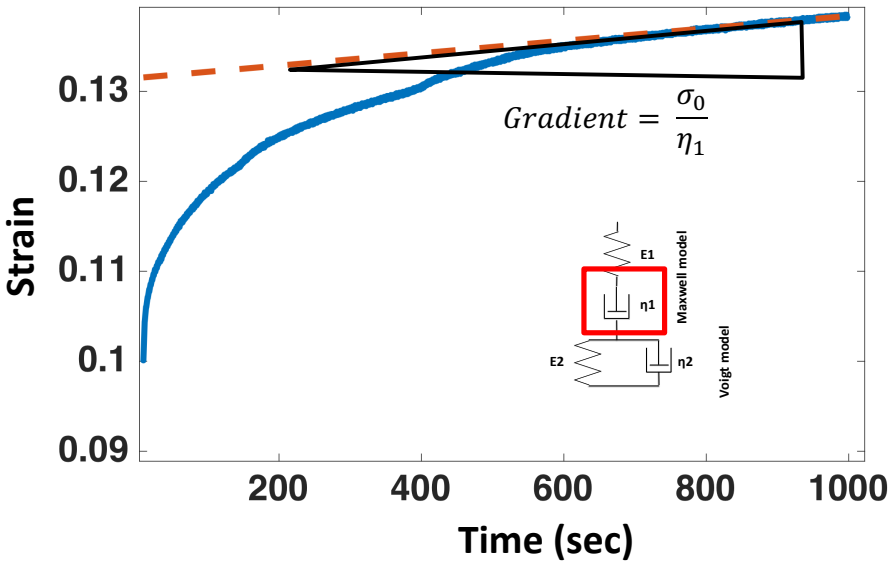

Figure 3.16: Obtaining η_1 from the sloipe of the response at long times.

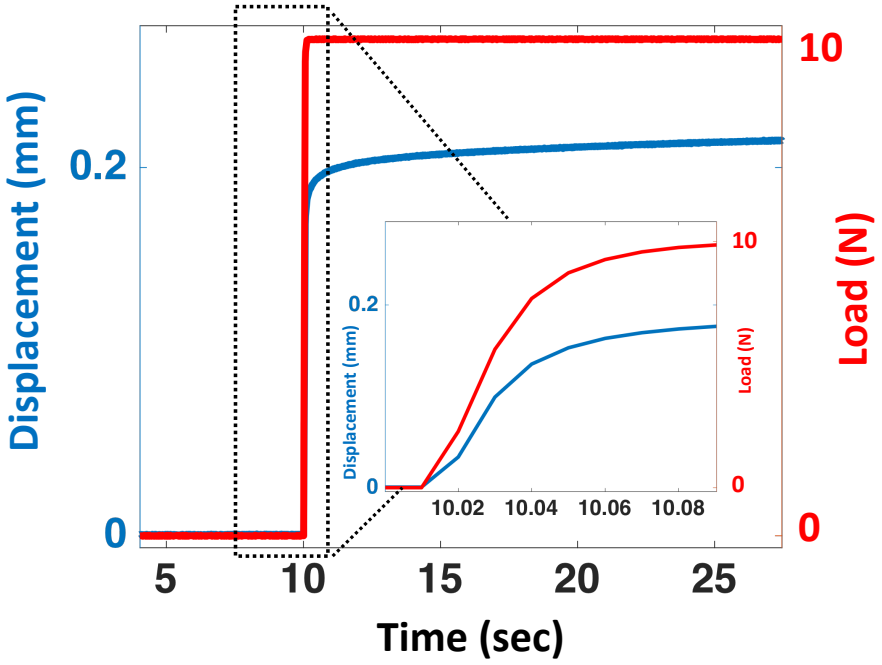

Figure 3.17: High frequency response

3.5.3 In plane strain response

Upon application of a longitudinal (in plane) strain the area of overlap of the electrodes increases, the dielectric thickness decreases and therefore the capacitance increases. In order to characterize the strain response the sensor is clamped at one end to suspend it vertically and weights are hung from the other end. The capacitive response to the applied load is shown in Figure 3.18 below. It is observed that upon stretching, the unclamped edges of the sensor curve inwards. This is due to the Poisson effect, where the width decreases with an increase in length - but only in the middle since the top and bottom ends are clamped. This manifests itself in the capacitive response shown below. The images on the top row are of the sensor being stretched vertically downwards. The bottom row is the capacitive response to the strain. Each bar plot represents the

4 X 4 array shown in the top row. The increase in capacitance of the two columns at the outer edges is less than the two inside columns.

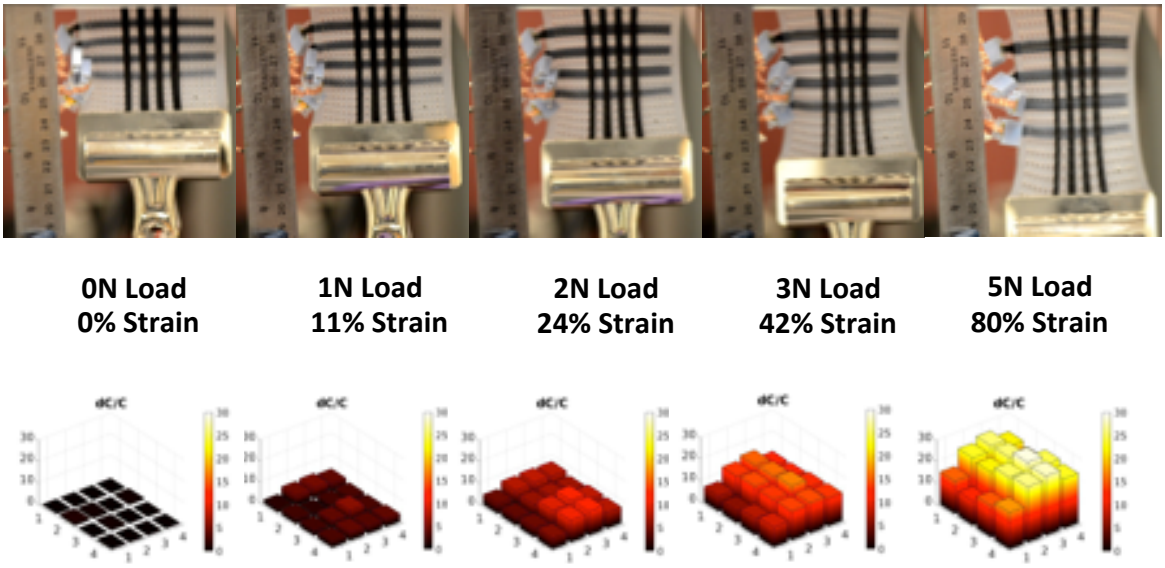

Figure 3.18: Sensor response to longitudinal strain. The top row shows photos of the sensor as load is increased from left to right. The bottom row shows the corresponding capacitance readings across the array.

The change in capacitance is plotted with strain in Figure 3.19. It is observed that the sensitivity or capacitive gauge factor is approximately 0.35 $\pm$ 0.007 $\Delta C/C_0$/strain. The uncertainty is due to the noise in the capacitance measurement. In theory the expected gauge factor should be 1 assuming a Poisson's ratio of σ=0.5. A strain in the y axis of ε_y should lead to a strain of $-\sigma\varepsilon_x$ and $-\sigma\varepsilon_y$ where σ=0.5. This leads to $C'=(1+\varepsilon_y)C_0$ (where C' is the new capacitance after stretch and C_0 is the baseline capacitance) and therefore a gauge factor of 1. However, the experimental gauge factor is much smaller. This is due to the baseline capacitance measured using the current readout circuit V1 being much larger than the actual readout circuit due to the addition of parasitic capacitance. Theoretically, incorporating the effects of fringe field the capacitance of a single taxel

of dimensions 4 mm X 4 mm with a dielectric thickness of 1.6 mm, should be ~ 0.6 pF following the equation (3-1) [82] while the actual measured capacitance is 1.5 pF.

The absolute change in capacitance measured due to 80% strain is ~0.45 pF. Using this value and the theoretical value of baseline capacitance the $\Delta C/C_0$ value obtained is 75% which is close to the expected value for a strain of 80% for a gauge factor of 1 (75/80=15/16).

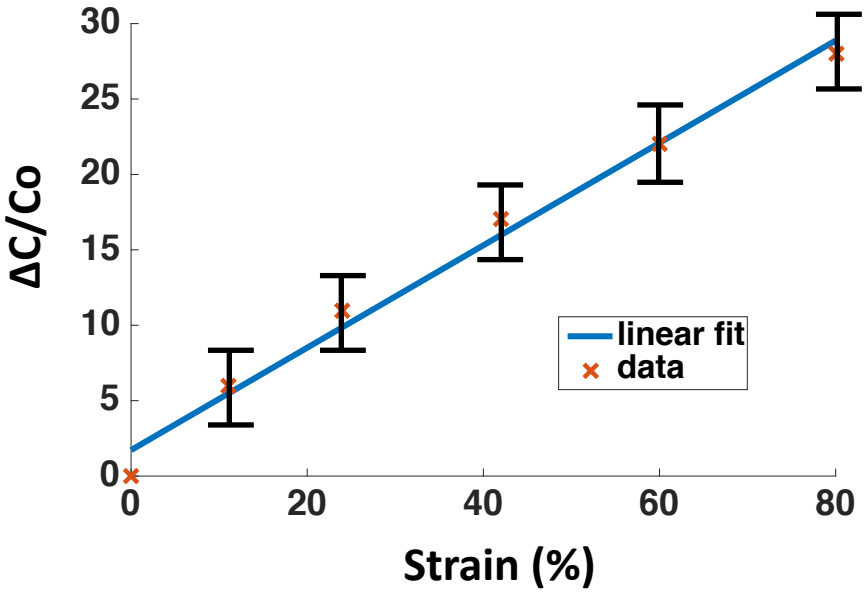

Figure 3.19: Change in capacitance with strain

A strain results in an increase in capacitance similar to a pressure. In order to differentiate between the two stimuli, the array structure is necessary. In the case of a pressure applied there is a localized increase in capacitance. However, in case of a strain, the entire array would experience an increase in capacitance as shown in Figure 3.18. Where the device is applied as a skin onto a rigid substrate, the differentiation is not necessary.

3.6 Conclusion

This soft multi-modal sensor has the ability to detect proximity and light touch by means of the mutual capacitance effect. It also detects pressure and strain by means of deformation of the sensor's overlap capacitor. Upon approach and light touch by a human finger, the mutual capacitance decreases (by approximately 5% and 10% respectively), while the application of a pressure or in plane strain leads to an increase of the overlap capacitance (with a sensitivity of 0.13% $\Delta C/C_0$/kPa and 0.35 gauge factor for strain respectively).

The opposing direction of response to the proximity and contact stimuli compared to the deformation-based stimuli enables easy differentiation. However, in case of a touch followed by a light pressure and a touch followed by a retraction of the finger both result in similar responses, which leads to ambiguity. Under these circumstances the information from the neighboring taxels is used to decipher the ambiguity. In order to aid this process of differentiation, the pressure sensitivity is enhanced using air gaps in the dielectric (similar to works in literature in [58], [81] and [3]), such that upon application of a small pressure, the capacitance increases beyond the baseline capacitance level.

Table 3.1 below shows a comparison of some stretchable pressure sensors in the literature. Although the literature shows greater sensitivities than this work, they do not offer the mutual capacitive benefits such as proximity and light contact of a human finger – abilities that are important for artificial skin applications in robotics.

Table 3.1: Comparison of sensor specification with literature

	Type	Pressure		Strain	
		Sensitivity	Range	Gauge factor	Range
Lipomi [14]	Capacitive	0.02%/kPa	0-1 MPa	0.004	50%
Park [18]	Capacitive and resistive	14%/kPa	0-25 kPa	1	30%
Chapter 3	Capacitive	0.15%/kPa	0-80 kPa	0.35	100%

Good pressure-sensitivity of such a soft sensor is in general a desired feature for a number of applications, especially in the field of artificial skin for robotics and prosthetics. However, one important stimulus for artificial skin applications is localized shear. This sense enables the system to interact with fragile objects and perform delicate manipulations. The next section of this thesis extends this work to incorporate shear sensitivity in addition to the existing range of stimuli.

Chapter 4: Artificial skin – proximity, touch, pressure and shear sensor

4.1 Summary

Having a robot feel its environment is a challenge, particularly using hard sensors that can make control of interactions challenging. Soft sensors that detect changes in capacitance in a similar way to touch screen are discussed in this thesis. Similar to the sensor in Chapter 3, this sensor can detect and differentiate between the proximity and light touch of a human, applied pressure and even shear. Shear sensing is important since it enables emotional interactions such as a caress and also helps control interactions with fragile objects such as eggs. Proximity is detected using fringing fields. Pressure and shear detection are made more sensitive thanks to the dielectric architecture that increased compliance in 3 axes. The sensing skin is as compliant as skin, and smooth, unlike many shear sensors. The simple fabrication method and low cost materials make it attractive to consider creating an array of sensors for use as a robot skin or even artificial skin for prosthetics.

4.2 Introduction

To accommodate for complex interactions between humans and robots, it is important to design a method for touch identification that can be active over most of the robot's surface area i.e. an "artificial skin" [1], [7]. Such a technology is also sought in the field of neurally controlled prosthetic devices to enhance motor control [83], [84].

Mechanically, human skin is non-linear and viscoelastic. According to the literature, the dermis is assumed to be the principal structure contributing to the mechanical properties of the skin [38]. The main components of the dermis include the collagen fibers (80% of the dermis dry weight) and elastin – an elastic protein which present elastic properties (Young's modulus from 150 to 300 kPa and up to 1 GPa) [38]. Their deformation mechanism is mainly responsible for the behavior of the skin. For small strains applied to the skin, the collagen fibers orientate in the direction of the stress. The skin related low stiffness is thus mainly due to the elastin mechanical properties. For large strains, both collagen and elastin fibers are stressed. Under these circumstances the high elastic modulus of the collagen fibers modifies the elastic response of the skin, which becomes stiffer. The viscosity in skin is due to the movement of the interstitial fluids. Figure 4.1 (a) shows the components of the skin as the skin is being strained and Figure 4.1 (b) shows the stress strain curve showing a small initial elastic modulus *E1* and later with larger strains a larger elastic modulus *E2*. Any form of artificial skin technology is expected to have a similar non-linear mechanical characteristic.

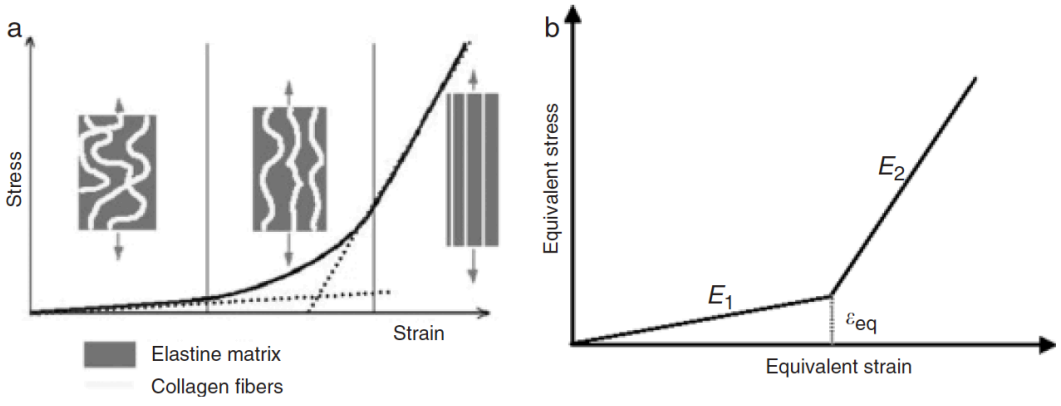

Figure 4.1: a) Components of the skin and their mechanical properties (b) stress-strain curve for skin [38]**.**

The functional requirements of an artificial skin are considered to include a skin-like surface, stretch-ability and the ability to sense tactile stimuli such as light touch, pressure and shear [1]. There is a plethora of work in literature on flexible touch and pressure sensors. These can be capacitive, resistive, or piezoelectric. The flexibility aspect is incorporated using active materials such as silver nanowires [13], carbon nanotubes [75], liquid metals [85], and hydrogel [17]. However, in addition to normal pressure sensing capabilities, shear sensing is an important ability to possess for an artificial skin when interacting with objects - especially fragile ones such as eggs. The shear sensing capability enables the user to ascertain just the right amount of pressure to apply such that it is not too low that the object will slip and the user does not need to overcompensate such that the that the object will be damaged [86].

Shear sensors are typically capacitive [4], [87] or piezoresisitive [50]. To render these sensors flexible and even stretchable the two main components – electrodes and substrate - need to be soft. As in pressure sensors, silver nanowires [13], carbon nanotubes [87], [88], liquid metal [27] and even ionically conductive gels [17] can be used as bendable and sometimes as stretchable electrodes. Silicone based elastomer substrates such as Ecoflex [85], [89] and PDMS [90] have been used to make the substrate stretchable.

Few soft sensors measure both shear and pressure. In one, Pang *et al.* [64] demonstrate a unique nano-hair based approach to detect pressure, shear and even twist. The sensor has a flat surface and is extremely sensitive to light pressures as low as a few Pascals. However, simultaneous application of all three stimuli makes it difficult to differentiate between them. There is also no information regarding the direction of the shear. Park *et al.* [91] demonstrate a micro-dome structured dielectric that enables piezoresistive sensing of pressure and shear. It loses the ability to distinguish between applied forces under simultaneous stimulation. There have been

several other shear sensors in literature that provide pressure and shear information [5], [37], [90]. These employ a protruding feature at each sensing location that is torqued when sheared. This angular deflection provides a deformation of the underlying material, which is detected capacitively. In the absence of these bumps, even soft elastomers are too stiff to deform substantially under light shear or pressure. While most shear sensors in the literature have a bump/protrusion, Charalambides *et al.* [92] demonstrates a flat surfaced shear sensor using PDMS as the elastomer with a pillar based approach. However, in this case the sensor does not buckle like human skin. The maximum shear displacement is small (max 250 μm in comparison to this thesis 1.5 mm and real skin that can be sheared a few mm). Additionally the sensor cannot detect the proximity or contact of a human, which is an important ability in case of robotics applications where the robot is expected to interact with humans

In this research, we present a soft and stretchable sensor that can sense the proximity and light touch of a human finger and deformations such as pressure and shear while differentiating between the different stimuli and providing directional information regarding the shear. The surface of the sensor is smooth and similar in stiffness to human skin (Figure 4.2 (left)). Like skin, it buckles and stretches with shear (Figure 4.2 (right)). It is able to detect the approach of a human (and of a grounded conductor) [42], but only shows a small response to insulating materials such as plastic and wood. In addition to functional aspects, this research also demonstrates mechanical similarity to skin that has not been discussed in the sensors in literature.

The sensor uses a combination of mutual capacitance to detect the proximity and a light touch of a human [2] and overlap capacitance to detect pressure and shear. A similar idea for shear and pressure measurement in capacitive electrodes has previously been proposed by Cheng *et al.* in [37] and Lee *et al.* in [5] but in these cases they rely on differential compression of capacitors

to detect shear, rather than change in overlap. Both employ bumps to produce a torque, rather than directly detecting shear. Overall, the key novelties here are : 1) most stretchable sensors in the literature detect shear by torqueing a protrusion, resulting in a normal force, but in this research the electrodes are laterally displaced hence a smooth skin-like interacting surface, 2) this sensor has the ability to detect the proximity/light contact of a human finger and 3) the dielectric architecture of this sensor enables high compliance in both the normal and lateral directions and 4) this architecture allows buckling and stretching - like human skin - *to be able* to shear locally. The novel aspect of the sensor design, which enables these features, is in the dielectric architecture. It is composed of two types of pillars – square cross-section and X cross-section, as shown in Figure 4.2 (f). The square cross-section pillars (square pillars) are bonded both on the top and the bottom surface of the dielectric while the X cross-section pillars (X pillars) are only bonded on the bottom surface as shown in Figure 4.2 (g). Upon application of a horizontal shear force, the part of the top layer of the sensor resting on the X-pillar is free to slide (being un-bonded) and the part that is bonded to the square pillar experiences a restoring force pulling the surface back to its original state once the shear force is released. The X design is chosen to mimic a scissor spring to aid in the restoring process while effectively holding up the surface of the sensor in the spaces between the square pillars. Such a dielectric architecture also provides a non-linear mechanical characteristic similar to skin as shown in Figure 4.1. The issue of matching mechanical properties of skin is not dealt with in the pressure/shear sensors in literature. This research is the first attempt at demonstrating both functional and mechanical analog to skin.

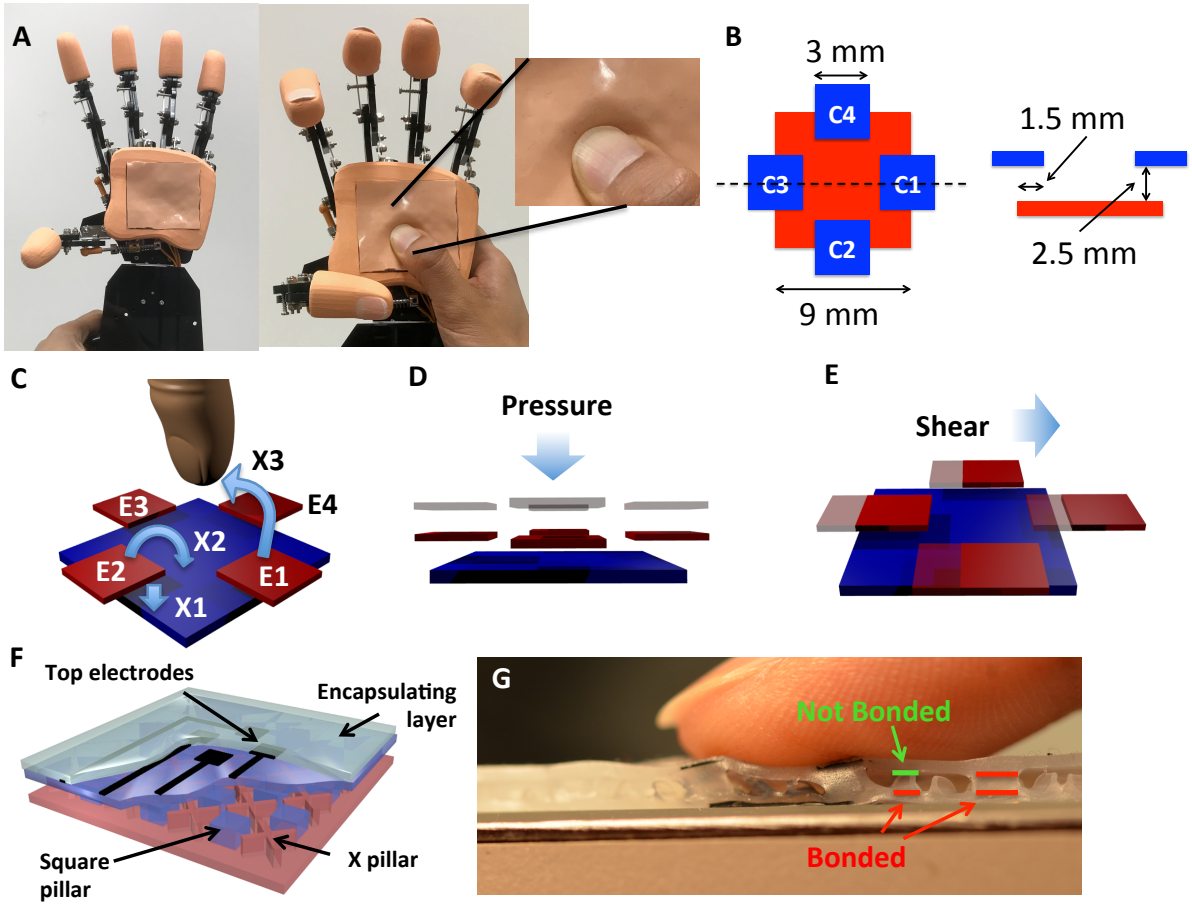

Figure 4.2: (a) Sensor on robotic palm (left) and being sheared demonstrating buckling (right), which localizes applied shear (b) Top view and cross-sectional view of electrode architecture, showing the 4 top electrodes in blue, which are separated from the bottom electrode in red. (c) Working principle of proximity and touch sensing. The arrows (X1-X3) are three representative field lines between the top electrodes and the bottom electrode. X3 is interrupted by the finger, reducing the capacitance between the top and bottom. (d) Application of pressure brings the top and bottom electrodes closer together (from grey to red), increasing capacitance of all four electrodes. (e) Applying shear changes the overlap capacitance between the top and bottom electrodes in the direction of shear. (f) 3D model of the sensor showing the dielectric architecture (g) Cross-section of sensor showing a change in overlap and buckling upon application of a shear.

4.3 Working Principle

The sensor is capacitive in nature and similar to the one in Chapter 3, using a combination of mutual capacitance and overlap capacitance to differentiate between the presence of a finger applying no force (light touch or proximity) and physical deformations such as pressure and shear. The key improvement from the sensor in Chapter 3 is the ability of this sensor to detect localized shear. Although capacitive pressure and shear sensors have been demonstrated in the literature [5], [37], the novelty here is in the sensor architecture. A combination of air gaps, square shaped pillars anchored both on top and bottom and X shaped pillars anchored only on the bottom provides the unique ability to buckle like real skin to enable detection of local shear in addition to enhanced compliance. The surface also feels similar to real skin, unlike the shear sensors in the literature [5], [37], that have protrusions to enable localized shear sensing ability.

A set of five independently connected electrodes is used for the capacitive sensing, enabling displacements and forces applied to the surface of the sensor to be resolved in 3 dimensions. Four top sense electrodes (E1~E4) and one bottom ground electrode are arranged as shown in (Figure 4.2 (b)). The top and bottom electrodes are coupled by electric fields both going through the dielectric (X1) and projecting outwards (X2) as shown in (Figure 4.2 (c)). The capacitances between each of the top electrodes and the bottom reference are sequentially measured. These change in a way that depends on the nature of the stimulus. The working principle is as follows. A human finger in proximity or lightly touching acts as a virtual ground and decouples the projected electric fields (labeled X3 in Figure 4.2 (c)) and thereby reduces all the capacitances C1~C4 in a similar manner, as previously demonstrated in [2]. Upon application of a pressure all four top active electrodes E1~E4 are displaced closer towards the ground electrode GND thereby increasing all four capacitances C1~C4 (Figure 4.2 (d)). Applying a shear force in

the positive x-axis moves E3 to the right (Figure 4.2 (e)), increasing the overlapping area of C3 (in Figure 4.2 (b)) with GND, and in turn increasing the magnitude of capacitance of C3. E1 also moves to the right (Figure 4.2 (e)), decreasing overlap area with GND, in turn decreasing C1 (Figure 4.2 (b)). The shear in this axis has minimal effects on C2 and C4. This combination of changes in C1~C4 is characteristic of a shear in the positive x-axis and provides information on the magnitude of the shear and its direction.

A simple flowchart of the process of identifying proximity, pressure and shear responses is shown below in Figure 4.3. All four capacitances are read and sorted in magnitude with the maximum negative change in capacitance from baseline being the first element of the array and the maximum positive change in capacitance from baseline being the last element in the array. If the changes are below the noise threshold then there was no stimulus. If all changes are negative then it is the proximity of a human finger or a touch depending on the magnitude of the negative change. If all changes are positive then it is a pressure applied. However, if there is a combination of a negative and positive change it is a shear applied. The direction is interpreted as in the flowchart in Figure 4.3. An array implementation of the sensor is necessary for differentiating between a light pressure applied with a human finger and proximity, similar to the case discussed in section 3.5.1. Further work needs to be done to analyze more complicated stimuli and sophisticated machine learning techniques may be required to interpret the complex stimuli and incorporate non-idealities in the sensor capacitance such as coupling of the trace interconnects discussed in a later section.

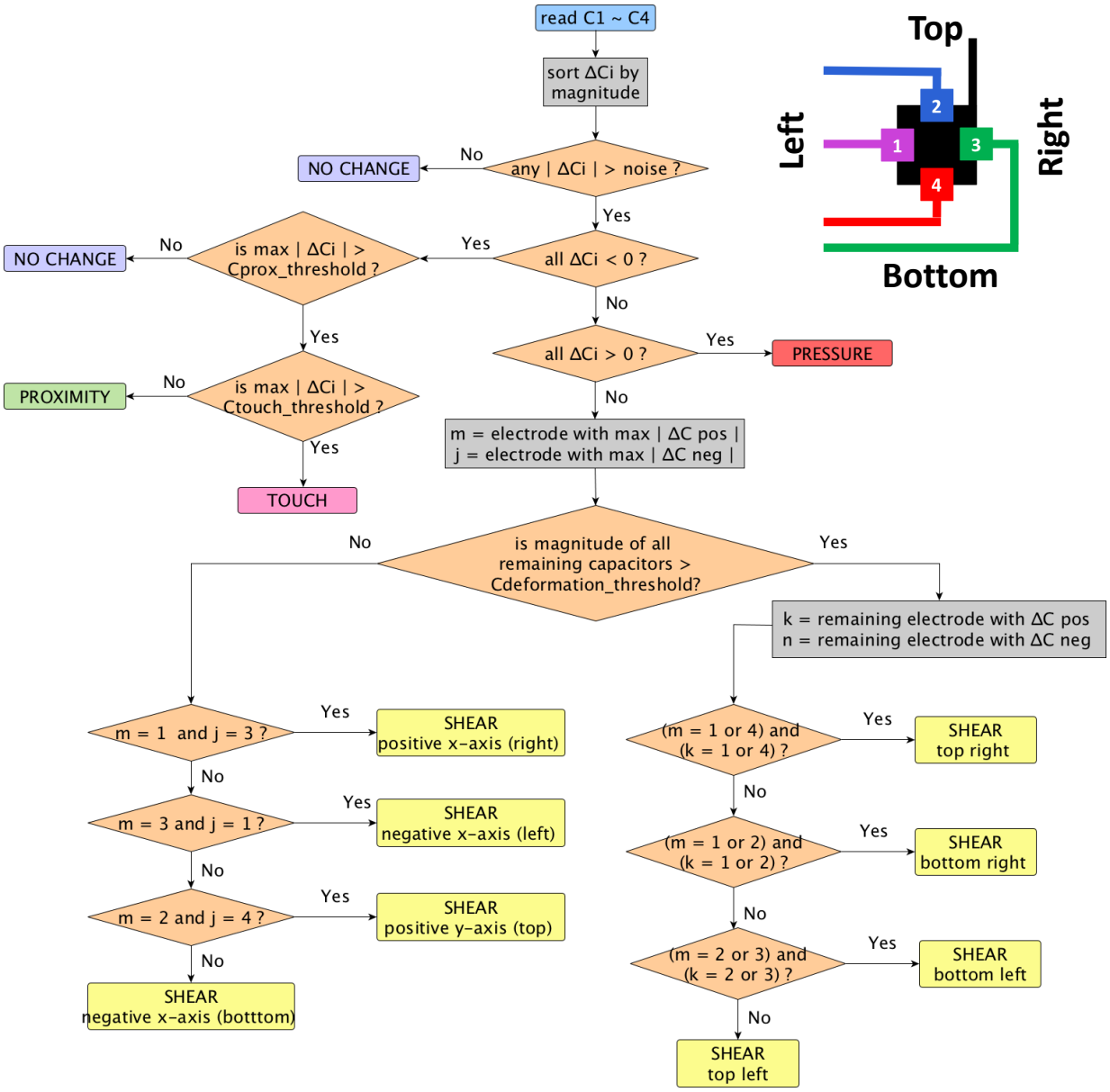

Figure 4.3: Flowchart showing working principle of sensor

To obtain a larger change in capacitance, localize the effect of shear and simulate the buckling and stretching of skin, a novel dielectric architecture is demonstrated, as shown in Figure 4.2 (f). The dielectric is not simply an elastomer, but also consists of a large pocket of air, with elastomer pillars supporting the top layer. There are two types of pillars – square ones with the

electrodes E1~E4 located on top of them (shown in blue) and X-shaped pillars (shown in pink). The spacing and aspect ratio of the square pillars are such that they can easily bend upon application of a shear at the top surface, making the device more sensitive compared to when a solid layer of elastomer was used. The square pillars are anchored on both the top and bottom layers, while the X pillars are only anchored to the bottom layer, as shown in Figure 4.2 (g). This allows for a smooth top layer by preventing it from collapsing at regions not supported by square pillars shown in Figure 4.2 (g), while simultaneously enabling a sliding motion of the top layer upon application of a shear. It is this feature that gives the sensor the ability to buckle and stretch in a localized region, mimicking human skin, as shown in Figure 4.2 (b). The dielectric architecture also provides a non-linear elastic modulus similar to human skin.

4.4 Fabrication

The materials and methods are deliberately chosen to be low cost and appropriate for large-format mass production. A simple three-step process mold-pattern-bond (MPB Fig 2A to D) produces a unibody sensor. The elastomer used is Ecoflex™. It is a common ingredient in toys, face masks, costumes etc. and provides a skin like feel. The stretchable electrodes are carbon black mixed with Ecoflex™. Although the resistivity of the carbon black based stretchable conductor is large (approximately 0.1 Ω-m), it is sufficient for capacitive sensing since this requires only very small currents.

A Stratasys Objet 3D Printer was used to print two molds (VeroWhitePlus RGD835). EcoflexTM 00-30 is first cured in the top and bottom molds (Figure 4.4 (a)) to build the top and bottom segments, with the two types of pillars in the two molds being 1.5 mm tall with a 0.5 mm thick top layer. The air pockets are 1.5 mm tall, the square pillars are 3 mm X 3 mm, and the X-

pillars are 5.8 mm long on each leg. Ecoflex was mixed in a 1 (part A) : 1 (part B) mass ratio for 3 minutes and degassed to remove air bubbles. The mixture was poured into the molds (shown in Figure 4.4 (a)) and leveled with a glass slide, degassed once more for 2 minutes and placed in an oven at 60°C for 10 minutes.

Masks for patterning the electrodes were cut manually from Staples multipurpose transparency sheets (120 μm in thickness). Each mask was manually aligned with the dielectric patterns on top of the cured Ecoflex mold layers while still in the mold, with the 4-electrode pattern laid down on the square-pillar piece and the bottom electrode laid down on the X-pillar dielectric. Carbon black (H30253 Carbon Black Super P® Conductive) was mixed with Ecoflex 00-30 in a 2 (carbon black) : 10 (part A) : 10 (part B) mass ratio for 4 minutes, then spread over the aligned mask exposed regions to cover the electrode region (Figure 4.4 (b)). A glass slide was used to level the conductive paste and remove excess material before liftoff of the mask, leaving the patterned electrode. Copper tape was laid adhesive-side down to overlap the uncured electrode paste by 5 mm and secured using polyimide tape to ensure electrical contact.

Ecoflex 00-30 uncured mixture was prepared using the same mixing and degassing method as above and spin-coated at 300 RPM on top of the patterned electrodes in the molds for 60 seconds to achieve an encapsulating layer of ~300 μm thickness (Figure 4.4 (c)). The molds were again placed in the oven for 10 minutes to cure the top layer.

The two molded pieces with patterned and encapsulated electrodes were peeled off of the molds. A 1:1 Ecoflex mixture was prepared and spin-coated onto a petri dish at 300 RPM for 60 seconds. The square-pillar layer was laid gently pillar-side-down on top of this uncured layer and lifted off to act as an adhesive layer on the bottom of the pillars. The dielectric piece with X-pillars was placed X side up and the square pillar piece was manually aligned such that the pillars fell in the center of the gaps between the Xs and gently pressed down to adhere the two layers and form

the full sensor (Figure 4.4 (d)). The sensor was cured in the oven for 10 minutes at 60°C to finish the curing process. The sensor is very soft with an elastic modulus in compression of approximately 160 kPa (skin has a modulus of ~ 400 kPa [93])

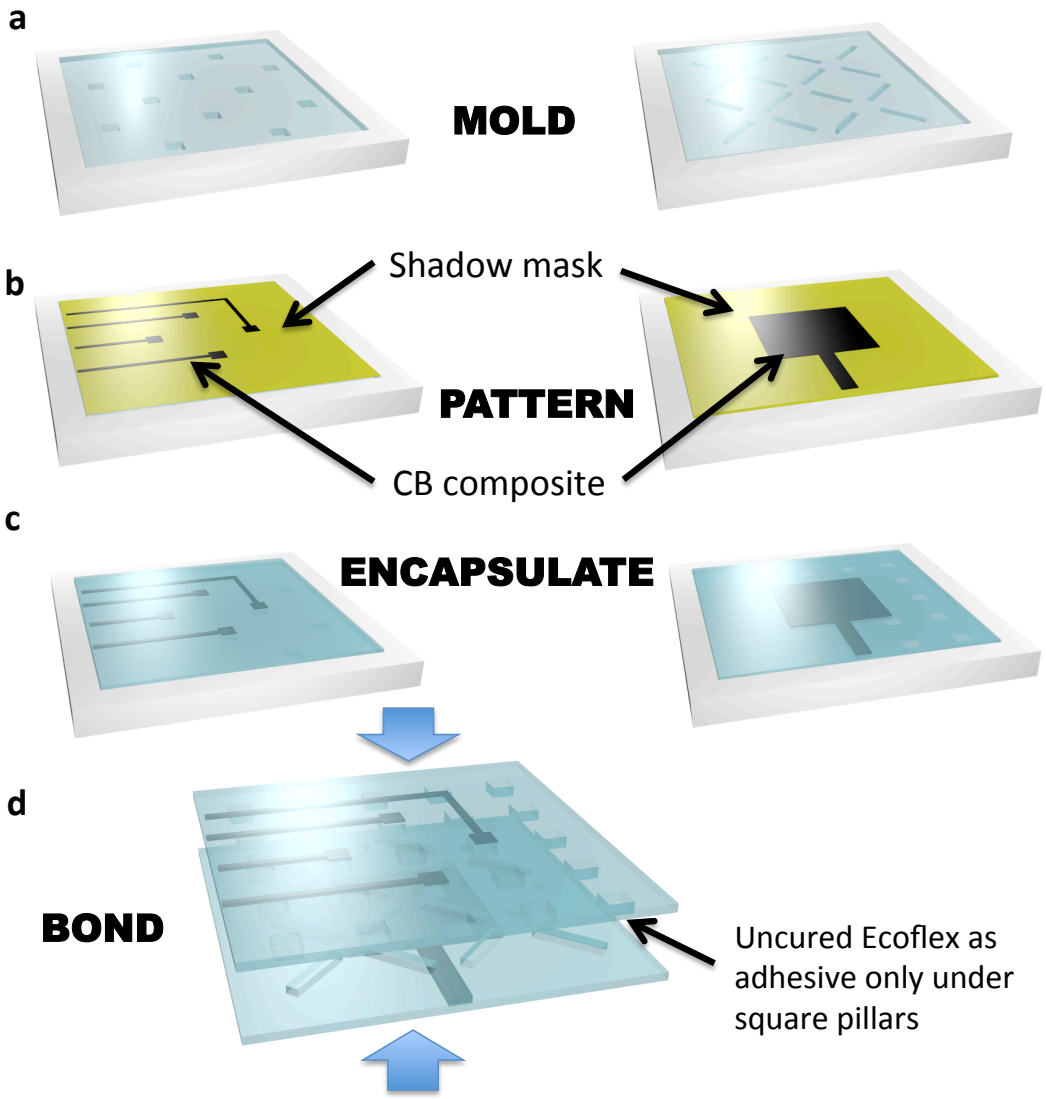

Figure 4.4: Fabrication steps

4.5 Results and discussion

In this section the range of stimuli mentioned earlier are applied on the sensor and the capacitive response to the different stimulus are plotted and analyzed. The sensor's sensitivity to the different stimuli and its ability to differentiate between them are discussed.

4.5.1 Overview of responses to different stimulus

To detect the range of stimuli mentioned earlier, a combination of mutual capacitance and overlap capacitance is used as shown in Figure 4.2 (c) – (e). Table 4.1 summarizes the behavior of the capacitances in response to the pure stimuli (proximity, touch, pressure and shear). The interaction with the skin can be interpreted based on the changes in the map, as shown in Figure 4.5. The four bars in the map correspond to the four capacitances C1~C4 shown in Figure 4.2 (b).

With the approach of a human finger the projected field couples increasingly with the finger and consequently the coupling between the active and reference electrodes will decrease. This will cause all four capacitances C1~C4 to decrease (Figure 4.5 (a)). The maps in Figure 4.5 (a) and Figure 4.5 (b) show the % decrease in the positive y-axis. The capacitances reach a minimum with a 10-12% decrease at the moment of contact, with the finger applying close to zero pressure, as shown in Figure 4.5 (b). The human finger acts as a virtual ground, which leads to the decrease in capacitance. The same effect is observed on the approach of a grounded metal. When approached or touched by a piece of cardboard or plastic, the capacitance shows a small increase (up to 2-3%). The response is small and in opposite in direction, and hence easily differentiable. The sensitivity to human approach is potentially interesting in robotics applications where the robot is expected to interact with humans in a delicate manner. It can be done through clothing,

and is sensitive at a distance of 1.5 cm for electrodes of this scale. Upon application of a pressure the dielectric thickness is decreased as shown in Figure 4.2 (d) and all four capacitances increase as shown in Figure 4.5 (c).

Figure 4.5 (d) shows the application of a shear and the sensor's response to it. The applied shear buckles the skin on the leading edge and stretches the skin on the trailing edge. This is achieved by the dielectric architecture in Figure 4.2 (f), which enables sliding of part of the surface, followed by the buckling. The capacitance response to a shear in the E1-E3 direction is shown in the map in Figure 4.5 (d). It is observed that the capacitor C1 at the trailing edge of the shear increases due to the increase in overlap area, as illustrated in Figure 4.2 (e). A fraction of this increase is due to the downward deformation at this location in the process of applying the shear, as seen in Figure 4.2 (g). The capacitance at the leading edge of the sensor decreases slightly as overlap with the reference is reduced. The two capacitances perpendicular to the axis of the shear force increase slightly due to a downward deformation component of the applied finger shear in a similar manner as to C1. In this way the combined information of the four capacitances provide both pressure and shear, including the direction of shear. However if a shear is applied in addition to a normal pressure, there the capacitors along the axis of the sheared direction will still demonstrate the characteristic increase and decrease but now with a positive offset due to the applied pressure.

Table 4.1: Response of the four capacitances to pure stimulus

Stimulus	**C1**	**C2**	**C3**	**C4**
Light touch	Down	Down	Down	Down
Pressure	Up	Up	Up	Up
Shear +ve X direction	Down	Unchanged	Up	Unchanged
Shear -ve X direction	Up	Unchanged	Down	Unchanged
Shear +ve Y direction	Unchanged	Up	Unchanged	Down
Shear -ve Y direction	Unchanged	Down	Unchanged	Up

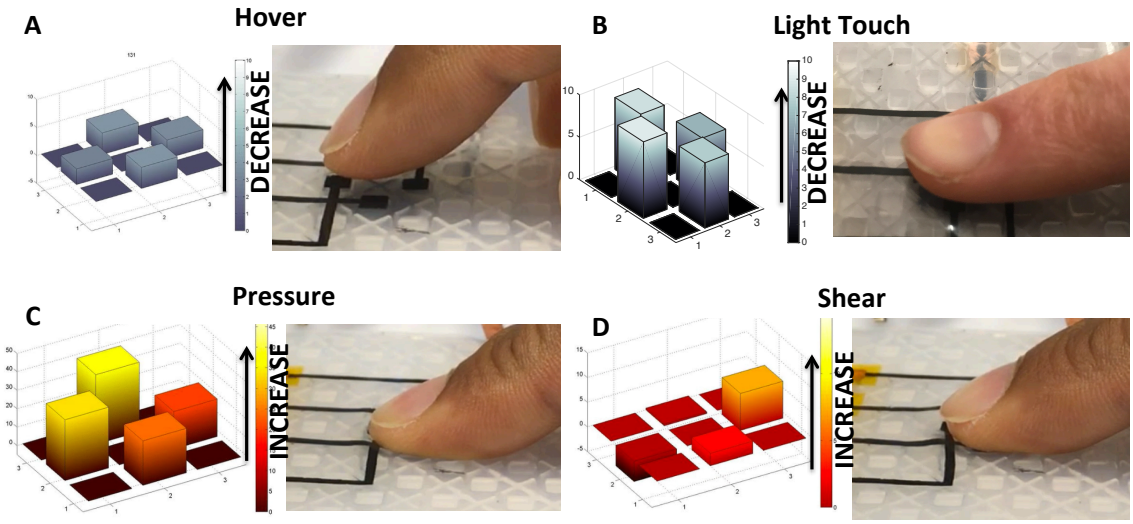

Figure 4.5: (A) Response to a hovering finger (B) a light touch (C) a press and (D) a shear.

4.5.2 Proximity and touch

To characterize the sensitivity of the sensor to a hovering finger and a light touch, a human finger was clamped and slowly brought close to the surface of the sensor such that it barely touches it. This is shown in Figure 4.6 below. The four dots at each data location correspond to the

capacitances C1-C4. At any given location the four dots are expected to coincide. However, since the baseline values of the capacitances are different (discussed in a later section) the $\Delta C/C_0$ values are different.

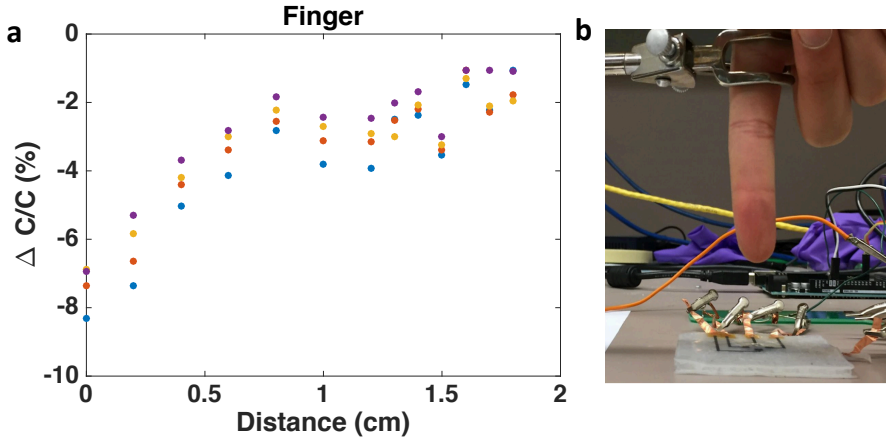

Figure 4.6: (a) Change in capacitance with finger distance from the surface of sensor (b) Experimental setup to measure change in capacitance with finger distance

It is observed that the sensor can detect a finger approximately 1 cm away from the surface of the sensor. The decrease in capacitance increases rapidly as the finger is closer than 0.5 cm. Upon light contact of just the tip of the finger with the sensor the capacitance reaches its minimum value of 8% for the given orientation and size of finger. The change in capacitance appears to increase slightly between 0.75 cm to 1.5 cm. This response does not adhere to the expected trend. The reason is likely the uncertainty in position. The finger is not perfectly stationery even in the clamp and also the orientation of the finger can change (i.e. the tip is not exactly pointing normal to the sensor surface). The maximum recorded decrease in capacitance when the entire finger tip is touching the surface of the sensor for a specific orientation that ensures maximum coupling of electric fields with the finger is 15%.

4.5.3 Pressure

To investigate the pressure sensitivity the sensor is mounted on a load cell and a 3D printed finger with a square cross-section of 12 mm X 12 mm is used to press on it. A Bose Electroforce dynamic mechanical analyzer is used to obtain the displacement and pressure data. A plot of pressure and % change in capacitance for a sinusoidal pressure is shown in Figure 4.7 (a). The stimulus is displacement controlled. It is observed that all four capacitances follow the pressure stimulus. The change in capacitance with the applied sinusoidal strain is plotted in Figure 4.7 (b). The strain is the displacement applied using the 3D printed finger divided by the thickness of the sensor (3.2 mm).

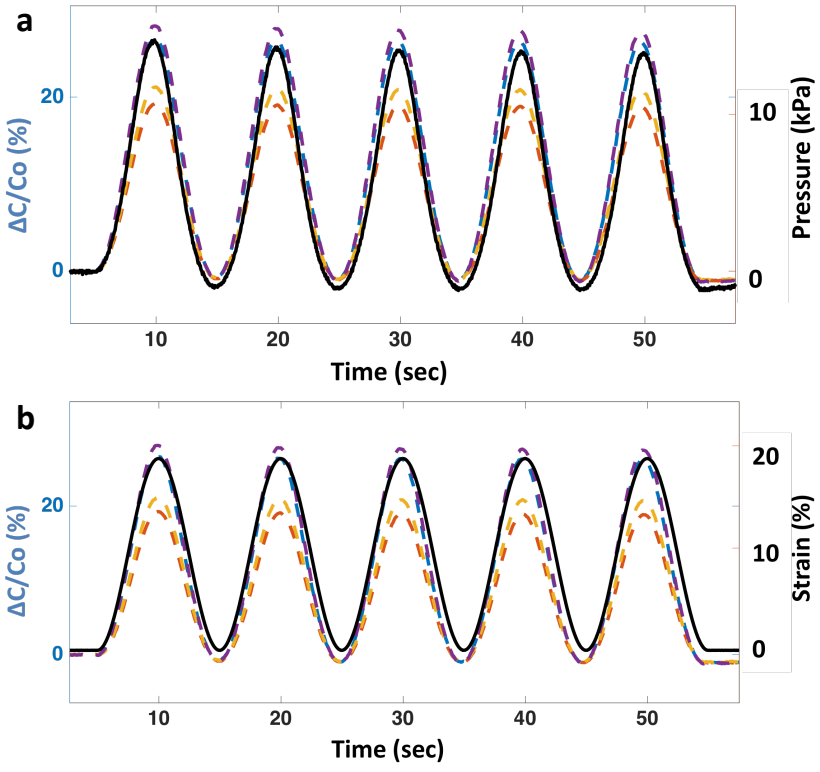

Figure 4.7: (a) % change in capacitance with pressure with a 0.1 Hz sinusoidal input (b) % change in capacitance with strain with 0.1 Hz sinusoidal input. The change in capacitance for each electrode is shown in a different color.

The magnitudes of the capacitance of the four sensor capacitors are plotted with the applied displacement and pressure of the 3D printed finger in Figure 4.8 (a) and (b) respectively. It is observed that the capacitance at zero displacement i.e. the baseline capacitance for the four capacitors are not the same. This is due to the coupling of the traces that connect the electrode capacitor electrode pads to the interconnects being asymmetric and therefore having different coupling with the bottom electrode. The largest baseline is the blue electrode (electrode 1) in Figure 4.8 that has its trace running most closely (therefore greatest coupling) to the trace of the bottom electrode. With an increase in displacement the capacitance appears to increase approximately linearly, however with pressure the capacitance appears to follow a parabola. A plot of change in capacitance ΔC with displacement and pressure (Figure 4.8 (c) and (d)) that shows the magnitude of change for the four capacitors for a given stimulus is approximately the same. This is inferred from the fact that the four plots are approximately overlapping each other. Finally a plot of $\Delta C/C_0$ in percentage with displacement and pressure applied is shown in Figure 4.8 (e) and (f). It shows with increasing magnitude of displacement, the $\Delta C/C_0$ values do not overlap even though the actual magnitude of change is similar. This is due to the different baseline values of the capacitors. This plot demonstrates a dynamic range of operation from 2kPa to 85 kPa with a sensitivity of approximately 1.3% change per kPa for the linear range of low pressures up to 25 kPa. The smallest detectable force is ~100 mN or 500 Pa. A very light press using a fingertip is approximately 50 g (magnitude was acquired by gently pressing on a weighing scale with the index finger) which corresponds to a pressure of 3.5 kPa assuming the cross-section of a fingerprint is 15 mm X 10 mm.

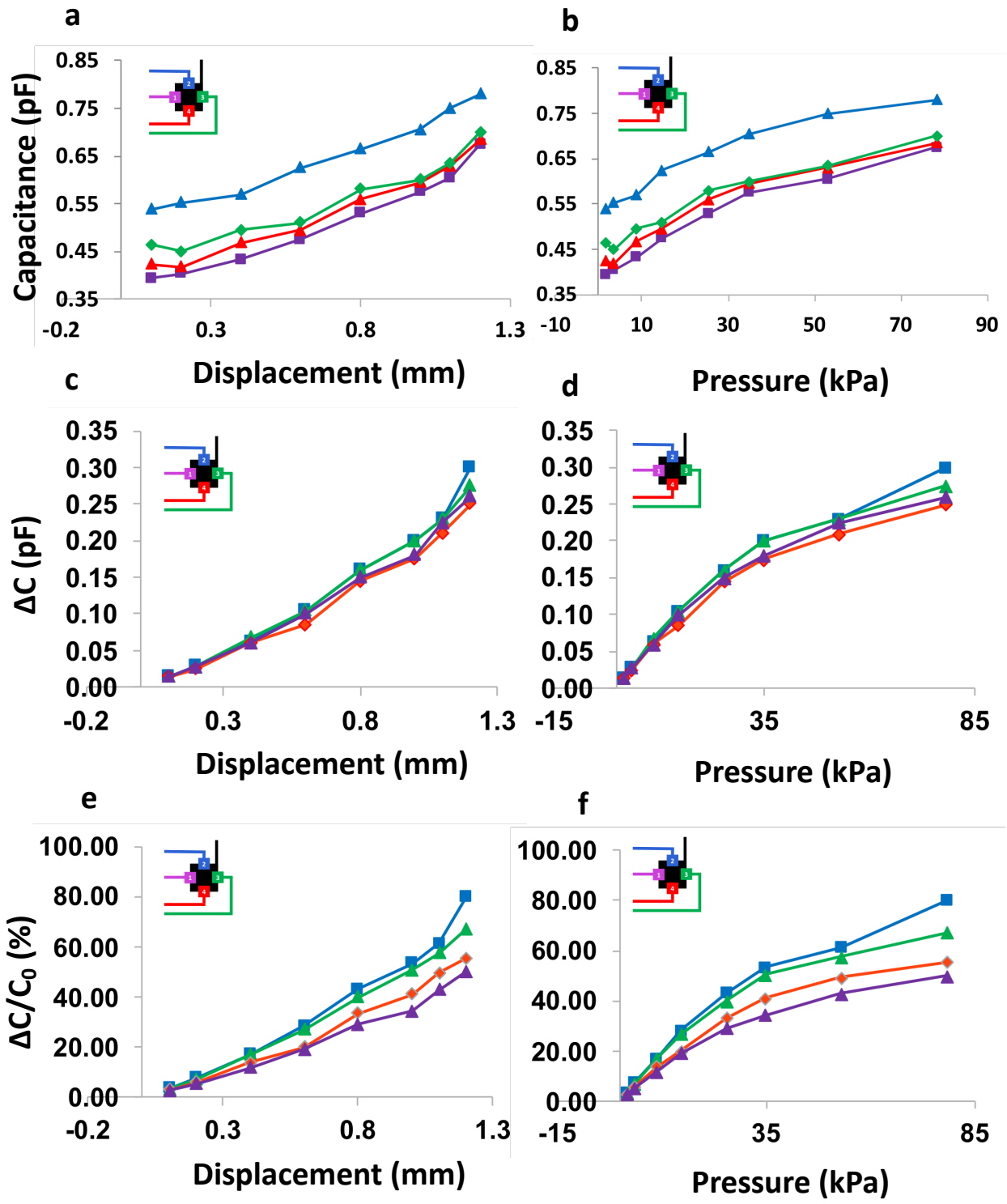

Figure 4.8: (a) Capacitance VS Displacement (b) Capacitance VS Pressure (c) ΔC VS Displacement (d) ΔC VS Pressure (e) $\Delta C/C_0$ VS Displacement (f) $\Delta C/C_0$ VS Pressure

Delalleau et al. discusses in [38] a non-linear elastic modulus of skin. The low elastic modulus region as shown in Figure 4.9 (a) is due to the strain on the elastin proteins only. In this region the collagen fibers begin to re-orient themselves. At a high strain the modulus increases since at this point the effective modulus is the combination of both the collagen fibers and the elastin. Plotting a stress-strain curve for this sensor, a similar non-linear behavior is observed. The gap between the loading and unloading cycle is characteristic of creep or a viscoelastic nature (discussed in Chapter 3) which is also characteristic of skin [38]. A low elastic modulus $E1 \approx 100$ kPa is observed until a strain of ~30% after which it increases to $E2 \approx 650$ kPa. The elastic moduli are calculated by approximating a straight line through the loading-unloading loop as shown in Figure 4.9 (b).

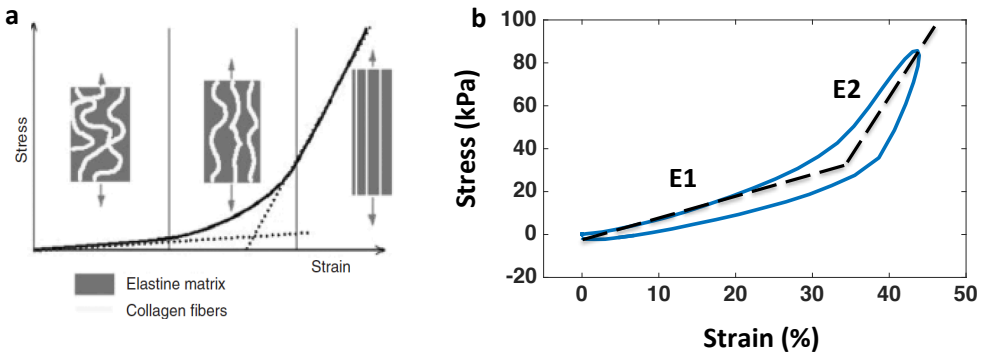

Figure 4.9: (a) Mechanical characteristics of skin (b) stress-strain curve of this sensor demonstrating similar non-linearity as skin

4.5.4 Shear

For artificial skin applications it is important to be able to detect a local shear over a large surface. In the literature the most widely implemented solution to attain localization is to fabricate a protrusion on the surface as seen in [5], [37]. An organic analogue for these protrusions can be skin warts. When a horizontal force is applied to such a protrusion, it is translated into a vertical component due to a resultant torque applied at the base of the protrusion. In such an implementation it is not the true surface shear that is being measured but a derived element. Additionally, for a skin implementation a smooth surface is preferred over such protrusions or warts.

In order to apply a controlled horizontal force for shear measurements, a 3D printed finger was used as shown in Figure 4.10 (a). The finger is connected to a load cell and is used to displace the surface of the sensor in the horizontal direction. The finger presses downwards on the surface of the sensor initially before starting the experiment to ensure proper adhesion and to prevent slip. This is shown in Figure 4.10 (b). A slight dip at the edges of the finger is seen due to the applied initial pressure. Horizontal displacements of varying magnitudes are then applied. Localized buckling of the surface of the sensor in front to the finger in the direction of shear is observed in Figure 4.10 (c). It is this ability of this sensor in addition to the non-linear elastic modulus that renders this sensor the closest analog to human skin in comparison to other artificial skin sensors in literature.

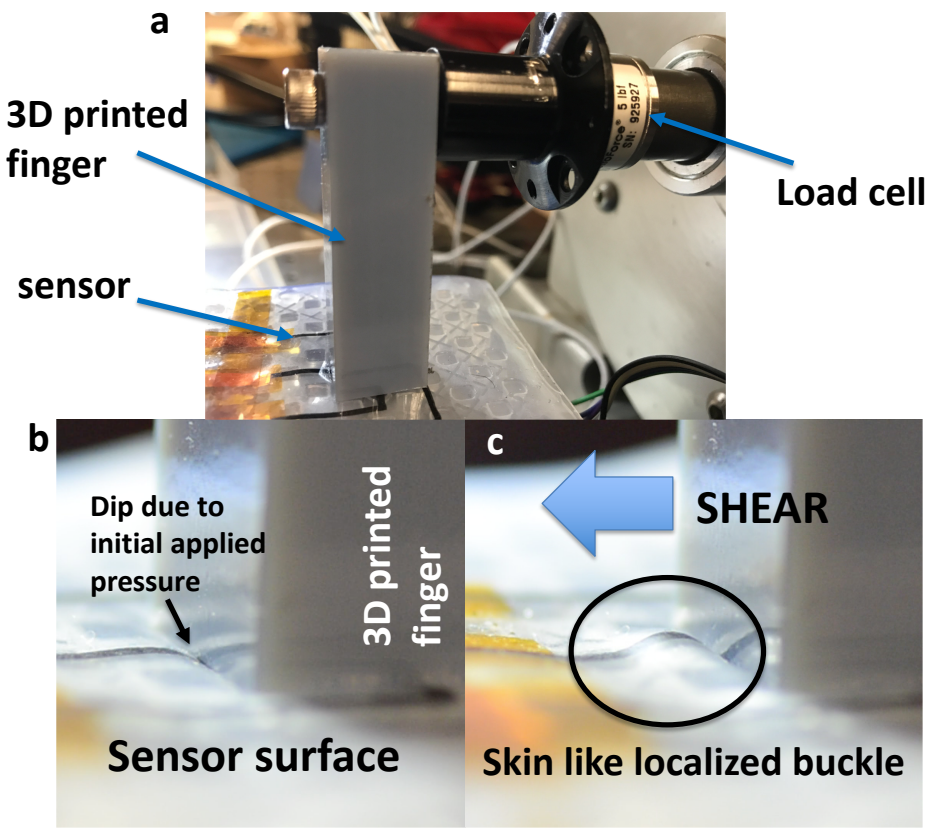

Figure 4.10: (a) Experimental setup to apply shear force on sensor surface (b) Close up image showing inital applied pressure before shear measurement (c) localized buckling on sensor surface due to applied shear (1 mm displacement)

The sensor is sheared with varying displacements ranging from 0.2 mm to 1.0 mm. The $\Delta C/C_0$ for the four sensor capacitors are plotted with respect to time for a sinusoidal stimulus of 0.1 Hz applying 0.2 mm and 1.0 mm shear displacement in Figure 4.11 (a). It is observed that the green electrode at the trailing edge (electrode 3) increases with increase in shear displacement due to an increase in overlap area and capacitive coupling with the bottom electrode. Corollary the purple electrode (electrode 1) decreases by a similar magnitude due to a decrease in overlap area and capacitive coupling with the bottom electrode. The off-axis electrode, electrode 4 (red) remains unchanged since the overlap area and coupling does not change substantially. However,

the off-axis electrode, electrode 2 (blue) shows a slight decrease in capacitance. This is due to the existence of comparably greater coupling between the trace running from electrode 2 -> interconnect and the bottom electrode -> interconnect (compared to the other electrodes). When the surface is sheared to the left (from electrode 3 towards electrode 1) these traces are moved apart and therefore the coupling reduces bringing about the slight decrease in capacitance.

The $\Delta C/C_0$ magnitudes are plotted with respect to applied shear displacement in Figure 4.12 (a) and with respect to shear force in Figure 4.12(b). Peak-to-peak shear displacement amplitudes as small as 0.2 mm and a shear force as small as 200 mN were applied, which is comparable to resolutions of 50 mN by Hu et al. in [94] and 50 mN by Cha et al. in [92]. The range of the shear force applied is 0-1 N which is comparable to literature of 0-0.4 N [37] and 0-0.5 N for Hu et al. [94] and 0-2 N for Cha et al. [92]. Although the smallest peak-to-peak amplitude is 0.2 mm, it is seen that the sensor even responds to a shear displacement of 15 μm (Figure 4.13) corresponding to a shear force of 20 mN. However, at this level the measurement is very close to the uncertainty in the displacement, which is $\pm$10 μm (discussed in a later part of this section).

The shear strain is calculated assuming the height of the square pillar is the vertical height that is bending upon application of a shear displacement i.e. h = 1.5 mm. Therefore, the strain corresponding to a shear displacement of 1 mm is 66%. The sensitivity to shear strain (also known as capacitive shear gauge factor) $\Delta C/C_0$/shear-strain is approximately 0.15 per unit shear strain (using the gradient of Figure 4.12 (a)), $\Delta C/C_0$/shear force is 11% per unit force (N) and the sensitivity $\Delta C/C_0$/shear-stress is 2.2% per kPa shear stress.

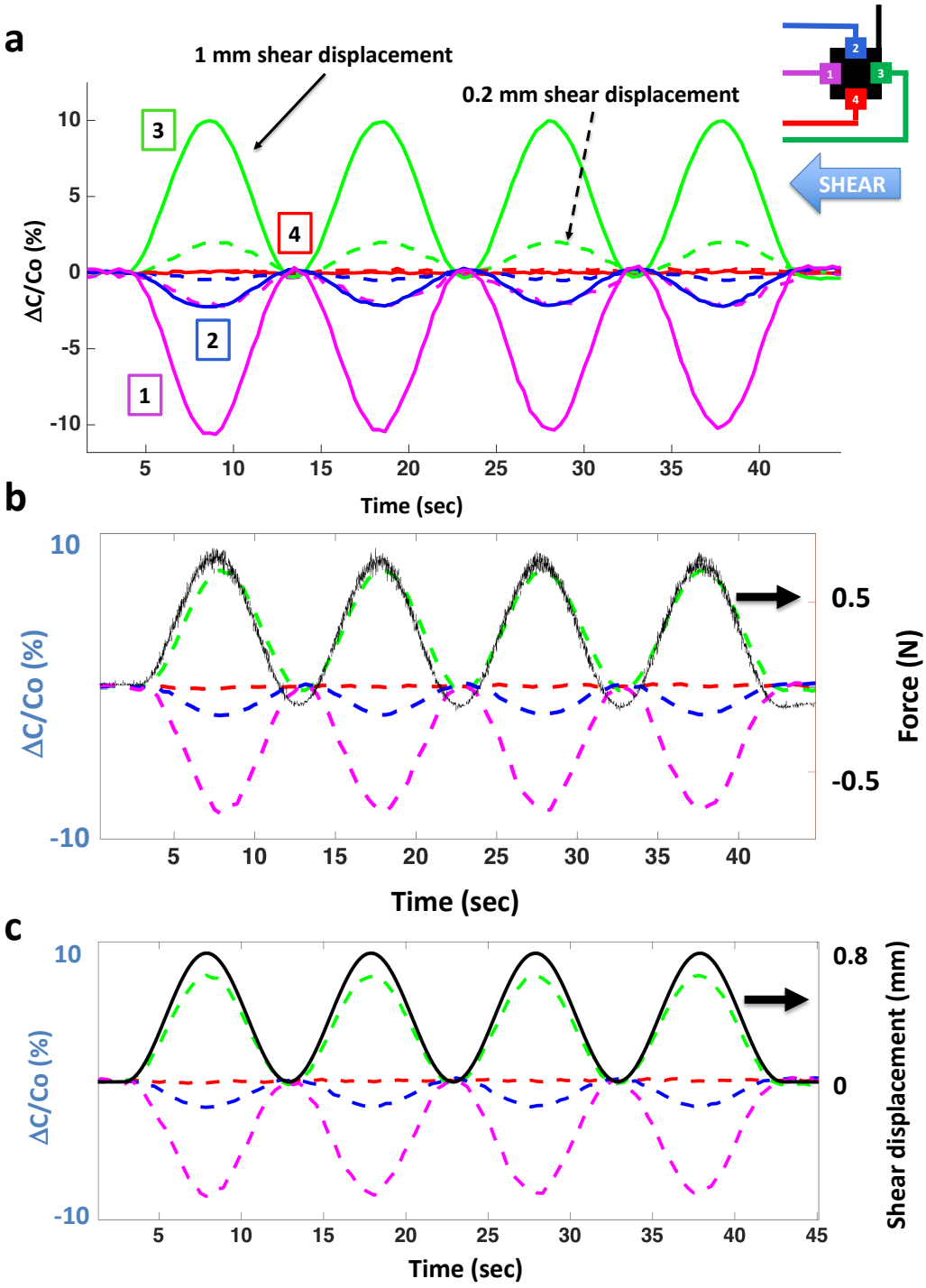

Figure 4.11: (a) Change in capacitance with 0.2 mm (dashed) and 1.0 mm (solid) shear displacement (b) $\Delta C/C_0$ of the four sensor capacitors (dotted lines) with shear force (black line) (c) $\Delta C/C_0$ of the four sensor capacitors (dotted lines) with shear displacement (black line)

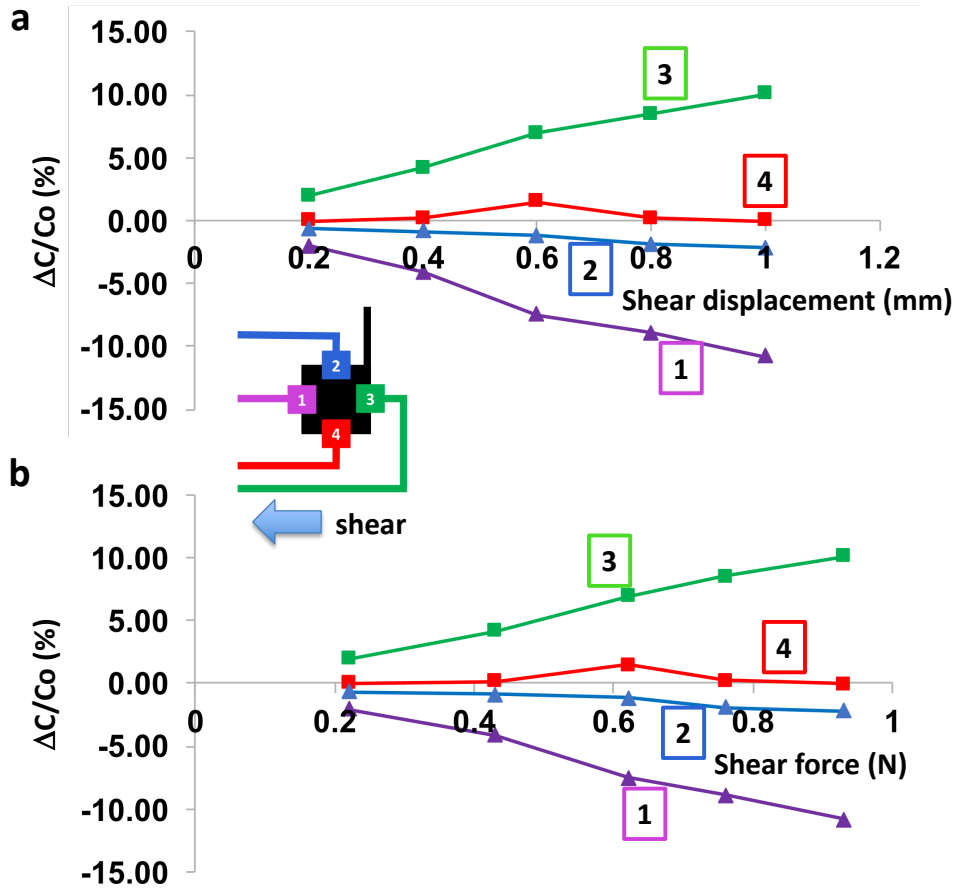

Figure 4.12: (a) $\Delta C/C_0$ VS shear displacement for four sensor capacitors (b) $\Delta C/C_0$ VS shear force for four sensor capacitors

In order to calculate the uncertainty in the shear measurement, a line is fit to the $\Delta C/C_0$ VS shear displacement data for a cycle of a sinusoidal shear displacement stimulus as shown in Figure 4.13. The error to the fitted line is calculated as in the Table 4.2 below. It is observed that the maximum error is 0.098% ~ 0.1%. Therefore, for any given reading of $\Delta C/C_0$ the actual measurement is $\pm$0.1%. From the gradient of the plot in Figure 4.13, a sensitivity of 0.15% $\Delta C/C_0$ per unit % shear strain is obtained. This is consistent with the previously obtained value of

sensitivity from Figure 4.12. An absolute value of uncertainty of 0.1% for the sensor $\Delta C/C_0$ response, with a sensitivity of 0.15 % $\Delta C/C_0$ per unit % shear strain, results in an uncertainty of ± 10 μm for shear displacement measurements.

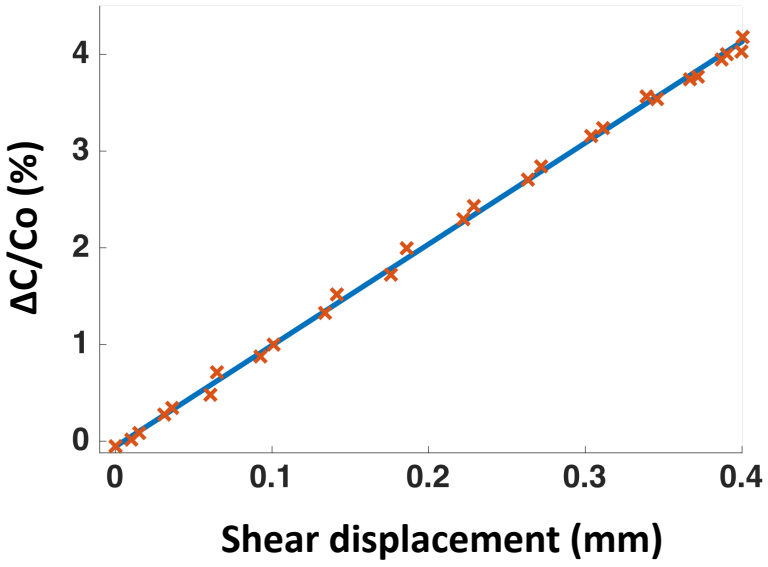

Figure 4.13: Fitting a linear function to $\Delta C/C_0$ VS shear displacement

Table 4.2: Table showing fit error for $\Delta C/C_0$ VS shear displacement

Shear displacement (mm)	$\Delta C/C_0$ (%)	Fit (%)	Fit Error (%)
6.47E-05	-0.0485201	-0.0552583	0.0067382
0.01541538	**0.08733624**	**0.10547479**	**-0.0181385**
0.036	0.33964095	0.32101178	0.01862918
0.06511666	0.70839398	0.62588576	0.08250822
0.101	0.9995148	1.0016122	-0.0020974
0.14163588	1.52353227	1.42710135	0.09643091
0.186	1.98932557	1.89162815	0.09769742
0.22851922	**2.43571082**	**2.33683736**	**0.09887346**
0.27186986	2.84327996	2.7907522	0.05252776
0.311441	3.23144105	3.20509275	0.0263483
0.34557114	3.54196992	3.5624618	-0.0204919
0.37192178	3.77486657	3.83837345	-0.0635069
0.39072758	4.00776322	4.03528472	-0.0275215
0.39937694	4.02717128	4.12585022	-0.0986789
0.4	4.18243571	4.13237418	0.05006153
0.387	3.94953906	3.99625409	-0.046715
0.367	3.73605046	3.78683858	-0.0507881
0.339	3.56137797	3.49365685	0.06772112
0.304	3.15380883	3.1271797	0.02662913
0.26354619	2.70742358	2.70359688	0.0038267
0.2218449	2.29985444	2.26695211	0.03290233
0.17614362	1.71761281	1.78842424	-0.0708114
0.134	1.32945172	1.34714781	-0.0176961
0.09287053	0.88306647	0.91649035	-0.0334239
0.06051989	0.47549733	0.57775405	-0.1022567
0.03116925	0.28141679	0.27043007	0.01098672
0.01	0.00970403	0.0487716	-0.0390676
0.001	-0.1261524	-0.0454654	-0.080687

A COMSOL simulation is done with the X-pillars bonded to the top surface as shown in Figure 4.14. The $\Delta C/C_0$ values for the capacitors are shown in Figure 4.14 (d) below. It is observed

that similar to the experimental values in Figure 4.12 (b) the trailing sense capacitor increases in capacitance, the leading capacitor decreases and electrode 2 decreases slightly. Figure 4.14 (f) shows the cross-section of electric field between the trace of electrode 2 and trace of bottom electrode. It shows that there exists electric field coupling between the traces, which upon deforming in the direction shown in Figure 4.14 (d) is decreased since the traces are moved apart. This also indicates that the design of the traces has a significant impact on the sensor capacitance. Quantitatively, the values of displacement don't match those measured in the sensors. It is observed that for an applied force of 1 N the displacement of the top surface is 0.6 mm, which is less compared to the experimental value of 1 mm. One likely reason is that in the model the X-pillars are bonded to the top surface due to constraints in the modeling environment. As expected, having the X-pillars unbonded at the top surface makes the sensor more compliant to a given shear force and therefore more sensitive to shear stimuli.

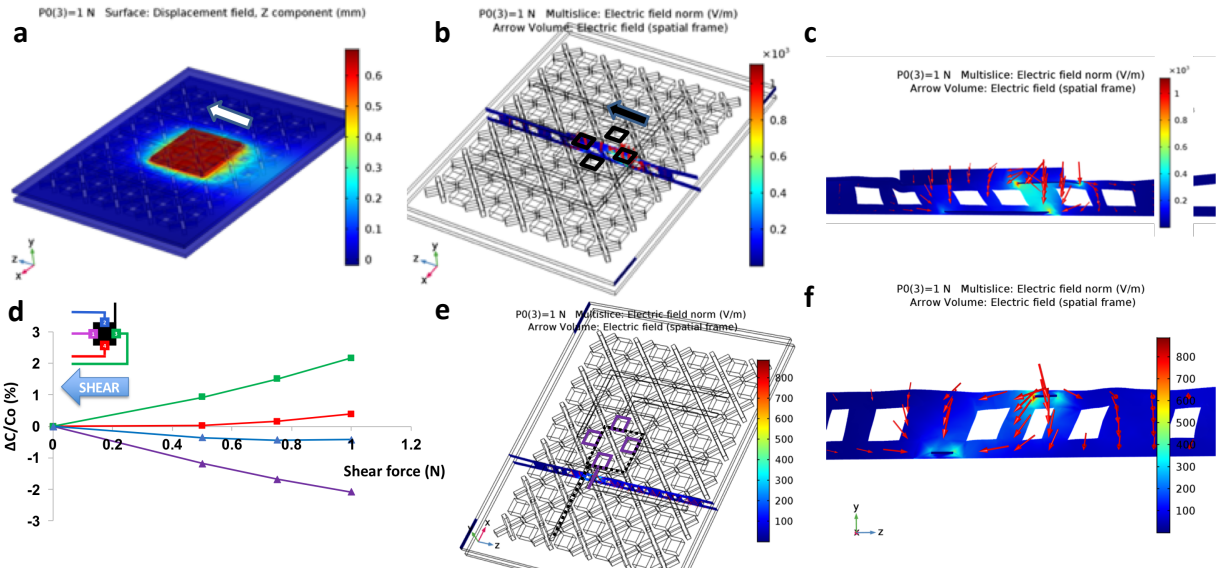

Figure 4.14: COMSOL simulation showing (a) shear displacement for a 1 N shear force applied (b) Cross-section through the active top electrode and bottom electrode in the axis of shear force showing electric field (c) close-up view of electric field in the cross-section (d) Simulated change in capacitance with applied shear (e) Cross-section showing electric field between traces of top electrode 2 and bottom electrode (f) close-up of electric field in the cross-section

This experimental setup is a first attempt at characterizing the shear capabilities of the sensor. There remains much work for the future to develop a more reliable method of shear sensing characterization and analysis of the response. This includes (i) a more robust method of applying the shear such that the applied shear displacement is perfectly horizontal (ii) verifying the actual distance by which the top electrodes translate (since there might be slippage), (iii) measurement of any normal force applied during the application of the shear, (iv) comparing the shear force measured with an off the shelf shear sensor.

4.6 Custom readout

In Chapter 3 it has been observed that the general readout circuit V1 (Figure 4.15 (a)) used for all the sensors, introduces a substantial amount of parasitic capacitance. The parasitic capacitance increases the baseline capacitance. This results in rendering the change in capacitance due to a stimulus to become a smaller fraction of the steady state capacitance. This makes the sensor apparently less sensitive than in reality. Reducing the parasitic capacitance is therefore an important task.

A new custom readout circuit V2 is designed for the artificial skin sensor as shown in Figure 4.15 (b). Since some applications for the skin requires it to be placed on a solid substrate e.g. a prosthetic arm or a robot arm, for these it is feasible to design a custom readout with a base for the sensor to be adhered on. This is shown in Figure 4.16 (b) and (c) where the copper tape interconnects are short in length and directly soldered on to the readout circuit as opposed to being clipped on to the crocodile clips in case of the previous readout circuit shown in Figure 4.16 (a).

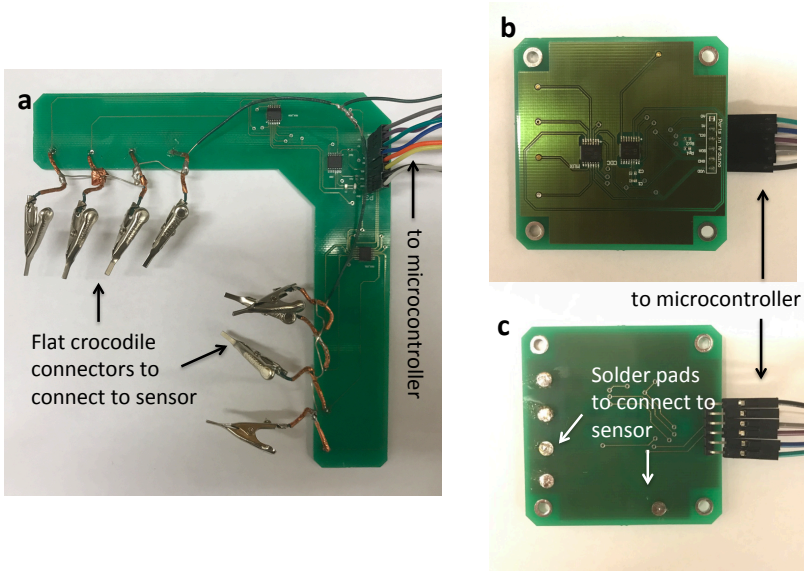

Figure 4.15: a) Readout circuit V1 b) Readout circuit V2 top view c) Readout circuit V2 bottom view

The removal of the crocodile clips and the custom design of the readout circuit decreases the parasitic component substantially. Without connecting any sensors readout circuit V1 shows a base capacitance of 0.2 pF while V2 shows a base capacitance of 0.015 pF. This is a 10 times decrease in base parasitic capacitance, mostly due to coupling between the connector clips and partially the long traces in the PCB.

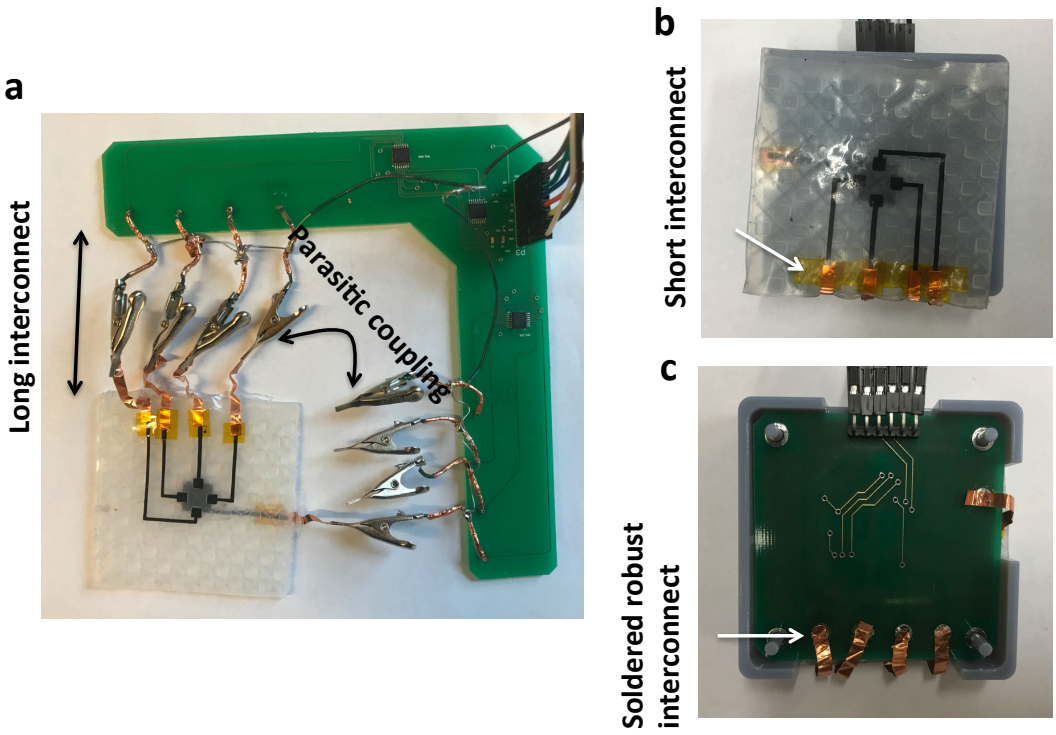

Figure 4.16: (a) Connecting sensor to readout circuit V1 (b) Top view of sensor connected to readout circuit V2 (c) Bottom view of sensor connected to readout circuit V2

When connected to a sensor the steady state capacitance read by readout circuit V1 and V2 are shown in Table 4.3 below.

Table 4.3: Comparison of readout circuit V1 vs V2

	C1 (pF)	C2 (pF)	C3 (pF)	C4 (pF)
V1	0.73	0.66	0.65	0.80
V2	0.36	0.34	0.33	0.47

The readouts for baseline capacitance of the sensor connected to readout circuits V1 and V2 are shown in Figure 4.17 (c) and (d) which are tabulated in Table 4.3. The responses of the sensor to the application of a sinusoidal displacement stimulus of 0.2 mm and 1.2 mm using the two readout PCBs are shown in Figure 4.17 (e)-(h). It is observed that for the larger stimulus the noise is almost imperceptible for both readout circuits, however for the smaller stimulus the noise is visibly apparent for the readout circuit V1 as shown in Figure 4.17 (e). The signal to noise ratio (SNR) is calculated as in equation 4-1:

$$SNR = 20\log\frac{|Signal|}{|Noise|} \quad (4\text{-}1)$$

The amplitude of signal is the magnitude of ΔC for a given stimulus and the amplitude of noise is half the magnitude of the average difference between the peak and trough of the noise signal. The SNR values for the four electrodes using the readout PCB V1 and V2 are shown in Table 4.4 below. It is observed that on an average there is an improvement of 7 dB using the PCB V2.

Table 4.4: SNR values for readout PCB V1 and V2 for sinusoidal displacement stimuli of 0.2 mm and 1.2 mm

Displacement		0.2 mm		1.2 mm	
PCB		Previous PCB	New PCB	Previous PCB	New PCB
SNR	Elec 1	29.2 dB	38.3 dB	45.2 dB	53.6 dB
	Elec 2	31.9 dB	38.5 dB	46.6 dB	55.0 dB
	Elec 3	30.4 dB	34.4 dB	44.8 dB	48.5 dB
	Elec 4	30.8 dB	38.0 dB	44.6 dB	53.3 dB

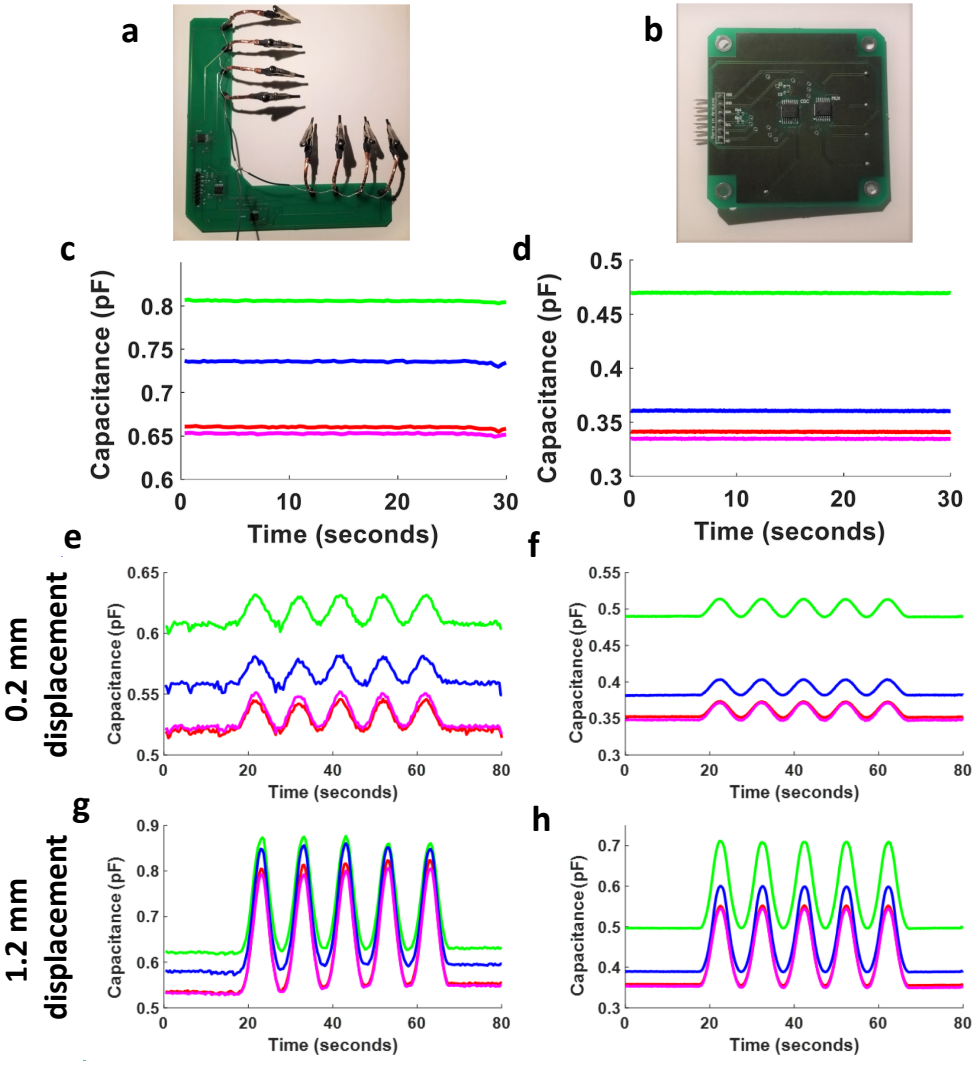

Figure 4.17: Image of readout PCB (a) V1 (b) V2. Baseline of sensor using readout PCB (c) V1 and (d) V2. Response of sensor to 0.2 mm sinusoid displacement using readout PCB (e) V1 (f) V2 and to 1.2 mm displacement using readout PCB (g) V1 (h) V2.

Designing a similar custom board for sensor II in Chapter 3 will increase the sensitivity for the sensor by reducing the baseline values of the capacitances of the sensor capacitors and reduce the noise levels in a similar manner.

4.7 Discussion and Conclusions

The sensor presented in this Chapter is seamless and smooth and has a non-linear elastic behavior like skin. Its modulus of compression is ~87 kPa for small strains (12%) and 160 kPa for large strains (40%), which is comparable to that of skin. This is the first smooth surfaced soft sensor that buckles like real human skin. It has the ability to detect proximity/light contact of a human finger and is able to distinguish pressure from the direction of shear. These analogue properties to skin are brought about by the novel dielectric architecture that enables the attainment of a smooth surface with the ability to buckle and stretch with the application of a shear force. This skin like performance is expected to be useful in robotics applications ranging from fruit picking, surgery to physically interacting with humans to aid in daily life.

Proximity and light contact lead to a decrease (maximum 15%) in capacitance of all four capacitors with the minimum being at the point of contact. The sensor offers good pressure-sensitivity (detecting change in pressure as low as 500 Pa or force of 100 mN) which is comparable to several works in literature (e.g. several kPa [95] [96]). Mechanoreceptors of human skin can detect forces as small as ~ 30 mN [97], corresponding to a pressure of 300 Pa (assuming the area of a finger tip is 10 mm X 10 mm) – so there is still work to do to match this sensitivity. To put this in perspective, 40 mN is how much a single sheet of letter size paper weighs.

Shear strains of up to 60% (assuming the normal height is the height of the deforming pillars) are detected by our sensor. In comparison to a notable work in literature by Pang *et al.* [64], this range is larger but sensitivity is lower. Pang's work shows the ability to detect a few % shear strain (with a maximum of 5%). The smallest shear force reported by Pang et al. [64] is 1 mN which is much smaller compared to shear force detected by the work in this thesis (20 mN). The range of force detected by this sensor is 0 – 1.5 N, which is larger than 0 – 0.4 N in Cheng *et al.* [37] . The reports showing high sensitivities [37], [64], with high sensitivities incorporate individual bumps to detect the shear. This makes the surface non-uniform and less skin-like. Additionally the sensors do not have the ability to detect a hovering finger and a light contact and some [64] have difficulty differentiating between different stimuli.

While most shear sensors in literature have a bump/protrusion (Table 4.5) Charalambiedes *et al.* [92] demonstrates a flat surfaced shear sensor using PDMS as the elastomer with a pillar based approach. However, in this case the sensor does not buckle like human skin. The range for a shear displacement is small (max 250 μm in comparison to 1.5 mm in this thesis and real skin that can be sheared a few mm). Additionally, the sensor cannot detect the proximity or contact of a human, which is an important ability in case of robotics applications where the robot is expected to interact with humans. Table 4.5 below shows a comparison with other shear capacitors in literature. None of the shear sensors in the literature are able to detect a proximity/contact of a human finger and most sensors are based on a bump/protrusion, which takes away the smooth feeling of real skin. Although the sensitivity of this work is less compared to some in literature it resembles skin the closest in a smooth skin-like feel, mechanical properties (having two elastic moduli for small strains and large strains) and has additional sensing modes such as proximity and light contact.

Table 4.5: Comparing shear sensors in literature

	Type	Shear			Normal		Bump	Proximity/ Contact
		Range (mN)	Resolution (mN)	Disp. (μm)	Range (mN)	Resolution (mN)		
Lee [98]	Capacitive	20	3	1	30	3	yes	no
Hu [94]	Resistive	500	25	-	5000	150	yes	no
Cha. [92]	Capacitive	2000	50	250	8000	190	no	no
Chapter 4	Capacitive	1500	20	1500	12000	100	no	yes

Regarding this sensor's ability to differentiate between the stimuli, there is a region of ambiguity between pressure and proximity. An approaching finger causes the capacitance to decrease. The capacitance increases back to baseline value upon retraction of the finger. The same response is seen if the finger approaches and pushes lightly on the sensor, with capacitance rising after contact due to compression of the capacitors. In order to resolve this ambiguity between light pressure and proximity, we can follow the time course of the capacitance, with an increase above the reference capacitance indicating that pressure has been applied, while an increase to the reference value suggests finger retraction. In an array format, neighboring sensor elements will provide information about the boundaries of any contact. In this case, a light touch will also lead to a small decrease in the capacitance of the neighboring sensing units and retracting the finger will return all the sensing units capacitances to their steady-state value. However, applying a pressure will cause the capacitance of the neighboring sensing units to remain in a decreased level while only the capacitance of the sensing unit being pressed on will increase. This is similar to the implementation in Figure 3.5 in Chapter 3.

A promising aspect of this technology is the combination of low cost materials (~\$1/m^2) with a simple and scalable fabrication process. Together these will enable the creation of arrays of

sensors at low cost over potentially very wide areas. Our previous work [2] suggests that the active area can be hundreds of square meters. The maximum area depends on refresh rate, the capacitance of the sensors, how resistive the contacts are and the density of sensors

An attractive feature of any capacitive technology is that its spatial resolution scales in proportion to the dimensions of the electrodes. Similar to a parallel plate capacitor whose dimensions are uniformly scaled up or down, the magnitude of the projected capacitance also scales linearly as do the vertical and lateral resolutions [2]. Devices can be constructed to sense at a much larger or smaller scales than the millimeter levels demonstrated here.

The combined pressure, shear and proximity sensor in its current form could be integrated into robot palms or fingertips. Next steps are to fabricate and test arrays that can form full skins, develop the electronics and electrical connects and work them into control systems. Success will help robots and prosthetics interact more safely and effectively with their environment.

Chapter 5: Conclusions

In this thesis three soft and stretchable sensors are demonstrated that are each able to detect a range of stimuli. Each sensor is an evolution from its predecessor. Table 5-1 below gives an overview off all three technologies.

The first sensor (Sensor I) in Chapter 2 is a soft, stretchable and transparent proximity and touch sensor. The substrate material is transparent silicone PDMS and the electrode material is transparent polymer hydrogel. The key novelty in this sensor compared to the existing literature is its ability to operate while being actively deformed. This is achieved using mutual capacitive technology and an electrode design that is minimally affected by deformations. This work is published in the journal Science Advances [2] and a PCT patent application is filed. Its applications include wearables, smart clothing and flexible hand-held devices. Its transparency renders it highly suitable for applications that require sensing in front of a display such that the sensor leaves the visualization of the display unobstructed.

Following this work, a soft and stretchable sensor (Sensor II) is developed that has additional sensing modes – pressure and strain. This work was presented at the Materials Research Society Spring Meeting in 2015. This is the first sensor that is able to detect and differentiate between proximity, light touch, pressure and strain. It uses a combination of mutual capacitive technology and overlap capacitive sensing. However, in the process we had to use a substrate (Ecoflex) and electrode material (Carbon black composite) that were not transparent and therefore limited its use to applications that did not require transparency. Its additional sensing modes make it suitable for applications in smart clothing, human motion mapping, health monitoring devices and artificial skin.

However, for artificial skin applications – including picking up and handling objects - shear sensing is an important mode of operation since it helps gauge the appropriate pressure and orientation needed to avoid slip.

The third sensor (Sensor III) developed in this thesis is an artificial skin technology that is able to detect the stimuli proximity, light touch, pressure and shear. This is the first sensor to have the ability to buckle locally like human skin and detect local shear in addition to proximity/light contact of a human finger. The sensor also has similar non-linear mechanical properties like skin. The substrate and electrode material are the same as the preceding sensor. The novelty is in the dielectric architecture. The combination of square pillars that are anchored both on top and bottom and X pillars that are anchored only on the bottom enable the top surface of the sensor to remain well supported, and also gives it the ability to slide when a shear is applied. The sensor is also more sensitive to pressures than the sensor described in Chapter 2. Although Sensor III is highly stretchable, since it is developed for robotic skin applications, it is expected to sit on a rigid prosthetic arm or robot arm and therefore in this application will not undergo stretch. This is the only sensor that can distinguish pressure, touch, shear and proximity – as shown for the case of an approaching finger.

Table 5.1: Comparison of the sensors

	Proximity	Light touch	Pressure (%/kPa)	Strain (capacitive gauge factor)	Shear (capacitive gauge factor)	Transparency
Sensor I (Chap 2)	**Yes**	15% (decrease)	**No**	**No**	**No**	90%
Sensor II (Chap 3)	**Yes**	10% (decrease)	0.13 (increase)	0.35 (increase)	**No**	**No**
Sensor III (Chap 4)	**Yes**	15% (decrease)	1.3 (increase)	**No**	0.15 (increase)	**No**

For future work, the sensor needs to be characterized further, existing limitations need to be addressed and the sensor needs to be developed further.

The shear response of the artificial skin was characterized by lightly pressing on the surface of the sensor initially such that the indenter does not slip. However, the sensor's shear response is expected to be dependent on the normal force being applied. Thus, the sensor needs to be thoroughly characterized using a setup that has the ability to measure normal force and horizontal force at the same time (e.g. with a 6-axis force sensor like the ATI Nano 17) and the sensor's response need to be investigated when a combination-stimuli such as a pressure and a shear is applied simultaneously. In addition to mechanical characterization the sensor needs to be characterized in terms of environmental parameters such as humidity and temperature. Also pertinent is characterizing the change in the performance of the sensor with time.

There are a few limitations of the sensor at this stage. Similar to Sensor II, this sensor will respond to a proximity/touch of a human, with a decrease in capacitance and then upon applying a pressure the capacitance will increase. However, at this point of time if the applied pressure is very small, the absolute capacitance reading will be difficult to interpret since it might mean that

the finger is being retracted or that a pressure is being applied. In Sensor II, this issue was addressed using data from the neighboring taxels so that is one route that can be undertaken to accomplish this task. In designing an array implementation caution needs to be exercised because the interconnect design has significant impact on the readout capacitance and on the sensor response to deformations. Alternative methods are being investigated to provide hardware level differentiation between the different stimuli ambiguity.

One limitation is the interconnect from the carbon black composite electrode to the copper strips that are soldered on the PCB. Being adhered solely by the adhesive on the copper tape, the connection is not very robust. A simple solution to this is to use a mechanical press-fit connector that clamps on at the interface making it stronger.

In terms of development, in addition to hardware level development to differentiate between different stimuli, algorithms need to be developed that can help interpret the sensor signals to recognize complex applied stimuli similar to the abilities of humans. These algorithms are widely used in touch screens [99] and need to be extended to multi-modal sensors.

Finally, the sensors will be tested in an application. We aim to implement the artificial skin on a robotic hand and design the control system to conduct complex maneuvers, interact with the physical world and in the end, become human – in touch.

Bibliography

[1] D. Silvera-Tawil, D. Rye, and M. Velonaki, "Artificial skin and tactile sensing for socially interactive robots: A review," *Rob. Auton. Syst.*, vol. 63, pp. 230–243, Jan. 2015.

[2] M. S. Sarwar, Y. Dobashi, C. Preston, J. K. M. Wyss, S. Mirabbasi, and J. D. W. Madden, "Bend, stretch, and touch: Locating a finger on an actively deformed transparent sensor array," *Sci. Adv.*, vol. 3, no. 3, 2017.

[3] S. C. B. Mannsfeld *et al.*, "Highly sensitive flexible pressure sensors with microstructured rubber dielectric layers.," *Nat. Mater.*, vol. 9, no. 10, pp. 859–64, Oct. 2010.

[4] D. P. J. Cotton, I. M. Graz, and S. P. Lacour, "A Multifunctional Capacitive Sensor for Stretchable Electronic Skins," *IEEE Sens. J.*, vol. 9, no. 12, pp. 2008–2009, Dec. 2009.

[5] Hyung-Kew Lee, Jaehoon Chung, Sun-Il Chang, and Euisik Yoon, "Normal and Shear Force Measurement Using a Flexible Polymer Tactile Sensor With Embedded Multiple Capacitors," *J. Microelectromechanical Syst.*, vol. 17, no. 4, pp. 934–942, Aug. 2008.

[6] T. . Chase and R. A. Luo, "A Flexible Capacitive Normal / Shear Tactile Force Sensor," in *Solid State Device Research Conference, 1995. ESSDERC '95. Proceedings of the 25th European*, 1995, pp. 351–355.

[7] M. L. Hammock, A. Chortos, B. C.-K. Tee, J. B.-H. Tok, and Z. Bao, "25th Anniversary Article: The Evolution of Electronic Skin (E-Skin): A Brief History, Design Considerations, and Recent Progress," *Adv. Mater.*, vol. 25, no. 42, pp. 5997–6038, Nov. 2013.

[8] H. Yousef, M. Boukallel, and K. Althoefer, "Tactile sensing for dexterous in-hand manipulation in robotics—A review," *Sensors Actuators A Phys.*, vol. 167, no. 2, pp. 171–187, Jun. 2011.

[9] Z. Kappassov, J.-A. Corrales, and V. Perdereau, “Tactile sensing in dexterous robot hands — Review,” *Rob. Auton. Syst.*, vol. 74, pp. 195–220, Dec. 2015.

[10] S. Xu *et al.*, “Soft Microfluidic Assemblies of Sensors, Circuits, and Radios for the Skin,” *Science (80-.).*, vol. 344, no. 6179, 2014.

[11] W. Zeng, L. Shu, Q. Li, S. Chen, F. Wang, and X.-M. Tao, “Fiber-Based Wearable Electronics: A Review of Materials, Fabrication, Devices, and Applications,” *Adv. Mater.*, vol. 26, no. 31, pp. 5310–5336, Aug. 2014.

[12] M. Stoppa and A. Chiolerio, “Wearable Electronics and Smart Textiles: A Critical Review,” *Sensors*, vol. 14, no. 7, pp. 11957–11992, Jul. 2014.

[13] W. Hu, X. Niu, R. Zhao, and Q. Pei, “Elastomeric transparent capacitive sensors based on an interpenetrating composite of silver nanowires and polyurethane,” *Appl. Phys. Lett.*, vol. 102, no. 8, p. 083303, Feb. 2013.

[14] D. J. Lipomi *et al.*, “Skin-like pressure and strain sensors based on transparent elastic films of carbon nanotubes.,” *Nat. Nanotechnol.*, vol. 6, no. 12, pp. 788–92, Dec. 2011.

[15] C. Gu, S. Chen, and X. Guo, “Transparent elastic capacitive pressure sensors based on silver nanowire electrodes,” *8th Annu. IEEE Int. Conf. Nano/Micro Eng. Mol. Syst.*, vol. 1, pp. 1183–1185, Apr. 2013.

[16] C. C. Kim, H. H. Lee, K. H. Oh, and J. Y. Sun, “Highly stretchable, transparent ionic touch panel,” *Science (80-.).*, vol. 353, no. 6300, pp. 682–687, Aug. 2016.

[17] J.-Y. Sun, C. Keplinger, G. M. Whitesides, and Z. Suo, “Ionic skin,” *Adv. Mater.*, Oct. 2014.

[18] S. Park *et al.*, “Stretchable Energy-Harvesting Tactile Electronic Skin Capable of Differentiating Multiple Mechanical Stimuli Modes,” *Adv. Mater.*, vol. 26, no. 43, pp. 7324–7332, Nov. 2014.

[19] J. Park *et al.*, “Tactile-Direction-Sensitive and Stretchable Electronic Skins Based on Human-Skin-Inspired Interlocked Microstructures,” *ACS Nano*, vol. 8, no. 12, pp. 12020–12029, Dec. 2014.

[20] Y. Tai *et al.*, “A highly sensitive, low-cost, wearable pressure sensor based on conductive hydrogel spheres,” *Nanoscale*, vol. 7, no. 35, pp. 14766–14773, 2015.

[21] J. -i. Yuji and C. Sonoda, “A PVDF Tactile Sensor for Static Contact Force and Contact Temperature,” in *2006 5th IEEE Conference on Sensors*, 2006, pp. 738–741.

[22] C. B. Cooper *et al.*, “Stretchable Capacitive Sensors of Torsion, Strain, and Touch Using Double Helix Liquid Metal Fibers,” *Adv. Funct. Mater.*, p. 1605630, Mar. 2017.

[23] R. D. Ponce Wong, J. D. Posner, and V. J. Santos, “Flexible microfluidic normal force sensor skin for tactile feedback,” *Sensors Actuators A Phys.*, vol. 179, pp. 62–69, Jun. 2012.

[24] G. Walker, “A review of technologies for sensing contact location on the surface of a display,” *J. Soc. Inf. Disp.*, vol. 20, no. 8, pp. 413–440, Aug. 2012.

[25] S. Yao *et al.*, “A Wearable Hydration Sensor with Conformal Nanowire Electrodes,” *Adv. Healthc. Mater.*, vol. 6, no. 6, p. 1601159, Mar. 2017.

[26] S. Takamatsu, T. Lonjaret, E. Ismailova, A. Masuda, T. Itoh, and G. G. Malliaras, “Wearable Keyboard Using Conducting Polymer Electrodes on Textiles,” *Adv. Mater.*, vol. 28, no. 22, pp. 4485–4488, Jun. 2016.

[27] M. D. Dickey, “Stretchable and Soft Electronics using Liquid Metals,” *Adv. Mater.*, vol. 29, no. 27, p. 1606425, Jul. 2017.

[28] B. Li, A. K. Fontecchio, and Y. Visell, “Mutual capacitance of liquid conductors in deformable tactile sensing arrays,” *Appl. Phys. Lett.*, vol. 108, no. 1, p. 013502, Jan. 2016.

[29] M. Amjadi, A. Pichitpajongkit, S. Lee, S. Ryu, and I. Park, “Highly Stretchable and

Sensitive Strain Sensor Based on Silver Nanowire–Elastomer Nanocomposite," *ACS Nano*, vol. 8, no. 5, pp. 5154–5163, May 2014.

[30] Y. Wang *et al.*, "A highly stretchable, transparent, and conductive polymer," *Sci. Adv.*, vol. 3, no. 3, p. e1602076, Mar. 2017.

[31] J. Shintake, E. Piskarev, S. H. Jeong, and D. Floreano, "Ultrastretchable Strain Sensors Using Carbon Black-Filled Elastomer Composites and Comparison of Capacitive Versus Resistive Sensors," *Adv. Mater. Technol.*, vol. 3, no. 3, p. 1700284, Mar. 2018.

[32] J.-Y. Sun *et al.*, "Highly stretchable and tough hydrogels.," *Nature*, vol. 489, no. 7414, pp. 133–6, Sep. 2012.

[33] C. Keplinger, J.-Y. Sun, C. C. Foo, P. Rothemund, G. M. Whitesides, and Z. Suo, "Stretchable, transparent, ionic conductors.," *Science*, vol. 341, no. 6149, pp. 984–7, Aug. 2013.

[34] H.-K. Kim, S. Lee, and K.-S. Yun, "Capacitive tactile sensor array for touch screen application," *Sensors Actuators A Phys.*, vol. 165, no. 1, pp. 2–7, Jan. 2011.

[35] A. P. Gerratt, H. O. Michaud, and S. P. Lacour, "Elastomeric Electronic Skin for Prosthetic Tactile Sensation," *Adv. Funct. Mater.*, vol. 25, no. 15, pp. 2287–2295, Apr. 2015.

[36] K. Kim *et al.*, "Polymer-based flexible tactile sensor up to 32 × 32 arrays integrated with interconnection terminals," *Sensors Actuators A Phys.*, vol. 156, no. 2, pp. 284–291, Dec. 2009.

[37] M.-Y. Cheng, C.-L. Lin, Y.-T. Lai, and Y.-J. Yang, "A Polymer-Based Capacitive Sensing Array for Normal and Shear Force Measurement," *Sensors*, vol. 10, no. 11, pp. 10211–10225, Nov. 2010.

[38] A. Delalleau, G. Josse, J.-M. Lagarde, H. Zahouani, and J.-M. Bergheau, "A nonlinear

elastic behavior to identify the mechanical parameters of human skin in vivo," *Ski. Res. Technol.*, vol. 14, no. 2, pp. 152–164, May 2008.

[39] K. Hinckley *et al.*, "Pre-Touch Sensing for Mobile Interaction," in *Proceedings of the 2016 CHI Conference on Human Factors in Computing Systems - CHI '16*, 2016, pp. 2869–2881.

[40] A. Braun, "Application and validation of capacitive proximity sensing systems in smart environments," *J. Ambient Intell. Smart Environ.*, vol. 7, no. 5, pp. 693–694, Sep. 2015.

[41] Barrett, "Projected-capacitive touch technology," *Inf. Disp.*, vol. 26, no. 3, 2010.

[42] G. Walker, "Fundamentals of touch technologies," in *Sunday Short Course (S-4), SID Display Week 2013*, 2013.

[43] G. Walker, "Fundamentals of Projected-Capacitive Touch Technology," Santa Clara, 2014.

[44] T. Tominaga and T. Mihara, "Pressure sensor having semiconductor diaphragm," 09-Jul-1979.

[45] I. Lee and H. J. Sung, "Development of an array of pressure sensors with PVDF film," *Exp. Fluids*, vol. 26, no. 1–2, pp. 27–35, Jan. 1999.

[46] Y. R. Wang, J. M. Zheng, G. Y. Ren, P. H. Zhang, and C. Xu, "A flexible piezoelectric force sensor based on PVDF fabrics," *Smart Mater. Struct.*, vol. 20, no. 4, p. 045009, Apr. 2011.

[47] R. Singh, Low Lee Ngo, Ho Soon Seng, and F. N. C. Mok, "A silicon piezoresistive pressure sensor," in *Proceedings First IEEE International Workshop on Electronic Design, Test and Applications '2002*, pp. 181–184.

[48] M. Amjadi, Y. J. Yoon, and I. Park, "Ultra-stretchable and skin-mountable strain sensors using carbon nanotubes–Ecoflex nanocomposites," *Nanotechnology*, vol. 26, no. 37, p.

375501, Sep. 2015.

[49] D. J. Cohen, D. Mitra, K. Peterson, and M. M. Maharbiz, “A highly elastic, capacitive strain gauge based on percolating nanotube networks.,” *Nano Lett.*, vol. 12, no. 4, pp. 1821–5, Apr. 2012.

[50] Y. Jung, D.-G. Lee, J. Park, H. Ko, and H. Lim, “Piezoresistive Tactile Sensor Discriminating Multidirectional Forces.,” *Sensors (Basel).*, vol. 15, no. 10, pp. 25463–73, Oct. 2015.

[51] K. Noda, K. Hoshino, K. Matsumoto, and I. Shimoyama, “A shear stress sensor for tactile sensing with the piezoresistive cantilever standing in elastic material,” *Sensors Actuators A Phys.*, vol. 127, no. 2, pp. 295–301, Mar. 2006.

[52] R. Surapaneni, K. Park, M. A. Suster, D. J. Young, and C. H. Mastrangelo, “A highly sensitive flexible pressure and shear sensor array for measurement of ground reactions in pedestrian navigation,” in *2011 16th International Solid-State Sensors, Actuators and Microsystems Conference*, 2011, pp. 906–909.

[53] F. Kreupl *et al.*, “Carbon nanotubes in interconnect applications,” *Microelectron. Eng.*, vol. 64, no. 1–4, pp. 399–408, Oct. 2002.

[54] M. Sarwar, “Dimensional modification of vertically aligned carbon nanotubes using miniaturized arc and glow discharges,” University of British Columbia, 2014.

[55] P. Chandrasekhar, *Conducting Polymers, Fundamentals and Applications*. Boston, MA: Springer US, 1999.

[56] Y. Wang *et al.*, “A highly stretchable, transparent, and conductive polymer,” *Sci. Adv.*, vol. 3, no. 3, 2017.

[57] S. Ma *et al.*, “Fabrication of Novel Transparent Touch Sensing Device via Drop-on-Demand Inkjet Printing Technique,” *ACS Appl. Mater. Interfaces*, vol. 7, no. 39, pp.

21628–21633, Oct. 2015.

[58] C.-L. Choong *et al.*, "Highly Stretchable Resistive Pressure Sensors Using a Conductive Elastomeric Composite on a Micropyramid Array," *Adv. Mater.*, vol. 26, no. 21, pp. 3451–3458, Jun. 2014.

[59] S. C. B. Mannsfeld *et al.*, "Highly sensitive flexible pressure sensors with microstructured rubber dielectric layers," *Nat. Mater.*, vol. 9, no. 10, pp. 859–864, Dec. 2010.

[60] W. Z. L. Wang X., Dong L., Zhang H., Yu R., Pan C., "Recent Progress in Electronic Skin," *Adv. Sci.*, vol. 2, no. 10, Oct. 2015.

[61] T. Someya, T. Sekitani, S. Iba, Y. Kato, H. Kawaguchi, and T. Sakurai, "A large-area, flexible pressure sensor matrix with organic field-effect transistors for artificial skin applications," *Proc. Natl. Acad. Sci.*, vol. 101, no. 27, pp. 9966–9970, Jul. 2004.

[62] M. S. us Sarwar *et al.*, "Transparent and conformal 'piezoionic' touch sensor," in *SPIE Smart Structures and Materials + Nondestructive Evaluation and Health Monitoring*, 2015, p. 943026.

[63] L. Cai *et al.*, "Super-stretchable, transparent carbon nanotube-based capacitive strain sensors for human motion detection.," *Sci. Rep.*, vol. 3, p. 3048, Jan. 2013.

[64] C. Pang *et al.*, "A flexible and highly sensitive strain-gauge sensor using reversible interlocking of nanofibres.," *Nat. Mater.*, vol. 11, no. 9, pp. 795–801, Sep. 2012.

[65] S. Park *et al.*, "Stretchable energy-harvesting tactile electronic skin capable of differentiating multiple mechanical stimuli modes.," *Adv. Mater.*, vol. 26, no. 43, pp. 7324–32, Nov. 2014.

[66] B. Zhang *et al.*, "Dual functional transparent film for proximity and pressure sensing," *Nano Res.*, vol. 7, no. 10, pp. 1488–1496, Aug. 2014.

[67] J. Friend and L. Yeo, "Fabrication of microfluidic devices using polydimethylsiloxane.,"

Biomicrofluidics, vol. 4, no. 2, 2010.

[68] M. Lake *et al.*, "Microfluidic device design, fabrication, and testing protocols," *Protoc. Exch.*, Jul. 2015.

[69] S. K. Sia and G. M. Whitesides, "Microfluidic devices fabricated in poly(dimethylsiloxane) for biological studies.," *Electrophoresis*, vol. 24, no. 21, pp. 3563–76, Nov. 2003.

[70] Y. Temiz, R. D. Lovchik, G. V. Kaigala, and E. Delamarche, "Lab-on-a-chip devices: how to close and plug the lab?," *Microelectron. Eng.*, vol. 132, pp. 156–175, Oct. 2014.

[71] Z. Wu, J. Walish, A. Nolte, L. Zhai, R. E. Cohen, and M. F. Rubner, "Deformable Antireflection Coatings from Polymer and Nanoparticle Multilayers," *Adv. Mater.*, vol. 18, no. 20, pp. 2699–2702, Oct. 2006.

[72] J. Wei, C. Yue, Z. L. Chen, Z. W. Liu, and P. M. Sarro, "A silicon MEMS structure for characterization of femto-farad-level capacitive sensors with lock-in architecture," *J. Micromechanics Microengineering*, vol. 20, no. 6, p. 064019, Jun. 2010.

[73] C. Larson *et al.*, "Highly stretchable electroluminescent skin for optical signaling and tactile sensing," *Science (80-.).*, vol. 351, no. 6277, 2016.

[74] T. Sekitani *et al.*, "Stretchable active-matrix organic light-emitting diode display using printable elastic conductors.," *Nat. Mater.*, vol. 8, no. 6, pp. 494–9, Jun. 2009.

[75] S. Park *et al.*, "Stretchable Energy-Harvesting Tactile Electronic Skin Capable of Differentiating Multiple Mechanical Stimuli Modes," *Adv. Mater.*, vol. 26, no. 43, pp. 7324–7332, Nov. 2014.

[76] Y. Enokibori, A. Suzuki, H. Mizuno, Y. Shimakami, and K. Mase, "E-textile pressure sensor based on conductive fiber and its structure," in *Proceedings of the 2013 ACM conference on Pervasive and ubiquitous computing adjunct publication - UbiComp '13*

Adjunct, 2013, pp. 207–210.

[77] S. Gong *et al.*, "A wearable and highly sensitive pressure sensor with ultrathin gold nanowires," *Nat. Commun.*, vol. 5, pp. 838–843, Feb. 2014.

[78] Y. Tai, M. Mulle, I. Aguilar Ventura, and G. Lubineau, "A highly sensitive, low-cost, wearable pressure sensor based on conductive hydrogel spheres," *Nanoscale*, vol. 7, no. 35, pp. 14766–14773, Aug. 2015.

[79] G. Schwartz *et al.*, "Flexible polymer transistors with high pressure sensitivity for application in electronic skin and health monitoring.," *Nat. Commun.*, vol. 4, p. 1859, Jan. 2013.

[80] R. Rocha, P. Lopes, A. T. de Almeida, M. Tavakoli, and C. Majidi, "Soft-matter sensor for proximity, tactile and pressure detection," in *2017 IEEE/RSJ International Conference on Intelligent Robots and Systems (IROS)*, 2017, pp. 3734–3738.

[81] B. Zhuo, S. Chen, M. Zhao, and X. Guo, "High Sensitivity Flexible Capacitive Pressure Sensor Using Polydimethylsiloxane Elastomer Dielectric Layer Micro-Structured by 3-D Printed Mold," *IEEE J. Electron Devices Soc.*, vol. 5, no. 3, pp. 219–223, May 2017.

[82] M. Hosseini, G. Zhu, and Y.-A. Peter, "A new formulation of fringing capacitance and its application to the control of parallel-plate electrostatic micro actuators," *Analog Integr. Circuits Signal Process.*, vol. 53, no. 2–3, pp. 119–128, Oct. 2007.

[83] J. E. O'Doherty *et al.*, "Active tactile exploration using a brain-machine-brain interface," *Nature*, vol. 479, no. 7372, pp. 228–231, Nov. 2011.

[84] S. Raspopovic *et al.*, "Bioengineering: Restoring natural sensory feedback in real-time bidirectional hand prostheses," *Sci. Transl. Med.*, vol. 6, no. 222, pp. 222ra19-222ra19, Feb. 2014.

[85] B. Li, A. K. Fontecchio, and Y. Visell, "Mutual capacitance of liquid conductors in

deformable tactile sensing arrays," *Appl. Phys. Lett.*, vol. 108, no. 1, p. 013502, Jan. 2016.

[86] M. Valero *et al.*, "Interfacial pressure and shear sensor system for fingertip contact applications.," *Healthc. Technol. Lett.*, vol. 3, no. 4, pp. 280–283, Dec. 2016.

[87] X. Wang, T. Li, J. Adams, and J. Yang, "Transparent, stretchable, carbon-nanotube-inlaid conductors enabled by standard replication technology for capacitive pressure, strain and touch sensors," *J. Mater. Chem. A*, vol. 1, no. 11, p. 3580, 2013.

[88] K. S. Karimov, M. Saleem, Z. M. Karieva, A. Khan, T. A. Qasuria, and A. Mateen, "A carbon nanotube-based pressure sensor," *Phys. Scr.*, vol. 83, no. 6, p. 065703, Jun. 2011.

[89] S. Yao and Y. Zhu, "Wearable multifunctional sensors using printed stretchable conductors made of silver nanowires," *Nanoscale*, vol. 6, no. 4, p. 2345, Jan. 2014.

[90] E.-S. Hwang, J. Seo, and Y.-J. Kim, "A Polymer-Based Flexible Tactile Sensor for Both Normal and Shear Load Detections and Its Application for Robotics," *J. Microelectromechanical Syst.*, vol. 16, no. 3, pp. 556–563, Jun. 2007.

[91] J. Park *et al.*, "Tailoring force sensitivity and selectivity by microstructure engineering of multidirectional electronic skins," *NPG Asia Mater.*, vol. 10, no. 4, pp. 163–176, Apr. 2018.

[92] A. Charalambides and S. Bergbreiter, "A novel all-elastomer MEMS tactile sensor for high dynamic range shear and normal force sensing," *J. Micromechanics Microengineering*, vol. 25, no. 9, p. 095009, Sep. 2015.

[93] M. Pawlaczyk, M. Lelonkiewicz, and M. Wieczorowski, "Age-dependent biomechanical properties of the skin.," *Postep. dermatologii i Alergol.*, vol. 30, no. 5, pp. 302–6, Oct. 2013.

[94] C.-F. Hu, W.-S. Su, and W. Fang, "Development of patterned carbon nanotubes on a 3D polymer substrate for the flexible tactile sensor application," *J. Micromechanics*

Microengineering, vol. 21, no. 11, p. 115012, Nov. 2011.

[95] C. Gerlach *et al.*, "Printed MWCNT-PDMS-Composite Pressure Sensor System for Plantar Pressure Monitoring in Ulcer Prevention," *IEEE Sens. J.*, vol. 15, no. 7, pp. 3647–3656, Jul. 2015.

[96] S. Miller and Z. Bao, "Fabrication of flexible pressure sensors with microstructured polydimethylsiloxane dielectrics using the breath figures method," *J. Mater. Res.*, vol. 30, no. 23, pp. 3584–3594, Dec. 2015.

[97] H. H. King, R. Donlin, and B. Hannaford, "Perceptual thresholds for single vs. Multi-Finger Haptic interaction," in *2010 IEEE Haptics Symposium*, 2010, pp. 95–99.

[98] H.-K. Lee, J. Chung, S.-I. Chang, and E. Yoon, "Real-time measurement of the three-axis contact force distribution using a flexible capacitive polymer tactile sensor," *J. Micromechanics Microengineering*, vol. 21, no. 3, p. 035010, Mar. 2011.

[99] R. Xiao, J. Schwarz, and C. Harrison, "Estimating 3D Finger Angle on Commodity Touchscreens," in *Proceedings of the 2015 International Conference on Interactive Tabletops & Surfaces - ITS '15*, 2015, pp. 47–50.